



Università degli studi ROMA TRE

SCUOLA DOTTORALE IN INGEGNERIA

Dottorato di ricerca in Scienze dell'Ingegneria Civile
XXI Ciclo

Tesi di Dottorato

Pseudo-dynamic tests on reinforced concrete
bridge piers repaired and/or retrofitted by means
of techniques based on innovative materials

Dottorando: Ing. Davide Lavorato

Docente guida: Prof. Camillo Nuti

Coordinatore del dottorato: Prof. Leopoldo Franco

Roma, febbraio2009

Collana delle tesi di Dottorato di Ricerca
In Scienze dell'Ingegneria Civile
Università degli Studi Roma Tre
Tesi n° 22

Sommario

In questa tesi sono presentati i risultati sperimentali di una campagna di prove su ponti in cemento armato con l'obiettivo di valutare l'efficacia di materiali innovativi (resine epossidiche, barre in acciaio inox, calcestruzzo autocompattante (SCC) e fasciature in fibre di carbonio(CFRP)) per la riparazione e il rinforzo di pile da ponte severamente danneggiate durante precedenti prove pseudodinamiche.

I provini fisicamente testati nel laboratorio sono rappresentativi di pile alte e basse in cemento armato con sezione circolare progettate secondo l'Eurocodice 8 e secondo la Normativa Sismica Italiana precedente al 1986.

Nella tesi è descritta la messa a punto di un sistema di prova per prove pseudodinamiche e del relativo software. La risposta sismica di due ponti è stata studiata sperimentalmente. Una pila in scala 1:6 è provata in laboratorio mentre il resto della struttura è simulato numericamente. Le prove pseudo dinamiche sono state seguite da prove cicliche per portare a rottura i provini.

Per questo scopo viene fornita la descrizione delle tecniche di riparazione e rinforzo delle pile così come la descrizione del sistema di prova per poi infine comparare il comportamento sismico e il danneggiamento delle pile originali con quello delle pile riparate e rinforzate.

Abstract

In this thesis the experimental results of a campaign of tests on r.c. bridges are presented with the aim of assessing the effectiveness of innovative materials (epoxy adhesive, stainless steel rebars, self compacting concrete and CFRP wrapping) in repairing and reinforcing of severely damaged piers during previous pseudo-dynamics tests.

The specimens physically tested in the lab, are representative of tall and squat circular r.c. piers designed according to Eurocode 8 and Italian Code before 1986.

In the thesis the pseudodynamic apparatus as well as the relative computer software has been developed and set up. Experimental seismic responses of two bridges are obtained. A representative pier scaled 1:6 is physically tested in the lab while the rest of the structure is simulated numerically.

The tests carried out are of pseudodynamic type as well as cyclic. To this end the description of the retrofitting of the piers as well as the description of test equipment is given and finally a comparison between the seismic behaviour of the original and the retrofitted piers are shown in terms of seismic response and final structural damage.

Contents

LIST OF FIGURES	IX
LIST OF TABLES	XVI
1. INTRODUCTION	1
2. RESEARCH OBJECTIVES.....	2
3. DEVELOPMENT OF EXPERIMENTAL METHODS	3
4. EXPERIMENTAL PROGRAM	8
5. CONCRETE BRIDGE STRUCTURES	9
5.1. DESIGN AND CONSTRUCTION OF ORIGINAL CONCRETE PIER SPECIMENS	10
6. PREVIOUS PSEUDO-DYNAMIC TESTS.....	12
7. DAMAGED CONCRETE SPECIMENS	14
8. SPECIMENS REPAIR	16
8.1. DAMAGED CONCRETE REMOVAL.....	16
8.2. CONCRETE CORE CONSOLIDATION	19
8.3. REINFORCING BAR RESTORATION.....	23
8.4. CONCRETE RESTORATION	30
8.5. SEISMIC RETROFITTING	38
8.5.1. DESIGN PROCEDURE.....	38
8.5.1.1. SQUAT PIERS	39
8.5.2. TALL PIERS.....	47
8.5.3. FRP WRAPPING	52
9. PSEUDO-DYNAMIC TEST.....	54
9.1. PSEUDO-DYNAMIC TESTING SOFTWARE.....	55
9.2. ACQUISITION PROGRAM.....	58
9.3. CONTROL PROGRAM	60
9.4. MAIN PROGRAM: PSEUDO-DYNAMIC TESTING PROGRAM	62
9.5. SOFTWARE TESTING.....	76
10. TEST EQUIPMENT	81

11. EXPERIMENTAL RESULTS	94
11.1. FREE OSCILLATIONS	95
11.1.1. OBSERVATIONS.....	95
11.1.1.1. PIER 7.....	96
11.1.1.2. PIER 8.....	96
11.1.2. HORIZONTAL-FORCE DRIFT-DEFORMATION RESPONSE	97
11.1.2.1. PIER 7.....	97
11.1.2.2. PIER 8.....	98
11.2. PSEUDO-DYNAMIC TEST.....	99
11.2.1. HORIZONTAL-FORCE DRIFT-DEFORMATION RESPONSE	100
11.2.1.1. PIER 7.....	100
11.2.1.2. PIER 8.....	107
11.3. CYCLIC TEST	114
11.3.1. OBSERVATIONS.....	115
11.3.1.1. PIER 8.....	115
11.3.2. HORIZONTAL-FORCE DRIFT DEFORMATION RESPONSE.....	115
11.3.2.1. PIER 7.....	116
11.3.2.2. PIER 8.....	119
1.1.1. STRAIN GAUGES	127
2. COMPARISON OF PREVIOUS EXPERIMENTAL AND RECENT TESTS	131
3. ANALYTICAL STUDIES	135
3.1. MATERIAL MODELS	137
3.1.1. STEEL	138
3.1.2. CONCRETE.....	141
3.2. FIBER MODELS.....	148
3.2.1. TALL PIERS.....	153
3.2.2. SQUAT PIERS.....	156
4. CONCLUSION.....	159
ACKNOWLEDGMENTS	167
REFERENCE.....	167

APPENDIX I	177
APPENDIX II.....	182

List of figures


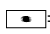
Figure 1 Layout of the bridge configuration, the central pier of the irregular bridge and the lateral one of the regular bridges, the ones experimentally tested.	10
Figure2: Main detected damages (h_c =cover expulsion extent in mm, l_b =buckled bar length in mm, δ =buckled bar deflection in mm, θ =shear crack inclination angle,  =damaged concrete,  =bar to be replaced).	15
Figure3. Repair and retrofitting of piers	16
Figure4 Damaged concrete cover removal (phase 1)	17
Figure5 Damaged concrete core removal and crack cleaning (phase 1)..	18
Figure6 Concrete core consolidation (phase 2)	20
Figure7 Tubes position at Injecting Zones (phase 2).....	21
Figure8 Tubes position (phase 2).....	22
Figure9 Injecting steps (phase 2).....	22
Figure 10 Welded joints (a) top (b) bottom.....	23
Figure 11 Monotonic tests in tension and compression ($\lambda=L/\varnothing=5$ (XMA), 11(XMC)) for $\varnothing 12$ stainless steel bars.	24
Figure 12 Cyclic tests –Stress strain relationship $\varnothing 12$ stainless steel bars.	25
Figure 13 Cyclic tests for $\varnothing 12$ stainless steel bars.....	26
Figure14 Reinforcing bar restoration (phase 3).....	27
Figure 15 Longitudinal Reinforcing bar restoration (phase 3).(Pier 6) ...	28
Figure16 Trasversal Reinforcing bar restoration (phase 3).....	29
Figure17 Reinforcing bar restoration (phase 3).....	30
Figure18 Concrete restoration (phase 4) (a) SCC production (b) formwork (c) SCC jet process.....	33
Figure19 Concrete restoration (phase 4). After removing the formwork, the SCC surface is smooth, compact and regular	34
Figure 20: hydraulic shrinkage-time diagram for SCC.....	36
Figure 21: (a) Shrinkage of different Concretes (NC=normal C., NCshr=shrinkage offset C., SCC=self compacting C., SCClow=SCC with low cement content) (b) Preparation technique effect on concrete expansion.....	37

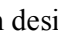
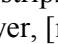
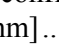
Figure 22 Elevation view of circular element confined with FRP strips.	44
Figure 23 FRP strips configuration designed for squat piers 6, 8;  1 layer, [mm] and for tall piers FRP strips configuration designed for tall piers 2, 4, 5;  3 layers,  1 layer, [mm].....	53
Figure 24 FRP strips application. Tall and squat piers.	54
Figure 25 Acquisition user interface.....	60
Figure 26 Procedure flow diagram	68
Figure 27 Pseudo-dynamic test software user interface.....	76
Figure 28 Comparison between the Force-Displacements cycles of the piers (7m) during pseudo-dynamic test and Takeda Model approximation.	77
Figure 29 Displacement history of piers 7m; simulated by previous pseudo-dynamic test software (red line), during the pseudo-dynamic test	78
Figure 30 Displacement history of piers 14m; simulated by previous pseudo-dynamic test software (red line), during the pseudo-dynamic test	79
Figure 31 Displacement history of piers 21m; simulated by previous pseudo-dynamic test software (red line), during the pseudo-dynamic test	79
Figure 32 Behavior of the specimen 7 during a previous elastic test (red line) and during the pseudo-dynamic test (blue line).....	80
Figure 33. Test equipment.....	82
Figure 34. Test equipment: vertical frame (mm).....	83
Figure 35. Test equipment: (a) vertical frame, (b) hinges constrains, (c) load system, (d) top hinge, (e) hydraulic jack, (f) load cell.	84
Figure 36. Test equipment real Side view.....	85
Figure 37. Disposition of the Vertical potentiometers (mm)	87
Figure 38. Disposition of horizontal potentiometers (mm).....	88
Figure 39. Disposition of diagonal potentiometers.....	89
Figure 40. Disposition of strain gauges on CFRP wrapping (mm); side view.....	90
Figure 41. Disposition of strain gauges on CFRP wrapping; cross section view	91
Figure 42. Disposition of strain gauges on CFRP wrapping.	92
Figure 43. Acquisition system.....	92

Figure 44. Load cells. The load cells Lc 14 and 15 measures the axial load applied at the top of the specimen whereas the load cell LC0 measures the horizontal restoring force.	93
Figure 45 Irregular bridge central pier – free oscillations – Force-Displacement cycles (real scale).....	98
Figure 46. Repaired irregular bridge central pier – free oscillations – Force-Displacement cycles (real scale).....	99
Figure 47 Irregular bridge central pier - pseudo-dynamic test Tolmezzo PGA=0.35g Force-Displacement cycles (real scale)	101
Figure 48 Irregular bridge, all piers - pseudo-dynamic test with Tolmezzo PGA=0.35g displacements time history; GD1 central pier (7m), GD2 lateral pier (14m), GD3 lateral pier (21m).	102
Figure 49 Irregular bridge, all piers - pseudo-dynamic test with Tolmezzo PGA=0.35g Relative displacements time history: GD1-GD2 between the piers GD1 and GD2, GD1-GD3 between the piers GD1 and GD3, GD2 between the pier GD2 and the near abutment, GD3 between the pier GD3 and the near abutment.	103
Figure 50 Irregular bridge central pier - pseudo-dynamic test Tolmezzo PGA=0.7g Force-Displacement cycles (real scale)	104
Figure 51 Irregular bridge, all piers - pseudo-dynamic test with Tolmezzo PGA=0.7g displacements time history; GD1 central pier (7m), GD2 lateral pier (14m), GD3 lateral pier (21m).	106
Figure 52 Irregular bridge, all piers - pseudo-dynamic test with Tolmezzo PGA=0.7g Relative displacements time history: GD1-GD2 between the piers GD1 and GD2, GD1-GD3 between the piers GD1 and GD3, GD2 between the pier GD2 and the near abutment, GD3 between the pier GD3 and the near abutment.	106
Figure 53 Repaired Irregular bridge central pier – first pseudo-dynamic test Tolmezzo PGA=0.35g Force-Displacement cycles (real scale).....	108
Figure 54 Repaired Irregular bridge central pier – second pseudo-dynamic test Tolmezzo PGA=0.35g Force-Displacement cycles (real scale)	109
Figure 55 Repaired irregular bridge, all piers – second pseudo-dynamic test with Tolmezzo PGA=0.35g displacements time history; GD1 central pier (7m), GD2 lateral pier (14m), GD3 lateral pier (21m)	110
Figure 56 Repaired irregular bridge, all piers – second pseudo-dynamic test with Tolmezzo PGA=0.35g. Relative displacements time history: GD1-GD2 between the piers GD1 and GD2, GD1-GD3 between the piers	

GD1 and GD3, GD2 between the pier GD2 and the near abutment, GD3 between the pier GD3 and the near abutment.....	111
Figure 57 Repaired irregular bridge central pier - pseudo-dynamic test Tolmezzo PGA=0.7g Force-Displacement cycles (real scale).....	112
Figure 58 Repaired irregular bridge, all piers – second pseudo-dynamic test with Tolmezzo PGA=0.7g displacements time history; GD1 central pier (7m), GD2 lateral pier (14m), GD3 lateral pier (21m).	113
Figure 59 Repaired irregular bridge, all piers – second pseudo-dynamic test with Tolmezzo PGA=0.7g. Relative displacements time history: GD1-GD2 between the piers GD1 and GD2, GD1-GD3 between the piers GD1 and GD3, GD2 between the pier GD2 and the near abutment, GD3 between the pier GD3 and the near abutment.....	114
Figure 60 Cyclic test on specimen 7; force-displacement cycles (specimen scale)	116
Figure 61 Damages of the specimen 7 at the end of cyclic test.....	119
Figure 62 Cyclic test on specimen 8; force-displacement cycles (specimen scale)	120
Figure 63 Damages of the specimen 8 during the loading sequence.	123
Figure 64 Specimen 8, Moment-Curvature cycles (base section).	124
Figure 65 Specimen 8, Moment-Curvature cycles (section 1).	125
Figure 66 Specimen 8, Moment-Curvature cycles (section 2).	125
Figure 67 Moment-Curvatures cycles – Section for which the moment-curvature relationships are calculated.	126
Figure 68 Repaired and retrofitted Pier (7m), evaluation of the displacement due to shear and flexure during cyclic test. Total: test response (real scale), Shear: displacement contribution due to shear....	127
Figure 69 Jacket Strain (level 1); strain gauges (Str) 1-3-5-7, cyclic test [mEpsilon].	128
Figure 70 Jacket Strain (level 1); strain gauges (Str) 2-4-6-8, cyclic test [mEpsilon].	129
Figure 71 Jacket Strain (level 2); strain gauges (Str) 9-11-13-15, cyclic test [mEpsilon].	130
Figure 72 Jacket Strain (level 2); strain gauges (Str) 10-12-14-16, cyclic test [mEpsilon].	130
Figure 73 Repaired Italian irregular bridge and irregular Italian bridge – first pseudo-dynamic test with Tolmezzo PGA=0.35g. Comparison between the response of the repaired specimen 8 including the initial horizontal load (REPAIRED PIER_tr) and the as-build Italian pier	

II71BN2 if the initial displacements are imposed in the direction D1(II71BN2_D1). (real scale).....	132
Figure 74 Repaired Italian irregular bridge and irregular Italian bridge – second pseudo-dynamic test with Tolmezzo PGA=0.35g. Comparison between the response of the repaired specimen 8 without the initial horizontal load(REPAIRED PIER_tr) and the as-build Italian pier II71BN2 if the initial displacements are imposed in the direction D1(II71BN2_D1). (real scale).....	133
Figure 75 Italian irregular bridge, all piers –pseudo-dynamic test with Tolmezzo PGA=0.35g displacements time history; GD1 central pier (7m), GD2 lateral pier (14m), GD3 lateral pier (21m).....	134
Figure 76 Italian irregular bridge–pseudo-dynamic test with Tolmezzo PGA=0.35g Comparison between the displacement time history of the repaired central pier and the as build Italian central pier. pseudodynamic test (Tolmezzo).....	135
Figure 77 Piers cross section: (a) repaired squat pier, (b) as-build tall pier	151
Figure 78 Opensees fiber model. The pier is divided into two nonlinear beamcolumnelement: one element (elem 4) represent the as-build portion of the pier and a second element (elem 2) the repaired one. The zerolenght element (elem.1) at the base models the strain penetration. The displacement history and the vertical load ia applied ath the top node the node 4. The node 1 is fixed at the ground.	152
Figure 79 Comparison between the Force-displacement cycles of tall pier (14m) of the regular bridge and the OpenSees model response during the pseudodynamic test.	154
Figure 80 EC8 regular bridge lateral piers – pseudodynamic test with Kobe Displacements history. This displacements History is applied on the Top of the Opensees Model.....	155
Figure 81 Confined (core) and unconfined concrete (cover) of the cross section of the as-build tall pier.-cyclic behavior of the model during the analysis (Displacements history applied at the top of the specimen during the pseudodynamic test (Kobe accelerogram).....	155
Figure 82 Steel fiber of the cross section of the as-build tall pier.-cyclic behavior of the model during the analysis (Displacements history applied at the top of the specimen during the pseudodynamic test (Kobe accelerogram)	156

Figure 83 Hosotani and Kawashima (1998) - SCC confined by CFRP discontinuous wrapping - (cover).	157
Figure 84 Hosotani and Kawashima (1998) - SCC confined by CFRP discontinuous wrapping and steel stirrups- (external part of the concrete core).....	157
Figure 85 Hosotani and Kawashima (1998) - concrete confined by CFRP discontinuous wrapping and steel stirrups- (repaired concrete core)....	158
Figure 86 Comparison between the monotonic displacement responses of the OpenSees fiber model of the retrofitted squat pier and the pseudodynamic and cyclic response of the specimen.(scale of the specimen).....	158
Figure 87 Repaired Italian irregular bridge and irregular Italian bridge – first pseudo-dynamic test with Tolmezzo PGA=0.35g. Comparison between the response of the repaired specimen 8 including the initial horizontal load(REPAIRED PIER_tr) and the as-built Italian pier II71BN2 if the initial displacements are imposed in the direction D2(II71BN2_D2).....	177
Figure 88 Repaired Italian irregular bridge and irregular Italian bridge – first pseudo-dynamic test with Tolmezzo PGA=0.35g. Comparison between the response of the repaired specimen 8 including the initial horizontal load(REPAIRED PIER_tr) and the as-built Italian pier II71BN1 if the initial displacements are imposed in the direction D1(II71BN1_D1).....	178
Figure 89 Repaired Italian irregular bridge and irregular Italian bridge – first pseudo-dynamic test with Tolmezzo PGA=0.35g. Comparison between the response of the repaired specimen 8 including the initial horizontal load(REPAIRED PIER_tr) and the as-built Italian pier II71BN1 if the initial displacements are imposed in the direction D2(II71BN1_D2).....	179
Figure 90 Repaired Italian irregular bridge and irregular Italian bridge – second pseudo-dynamic test with Tolmezzo PGA=0.35g. Comparison between the response of the repaired specimen 8 without the initial horizontal load(REPAIRED PIER_tr) and the as-built Italian pier II71BN2 if the initial displacements are imposed in the direction D2(II71BN2_D2).....	180
Figure 91 Repaired Italian irregular bridge and irregular Italian bridge – second pseudo-dynamic test with Tolmezzo PGA=0.35g. Comparison between the response of the repaired specimen 8 without the initial	

horizontal load(REPAIRED PIER_tr) and the as-build Italian pier II71BN1 if the initial displacements are imposed in the direction D1(II71BN1_D1).....	181
Figure 92 Repaired Italian irregular bridge and irregular Italian bridge – second pseudo-dynamic test with Tolmezzo PGA=0.35g. Comparison between the response of the repaired specimen 8 without the initial horizontal load(REPAIRED PIER_tr) and the as-build Italian pier II71BN1 if the initial displacements are imposed in the direction D2(II71BN1_D2).....	182
Figure 93 Pseudodynamic test software –USER INTERFACE.....	183
Figure 94 Pseudodynamic test software –Block diagram-.....	184

List of tables

Table 1 Experimental program	9
Table 2 Pier specimens characteristics (D =diameter [mm], H =height [mm], C =cover [mm]) and design criteria. Original spiral is the design spiral whereas the Actual spiral is the detected or the new transversal reinforcements (repaired piers).....	11
Table 3:Material mechanical properties of the as build specimen; f_{cm} mean value of the concrete strength, \emptyset longitudinal bar diameter, f_{sy} steel yield stress, f_{st} steel maximum stress, ϵ_{su} steel ultimate strain, ϵ_{sh} steel strain at hardening initiation	12
Table 8.3.1. Mechanical properties of stainless steel bars	26
Table 2 SCC standard cubic strength- Mean value and Standard deviation	35
Table 3 Testing fresh self compacting concrete: D_m = the largest diameter of the flow spread, T_{50} = the period between the moment the cone leaves the base plate and SCC first touches the circle of diameter 500 mm, T_e = the V-funnel flowtime, T_{e5} = the V-funnel flowtime after 5 minutes.....	36
Table 4 Shear resistance of plastic hinges and Shear resistance outside of plastic hinges of the as-build Italian squat piers.....	42
Table 5 The CFRP contribution to the shear capacity in plastic hinges and outside of plastic hinges	45
Table 6 CFRP Discontinuous wrapping for Italian tall pier. Design procedure	51
Table 7 Discontinuous CFRP wrapping of the tall piers. Design parameters	51
Table 8 Shear resistances of the specimen; outside plastic hinge (o.p.h.) and in plastic hinge (p.h).....	52
Table 9 Integration procedure.....	66

1. Introduction

Strengthening and rehabilitation of existing reinforced concrete (r.c.) bridge can lead to considerable savings by eliminating or reducing the need to take a structure out of service while it is repaired and/or retrofitted.

Therefore, it can be interesting to study the efficacy of quick repair and retrofit techniques able to assure sufficient protection or to enhance seismic performance of concrete dissipative elements damaged under a severe earthquake

Considering that, a bridge pier if it is used as dissipative element, may be significantly damaged in plastic hinge zone, the only alternative to repair is its replacement, which is typically the most expensive solution. In addition, the rebuilding alternative involves the closure of traffic lanes and a lengthy disruption of traffic.

Clearly, a repair and/or a retrofit option should be considered to ensure a quick problem resolution.

This study attempts to propose a usability procedure to fast repair of piers, which provides: improvement of strength of damaged concrete core, that is comparable with that of original concrete core, the effectiveness of strengthening concrete columns by placing concrete jackets, corrosion protection by using inox rebars in critical zone, fast and economic seismic retrofitting by means of CFRP wrapping.

This system can be as alternatives to traditional materials and techniques (externally bonded steel plates, steel or concrete jackets).

In the practical problems described above, difficulties may be encountered. This paper discusses a number of practical problems in repairing structures as well as their solutions. Further innovative construction materials that have potential for use in seismic rehabilitation of existing structures, more and more used by architects and engineers to build new structures, will be proposed.

It is important to note that these materials allow overcoming many of the difficulties that have previously limited similar solutions.

However it is necessary to undertake an experimental validation of the presented repair techniques. To provide an experimental validation for repair techniques of damaged piers elastic, pseudo-dynamic and cyclic tests were performed at the Laboratory of experiments on materials and structures of the University of Roma Tre.

In previous research (De Sortis & Nuti 1996)[52] some columns were tested until collapse by pseudo-dynamic tests but others are still entire.

The column specimens are representative of tall and squat circular r.c. piers designed according to Eurocode8 (1998-2) [57] and Italian Code (D.M. LL.PP. 24.01.86)[54].

An accurate study to detect the level of degradation in materials, as the case of real structures after an earthquake, is now performed. Then, based on the evaluation done, EC8 columns are repaired and the Italian ones retrofitted by mean of FRP jacket, longitudinal stainless steel and self compacting concrete. Actual tests pseudodynamic and cyclic aim to evaluate the effectiveness of this technique. Repairing and retrofitting operations, test equipment and planned tests are presented.

In the thesis the pseudodynamic apparatus as well as the relative computer software has been developed and set up. Experimental seismic responses of two bridges are obtained. A representative pier scaled 1:6 is physically tested in the lab while the rest of the structure is simulated numerically.

The tests carried out are of pseudodynamic type as well as cyclic. To this end the description of the retrofitting of the piers as well as the description of test equipment is given and finally a comparison between the seismic behaviour of the original and the retrofitted piers are shown in terms of seismic response and final structural damage.

2. Research objectives

The primary objective of the research effort presented here, was to analytically and experimentally investigate the effectiveness of using epoxy adhesive, self compacting concrete (SCC), stainless steel rebar and CFRP discontinuous wrapping to repair and retrofit severe damaged vertical elements. In particular it is interesting to focus the attention on reinforced concrete circular bridge piers.

The proposed research project consists of three major tasks: (1) repair and retrofit of damaged piers, (2) experimental work, (3) comparison with previous tests, (4) analytical phase.

The primary objective of the test program was to determine the ultimate flexural, shear, deformation and energy dissipation capacity of the repaired and or retrofitted specimens.

The experimental program consists of scale (1:6) pier models with circular cross-section. The specimens are divided into 2 groups, tall and squat piers, of 2 piers each.

The pseudo dynamic testing was used to evaluate the seismic performance of repaired and/or retrofitted regular and irregular bridges.

In addition, the proposed work aims at providing an assessment of the adequacy and the calibration of the existing analytical tools in OPENSEES to predict the seismic response of specimens.

3. Development of experimental methods

In the recent years, several real-time hybrid test methods have been presented to study the seismic behavior of structures and soil-structure systems.

These test methods are experimental techniques which use feedback signals from a specimen of a key component of the structure in a numerical analysis of the surrounding structure interact in real-time to solve the equations of motion step by step.

The on-line computer controlled test concept first proposed by Hakuno et al. (1969) [[4] and Takanashi et al. (1974)

[21] are at the basis of these methods.

The pseudo-dynamic test method was developed under the US-Japan Cooperative Earthquake Programme in the early 1980s (Mahin and Shing, 1985; Takanashi and Nakashima, 1987). The pseudo-dynamic technique was first proposed in Japan about 25 years ago by Takanashi et al but the success of this technique is attributed to the researches of several authors (Shing and Mahin 1983, Nakashima and Kato 1987 [11], Shing et al. 1991 [18]).

In fact thanks to these studies, it was possible to understand better the influence of experimental errors on the test results and some effective methods are proposed to mitigate the effect of these errors. This test runs

on an timescale of the order of 100 times the actual timescale (Mahin et al., 1989).

It is important to remind the developed of the substructure test method by Dermitzakis and Mahin (1985) [3] and later improved by a several researchers (Nakashima et al. 1990 [[12], Shing et al. 1994 [[20], Pinto et al. 2004). This method consist to test only the element of a structure for which it is not possible to predict analytically the seismic behavior while the rest of the structure is modeled in a computer.

Nakashima et al. (1990) and Combescure and Pegon (1997) proposed the operator splitting method, which combines the positive attributes of both implicit and explicit integration schemes.

Finally it is necessary to remind the real-time pseudo-dynamic testing, first successfully conducted by Nakashima et al. (1992) [[13] that by-pass the rate-of-loading problem. In this test actuators were kept in continuous motion and the equations of motion are solved using a staggered solution approach. The same author (Nakashima et al. 1999 [14]) extends this method at a real-time test method that uses extrapolation and interpolation to calculate displacement to move actuators continuously at high speed.

A high-speed continuous substructure test method is proposed by Magonette et al. (1998) [[8] in which the equations of motion for the tested substructure are solved with an explicit scheme, whereas those for the analytical substructure using an implicit method.

Subsequently, Reinhorn et al. (2004) [[16] used a hybrid test technique. The proposed method combines shake table excitation with dynamic actuators and it is used to test soil-structure interaction.

Recently, Shing et al. 2004 [[19] have developed a fast hybrid test system as part of the George E. Brown, Jr. Network for Earthquake Engineering Simulation (NEES) Program sponsored by the US National Science Foundation. This system has a general structural analysis framework to simulate the nonlinear behavior of the analytical substructure using unconditionally stable implicit time integration scheme.

The implicit time-stepping algorithms recently used to test stiff multiple-degree-of-freedom structures and substructures are all adaptations of the α -method proposed by Hilber et al.

The development of the implicit scheme began thanks to Thewalt and Mahin. The authors proposed the first successful implicit scheme for testing inelastic multiple-degree-of-freedom structures based on a hybrid digital-analog, which is based on the α -method developed by Hilber et al.

An alternative solution was proposed by Nakashima et al. for testing structural subassemblies, which have high-frequency components introduced by the interface degrees of freedom. This procedure uses an unconditionally stable algorithm, the Operator-Splitting algorithm, based on a technique proposed by Hughes et al and using a predictor-corrector approach it does not require any numerical iteration (recently Tsai et al [6] has used this method).

Shing et al for testing general multiple-degree-of-freedom structures has developed another integration scheme. This is an implicit algorithm based on the α -method of Hilbert et al, which uses a modified Newton-type iterative procedure.

Then the procedure is modified introducing an adaptive time-stepping procedure in order to test structural models which may exhibit severe strain softening.

Numerical integration schemes can be classified into implicit and explicit types.

Most explicit schemes are conditionally stable while the implicit scheme can be unconditionally stable but require a Newton-type iterative method when the structure exhibits a nonlinear behavior.

Explicit schemes compute the displacement increment directly from the results of the previous time step but are conditionally stable and require the use of a short time step. To assure the stability it has to be respected that $\pi/\min T \leq \Delta$, where T_{\min} is the shortest period of the structure. These methods are used when the tested structures have a high mass to stiffness ratio and few degrees of freedom.

Implicit methods require the values of the acceleration at the end of the current time step, which can only be achieved using a iterative procedure. These methods are used when the test structure is stiffer and/or more complex. In fact in this case it is necessary an unconditionally stable integration scheme. Therefore, implicit integration algorithms perform numerical dissipation using approaches such as the α -shifted Newmark scheme (Hilber et al. 1977).

On the basis of the above considerations, explicit schemes were used for pseudo-dynamic tests in years [22][10] and for real-time pseudo-dynamic tests [14],[5],[29],[30].

It is possible to find unconditionally stable numerical schemes which do not require an iterative correction. The OS method by Nakashima et al.

[24], the “explicit” scheme by Chang [31], and the predictor-correct method by Bonelli and Bursi [32] are some examples.

In particular the extended OS method is applied to the real-time testing of nonlinear viscous fluid dampers by Wu et al. [33]. This method uses an explicit prediction-implicit correction approach. The displacements are computed with explicit prediction and then are imposed on the specimen. However if the structural response is highly nonlinear, the accuracy of this method is inferior to implicit methods with Newton-type iteration [33], [34].

The explicit scheme of Chang [31] is based on an explicit prediction using the initial elastic stiffness of a structure.

Note that the comparison of the accuracy of this method with that of the OS method is not investigated schemes when it is used to evaluate the nonlinear response of a structure.

Finally the above real-time pseudodynamic test system developed for the Fast Hybrid Test (FHT) facility at the University of Colorado, Boulder uses an unconditionally stable implicit time-integration method for real-time tests. This method uses a nonlinear solution strategy and combines a Newton-type iterative method with subincrementation [37].

Bayer et al. [1] has proposed a similar approach to test substructure testing in which the experimental substructure is subjected to truly dynamic shaking

Among the recent applications of this algorithm it is important remind the pseudodynamic testing of a stiff full-scale, multiple-storey, masonry structure* and a subassembly of a steel braced frame.

The study of the experimental errors is a key element of the pseudo-dynamic test method. The error-propagation characteristics of the hybrid method proposed by Thewalt and Mahin' have been studied by Peek and, Shing and Vannan.

In this brief summary it is possible remind that Nakashima and Kato, Comberscure and Pegon have studied the error-propagation characteristic of the Operator-Splitting scheme whereas the error-propagation characteristics of the iterative scheme of Shing et al have been thoroughly investigated by Shing et al and Comberscure and Pegon. Then different error-compensation techniques^{3*} ' * 0%\$-'' have been developed.

However, it is interesting the error-compensation technique proposed by Nakashima and Kato which relies on the predictor stiffness of a structure and the difference between the commanded and measured displacements.

Finally Nakashima et al. have considered that experimental error growth can be controlled by the dissipative properties of the integration scheme (α -method) whereas Shing et al use a correction procedure for residual errors that can eliminate effectively the spurious higher-mode response of a structure.

The most important experimental methods to evaluate the seismic response of the structures are: Pseudo-dynamic test, real time test methods, shaking tables tests.

The Pseudo-dynamic testing is a hybrid method which computes the structural displacements due to the input excitation (i.e. earthquake) using an integration procedure step by step and imposes these displacements quasi-statically to the test specimen.

In this procedure the restoring forces of the specimen are measured and fed-back to the analytical model as part of the input for the next calculation step. The timescale of the test is in the order of about 100 times the actual timescale.

The real time test methods are used to include the rate-dependent effects of the dissipative devices (i.e. dampers, rubber bearings) and the loading rate is increased above that of a normal Pseudo-dynamic test and the hold period eliminated (Takanashi and Nakashima, 1987; Magonette, 2001). There are two possible approaches: a real-time substructure testing is practically a fast version of the substructure approach to PsD testing, and effective force testing in which, the actuators operate under forces control in order to apply the seismic forces in real-time.

Shaking tables are tests in which a specimen of a structure is placed on a stiff platform. This platform is shaken to apply the base motion and to generate the inertia forces on the structure.

It is possible to reproduce the desired motion by means of high-quality equipment and sophisticated control engineering.

4. Experimental program

An experimental research program is realized to evaluate the effectiveness of repairing and retrofitting of existing reinforced concrete vertical elements.

In order to verify the seismic behavior of repaired and retrofitted piers, preliminary free oscillation, pseudo dynamic and quasi-static cyclic tests, are carried out.

The experimental program consisted of three parts:

- the preliminary elastic test (free oscillations)
- two pseudo-dynamic tests, one using a selected accelerogram used in previous test [52] and the second with the same accelerogram scaled to 2, which are intended to examine the seismic response of a bridge and to induce damage that can underline the seismic capacity of the elements,
- cycling test to evaluate the ultimate resistance, ductility and energy dissipation of the element. During all test is applied the same constant axial compressive load.

The program consisted of 4 specimens, two tall and two squat piers tested under quasi-static loading conditions. Loads, deformations, and fiber strains are measured. Stiffness, strength and ductility of specimens are determined.

Two groups of experimental testing are conducted on a total number of four specimens.

In the first group, two squat piers are tested under quasi-static lateral load, In particular pseudo-dynamic and cyclic tests are performed with a constant axial compressive load. In the second group, two tall piers will be tested to examine the performance of a flexural reinforcing bridge pier under earthquake excitations.

In addition the squat specimens 7 previously damaged, is used to verify equipment setup and for calibration of pseudo-dynamic program.

Applied displacements simulate that might occur on the piers from a seismic excitation.

Today two specimens were instrumented and tested in the experimental program (specimen 7 and 8)

n	tests	objectives
1	preliminary free oscillation	retrofitting Validation measured strain in fiber ultimate capacity
3	pseudo dynamic (Kobe)	
	pseudo dynamic (Kobe scaled to 2) quasi-static cyclic	
6	preliminary free oscillation	repair and Retrofitting Validation measured strain in fiber ultimate capacity
8	pseudo dynamic (Tolmezzo)	
7	pseudo dynamic (Tolmezzo scaled to 2)	test equipment validation damaged piers seismic behavior ultimate capacity
	quasi-static cyclic	

Table 1 Experimental program

5. Concrete bridge structures

The prototype structures are two existing reinforced concrete highway bridges constructed in Italia in '70.

Two bridges (one regular and one irregular) have been designed both accordingly to Eurocode 8 Part 1 [56] and Eurocode 8 Part 2 [57] for the design of bridges in seismic areas and Eurocode 2 [8] for the general rules on concrete structures and Italian Seismic Code D.M. LL.PP. 24.01.86 Figure 1 shows both regular and irregular bridges geometry.

The bridge configurations which were investigated, ranged from regular symmetric to irregular asymmetric which are identified based on the distribution of the piers.

A regular bridge configuration presents piers of equal height (14m) on sides and the middle pier (21m) that is greater than that of the side piers.

In an irregular configuration, the bridge piers are of unequal height with the shortest pier 7m in the middle and two piers with different height (14m and 21m) on sides.

The bridges have a continuous box girder hinged on the circular section piers and on the abutments. It consists of four bridge spans with an equal span length of 50m.

0.35g peak ground acceleration is assumed for the elastic response spectrum together with a behavior factor of 3 for horizontal and 1 for vertical component of the input motion.

Pier concrete strength is fixed at 25 N/mm², steel yielding stress at 500 N/mm². Deck self weight and dead load was 200 KN/m.

Elastic stiffness of the deck is calculated on the basis of the gross section; the piers stiffness instead based on the cracked section (50% that of the gross section)

In fact before the severe earthquake, the bridge piers already had some structural cracks that could be due to a previous moderate earthquake, shrinkage of reinforced concrete and temperature fluctuations

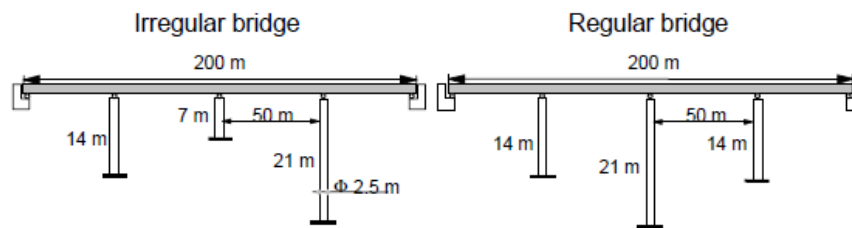


Figure 1 Layout of the bridge configuration, the central pier of the irregular bridge and the lateral one of the regular bridges, the ones experimentally tested.

5.1. Design and construction of original concrete pier specimens

Geometry and reinforcement configurations of pier specimens together with relative design criteria are summarized in Table 2.

Because the specimens do not show the mark used to identify them (did not write directly on a specimen), it is directly not possible to associate the experimental data recorded with specimens.

However, an inspection of a specimen using a concrete cover meter or pachometer can nondestructively reveal the depth of the concrete cover above the steel reinforcement, the location of the reinforcement and also its diameters. Sometimes it is necessary to remove concrete cover to reveal reinforcement.

In this way it has been possible to detect the design procedure for tall and squat pier specimens.

pier	#	design	D	H	C	bars	Original spiral	Actual Spiral
tall	1	DM	420	2340	30	24 \varnothing 10	\varnothing 6/100	\varnothing 5/80
	2	DM	420	2340	30	24 \varnothing 10	\varnothing 6/100	\varnothing 5/100
	3	DM	420	2340	30	24 \varnothing 10	\varnothing 6/100	\varnothing 5/100
	4	DM	420	2340	30	24 \varnothing 10	\varnothing 6/100	\varnothing 5/80
	5	EC8	420	2340	30	24 \varnothing 10	\varnothing 5/30-60-100*	\varnothing 6/40
squat	6	DM	420	1170	39	12 \varnothing 12	\varnothing 6/120	\varnothing 5/114
	7	DM	420	1170	30	12 \varnothing 12	\varnothing 6/120	\varnothing 6/120
	8	DM	420	1170	45	12 \varnothing 12	\varnothing 6/120	\varnothing 5/114

Table 2 Pier specimens characteristics (D =diameter [mm], H =height [mm], C =cover [mm]) and design criteria. Original spiral is the design spiral whereas the Actual spiral is the detected or the new transversal reinforcements (repaired piers).

Longitudinal and transverse reinforcement configurations and concrete cover thickness have some differences with respect to design drawings as sometimes it happens in practice. Concrete with $R_{ck}=25$ MPa and FeB44k steel were fixed in design. Tested concrete strength was about the same of the design one whilst steel yielding varied from 550 MPa to 600 MPa, therefore exceeding the design one.

	concrete		steel			
	f_{cm} [MPa]	\varnothing [mm]	f_{sy} [MPa]	f_{st} [MPa]	ϵ_{su} [%]	ϵ_{sh} [%]
1, 2, 3, 4	17,209	5; 6*	445,46	680,40	16	1,40
		10	513,69	608,04	15,68	2,67
5	17,347	6	444,19	680,82	21,81	1,4
		10	537,61	618,01	16,70	4,00
6, 8, 7	17,440	6	445,46	680,40	16	1,40
		12	574,37	666,24	12,76	2,25

Table 3: Material mechanical properties of the as build specimen; f_{cm} mean value of the concrete strength, \varnothing longitudinal bar diameter, f_{sy} steel yield stress, f_{st} steel maximum stress, ϵ_{su} steel ultimate strain, ϵ_{sh} steel strain at hardening initiation

6. Previous pseudo-dynamic tests

In a previous research program, eleven specimens were constructed and tested [52]. Testing apparatus was set up in house and software for instrumentation control and numerical integration was purposely developed.

In this study the use of alternative scaling criteria for large structures such as RC bridge piers is investigated. Similitude criteria between model and prototype are developed with respect to global quantities, such as: flexural and shear strength, confinement effect, post-elastic buckling and pullout of rebars.

This approach does not imply the "perfect" geometrical scaling of aggregate granulometry, reinforcing bar diameters and deformed bar shape and spacing, allowing the use of ordinary concrete mixing and commercial reinforcing bar.

An improved anchorage detail of the longitudinal bars to improve the bond-slip scaling accuracy has also been investigated.

The irregular bridge was subjected to the E-W component of the 1976 Italian Tolmezzo earthquake (PGA= 0.35g), the regular one to the N-S component of the accelerogram recorded at Kayou Weather Bureau during the 1995 Kobe earthquake (PGA = 0.82g).

Subsequently, new pseudo-dynamic tests were performed and the specimens were subjected to bigger earthquakes. The second excitation used in the tests, is derived by scaling to double the previous accelerograms.

The Bridges designed to EC8.2 have shown a large capability to undergo inelastic deformations with limited damage.

In particular, the behavior of the irregular bridge was very satisfactory: significant flexural and shear deformation occurred in the tested pier, which nonetheless showed enough strength and ductility to resist the stresses imposed by earthquakes.

Comparison between models with and without special anchorage detail showed that the response was highly influenced by pullout scaling, especially in squat piers. Thus, the tests confirmed the importance of an accurate scaling of the longitudinal rebars anchorage in the foundation.

Italian piers have been tested with the same accelerograms and cyclic load history of the Eurocode ones.

The results for the Bridges designed using the 1986 Italian Code have demonstrated acceptable seismic behavior for the regular bridges configuration, similar to the EC8 one, while the irregular one had a different response, showing a higher degradation of the cyclic response, given the large difference in longitudinal reinforcement.

In case of irregular bridge layout the performance of the Italian Bridges has proved to be less satisfactory but still providing sufficient protection.

Furthermore, the results from this study have demonstrated that the shear deformation represents an important contribution to the total displacement and strongly reduces the stiffness of squat piers and then the structural irregularity.

7. Damaged concrete specimens

Prior to flexural testing, the piers were visually surveyed for damage relating to the previous tests.

Piers 2 (tall DM), 4 (tall DM), 5 (tall EC8), 6 (squat DM) and 8 (squat DM) were tested until collapse in previous pseudo-dynamic and cyclic tests thus they are damaged while piers 1 (tall DM), 3 (tall DM) have not been subjected to tests and are intact. Pier7 (squat DM)

Figure2 cover spalling, longitudinal bar buckling and rupture, yielding in transverse reinforcement and concrete core crushing are highlighted.

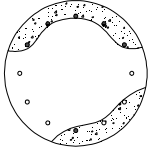




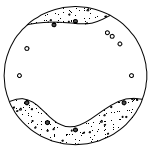




n.	section	front	back
6			
<p>Concrete cover spalling ($h_c=130-350$); Spread shear cracking ($\theta=56^\circ$) Longitudinal bar buckling ($l_b=145$, $\delta=21$) Yielding of hoops</p>			
7			
<p>Wide crack at the base</p>			
8			
<p>Concrete cover spalling ($h_c=200-250$); Spread shear cracking ($\theta=52^\circ$) Longitudinal bar buckling ($l_b=160$, $\delta=22$); Rupture of 1 longitudinal bar Yielding of hoops</p>			

Figure2: Main detected damages (h_c =cover expulsion extent in mm, l_b =buckled bar length in mm, δ =buckled bar deflection in mm, θ =shear crack inclination angle, =damaged concrete, =bar to be replaced).

8. Specimens repair

Foreseen operations on seriously damaged piers 2, 4, 5, 6, 8 are (for example piers 6 and 8 in Figure3): mechanical removal of damaged concrete cover and cleaning of substrate from residue particles (phase1), concrete core repair with resin injections (phase2), substitution of damaged (yielded, buckled or broken) bars using stainless steel ones (phase 3), restoration of damaged concrete cover with self compacting concrete (SCC) (phase 4) and C-FRP strips application (phase 5).

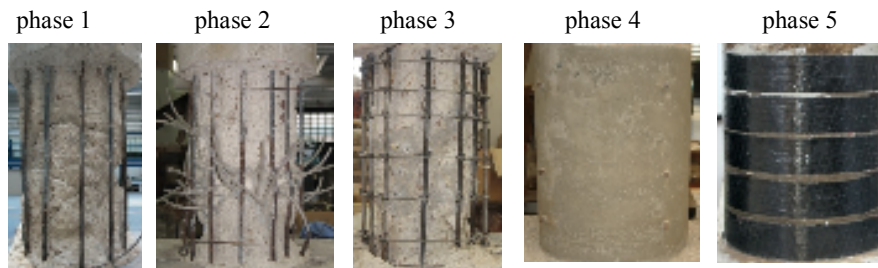


Figure3. Repair and retrofitting of piers

8.1. Damaged concrete removal

Cracked and nearly detached part of concrete cover and core have been completely removed over a height of 550 mm (plastic hinge length plus overlap splice of restored longitudinal bar) from the pier base. About 20 mm of concrete around reinforcing bars have been removed and the latter accurately cleaned in order to guarantee optimal bond with the repairing material. The quality of the interface between the existing concrete and the repairing material is essential for durability and effectiveness of restoration. In particular, lack of surface roughness makes the interface a preferential plane for rupture: mechanical removal followed by cleaning

of substrate from residual particles was used to provide good bond (Figure3:: phase 1).

Figure4 Damaged concrete cover removal (phase 1)

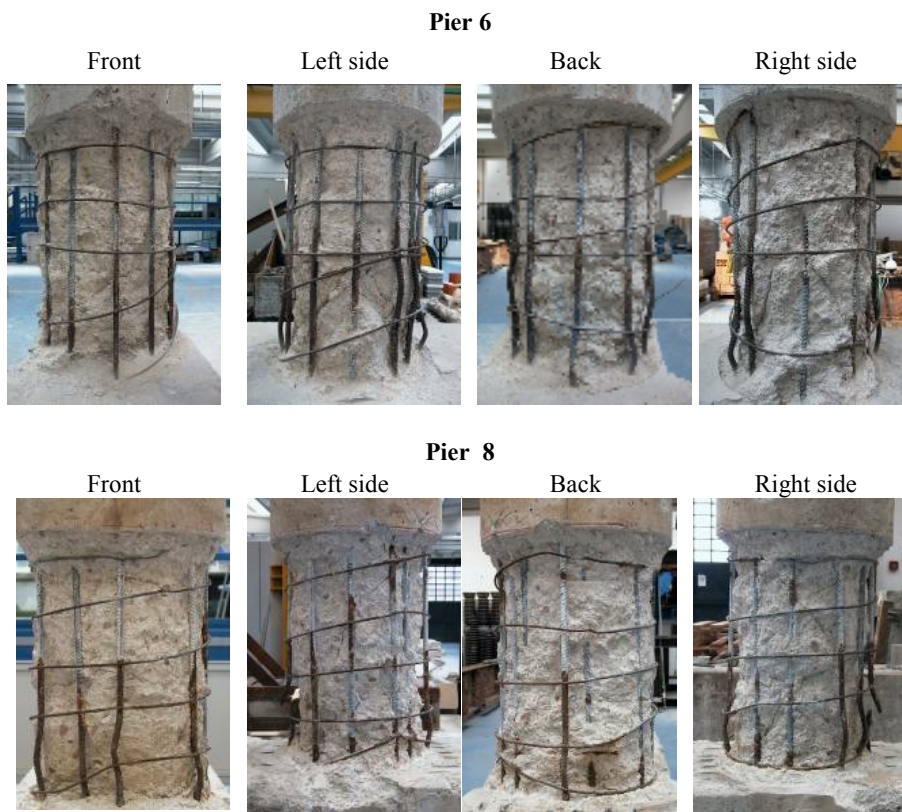
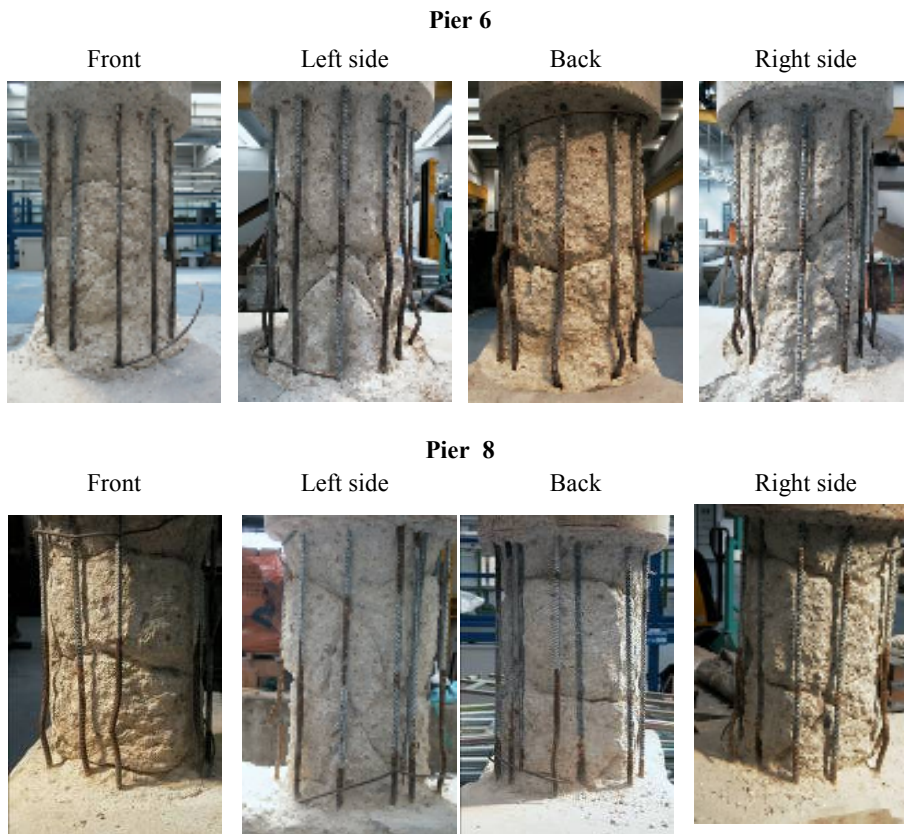


Figure5 Damaged concrete core removal and crack cleaning (phase 1)



8.2. Concrete core consolidation

Injection of concrete core with bicomponent epoxy resin (EPOJET LV with 70 MPa and 20 MPa compressive and flexural strength respectively at 7 days and adhesion to concrete higher than 3.5 MPa) with very low viscosity (140 mPa.s Brookfield viscosity with 1 hour workability time at 20°C) have been used. About 20-40 mm deep perforations have been performed to place small plastic tubes. Cracks were closed by spreading with thixotropic bicomponent epoxy plaster (MAPEWRAP12 with 30 MPa tensile strength after 7 days - ASTM D 638, adhesion to concrete higher than 3 MPa and setting time at 23°C of about 5 hours) in order to obtain a sort of pipe system inside the core ending with the tubes. Ø2-5 mm sand obtained by crushing was fixed on the fresh plaster to make its surface rough. Compressed air was insufflated in order to remove powder and to check the communicability between inner pipes. The injections were performed from the bottom towards the top until inner cracks complete filling (Figure3:: phase 2).

.The resin passes also through the hairline cracks and penetrates deep down into the concrete core. The injection is easy to do and very fast.

Figure6 Concrete core consolidation (phase 2)

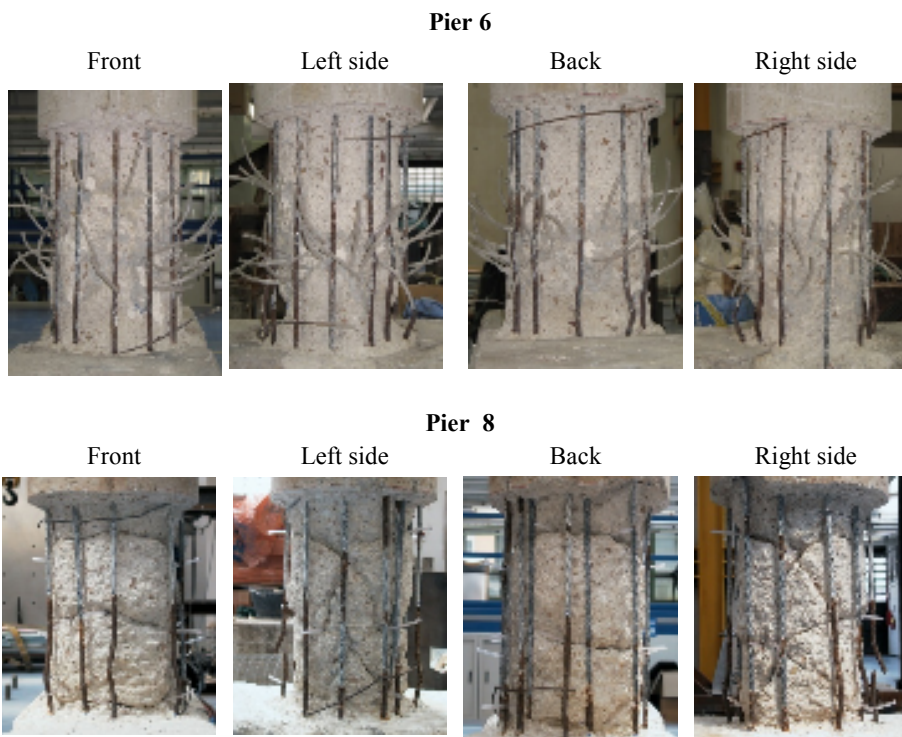
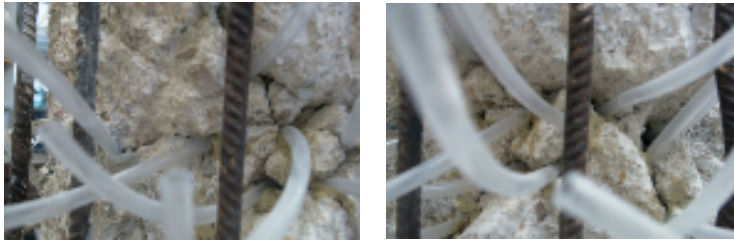


Figure7 Tubes position at Injecting Zones (phase 2)

Pier 6



Pier 8



Pier 8



Figure8 Tubes position (phase 2)

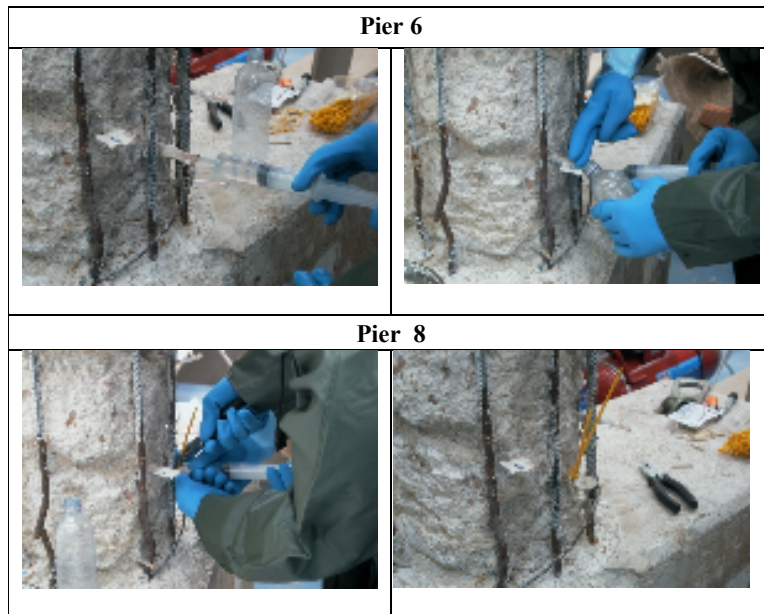


Figure9 Injecting steps (phase 2)

8.3. Reinforcing bar restoration

Austenitic stainless steels combine very good corrosion behavior with excellent mechanical properties (strength and toughness). Although initially more expensive, it offers cost savings in the long term because of reduced maintenance and protection operations and increasing life of the structure. These characteristics make it suitable for restoration of existing damaged reinforcing bars and for seismic retrofitting. Stainless steel (AISI304) $\varnothing 12$ bars were used for damaged reinforcing bar substitution. First, the spiral reinforcement was cut and removed; the ends of embedded hoop were welded to remaining longitudinal bars. Yielded and buckled longitudinal rebars were cut and removed too. Remaining rebars were cleaned, by mean of a metallic brush, to eliminate rust layers and residual concrete, plaster and resin. Single new bars were placed aside the existing ones trying to keep inner lever arm and cover thickness equal to the original ones: it was impossible to apply them in pairs to avoid asymmetries because of the congested reinforcement of the foundation. Welding was performed away from the potential plastic hinge (Figure 10): since the portion of damaged bar often extends into the foundation, it was necessary to dig it (at least 70-80mm deep) around the bar before welding.

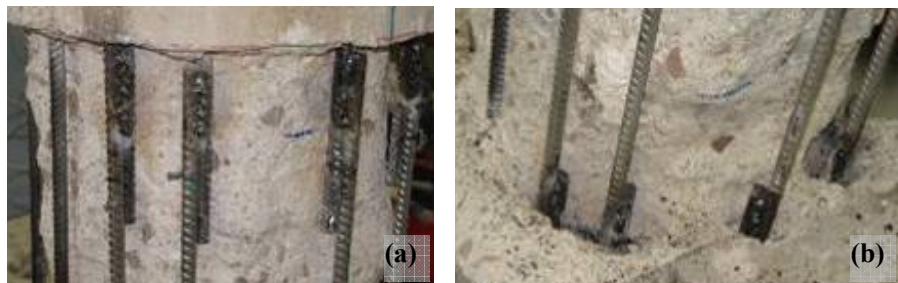


Figure 10 Welded joints (a) top (b) bottom

Welding was the only practicable solution since the congested reinforcement of the foundation did not allow performing holes deep enough and in the right position to guarantee effective bond even using resin. Practical difficulties in welding due to reduced space around the

bars made it necessary to realize two 50 mm weld puddles (the design length of a single puddle was 35 mm only). Removed spiral reinforcement was replaced with circular stainless steel $\varnothing 5$ stirrups; spacing was calculated to assure the original design ratio $f_t A_s/s$ (A_s =hoop cross section, s =spacing, f_t =peak strength). Stirrups were fixed with intercrossed metallic fastenings to avoid welding that could produce dangerous local deformation in bars with such a small diameter. Anyway, 20 mm length welding was necessary to close stirrups (Figure3: phase 3). Stainless steel reinforcing ribbed bars have been tested and their mechanical properties determined both for monotonic and cyclic behavior including post-elastic buckling (Albanesi et al. 2006)[46]. Monotonic tests in tension and compression on $\varnothing 12$ bars (Figure 11) used in restoration have been performed according to the European Code UNI EN 10002-1 (2004)[67]. Table 8.3.1 shows the mechanical properties of stainless steel bars. Fig shows the results of cyclic test on $\varnothing 12$ stainless steel bars ($\lambda=L/\varnothing=5$, 11). The study is in progress and the inox rebars present a behavior similar to the standard steel. The strength and the yield stress are greater than those of the standard steel. It is not observed hardening phenomenon.

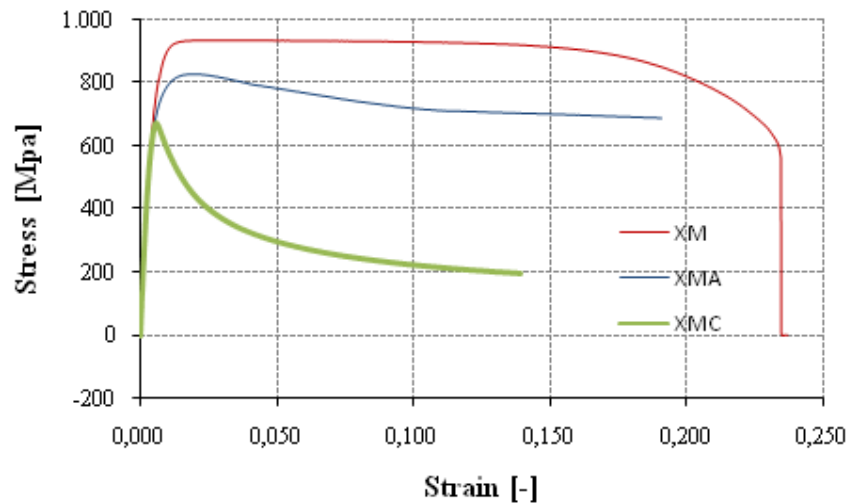


Figure 11 Monotonic tests in tension and compression ($\lambda=L/\varnothing=5$ (XMA), 11(XMC)) for $\varnothing 12$ stainless steel bars.

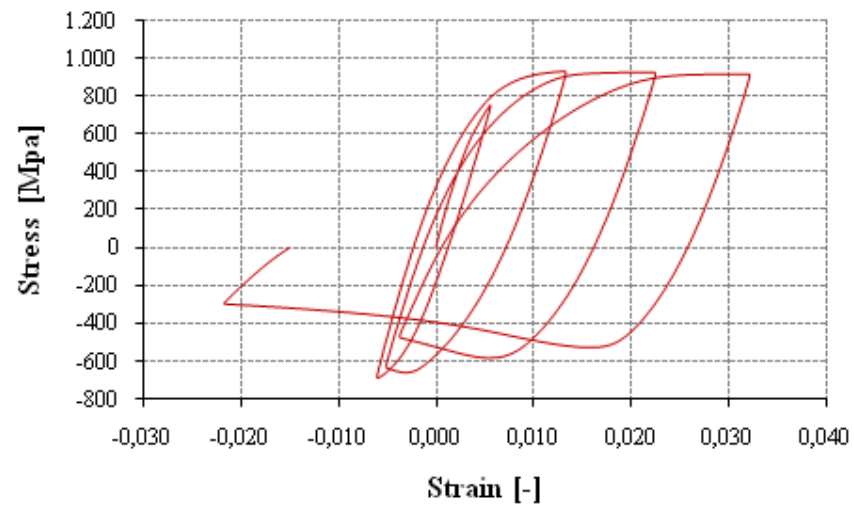
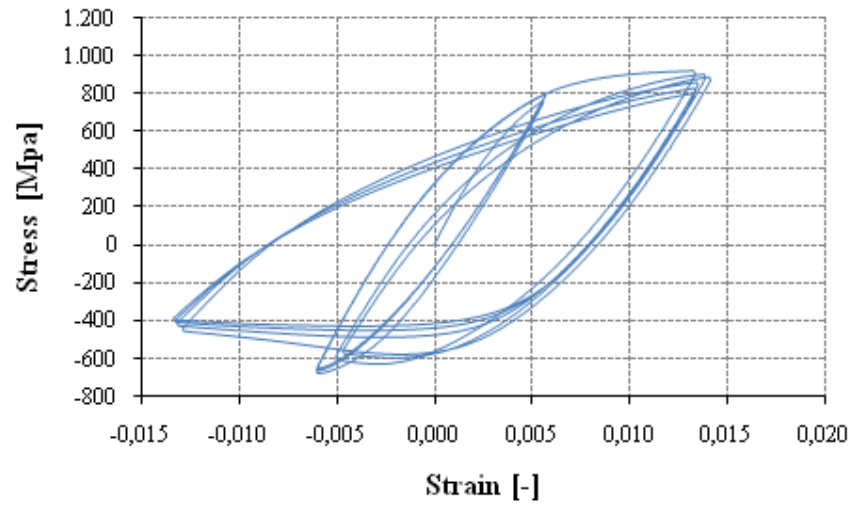


Figure 12 Cyclic tests –Stress strain relationship Ø12 stainless steel bars.

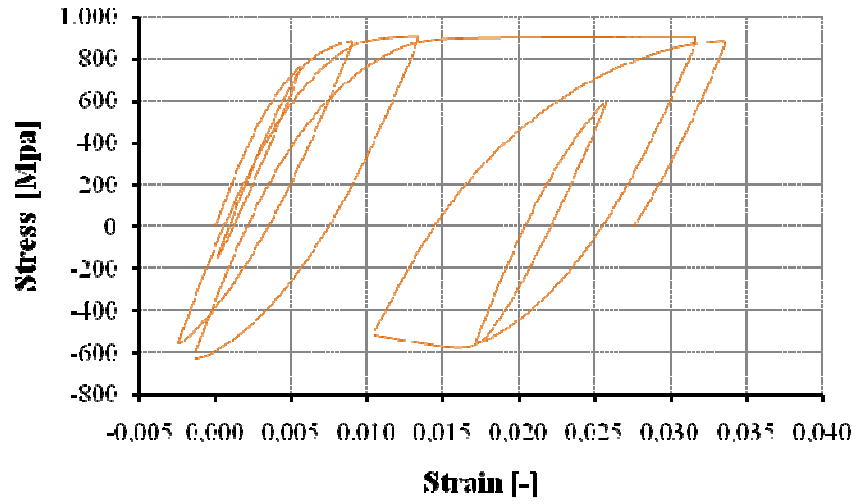


Figure 13 Cyclic tests for Ø12 stainless steel bars.

\varnothing [mm]	f_{sy} [MPa]	f_{sm} [MPa]	f_{sm}/f_{sy} [-]	A_{gt} [%]	A_{su} [%]
5	829,4	927	1,19	5	22,6
12	790	941	1,19	5	22,0

Table 8.3.1. Mechanical properties of stainless steel bars
(mean values of strength and elongation).

Figure14 Reinforcing bar restoration (phase 3)

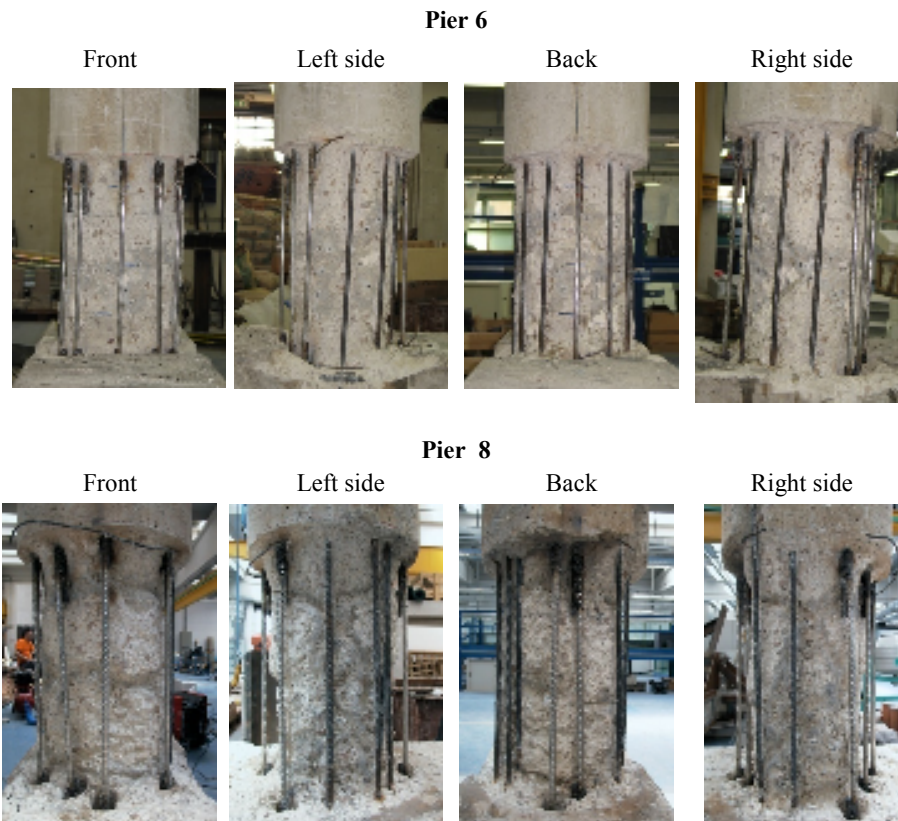




Figure 15 Longitudinal Reinforcing bar restoration (phase 3).(Pier 6)

Figure16 Trasversal Reinforcing bar restoration (phase 3)

Pier 6

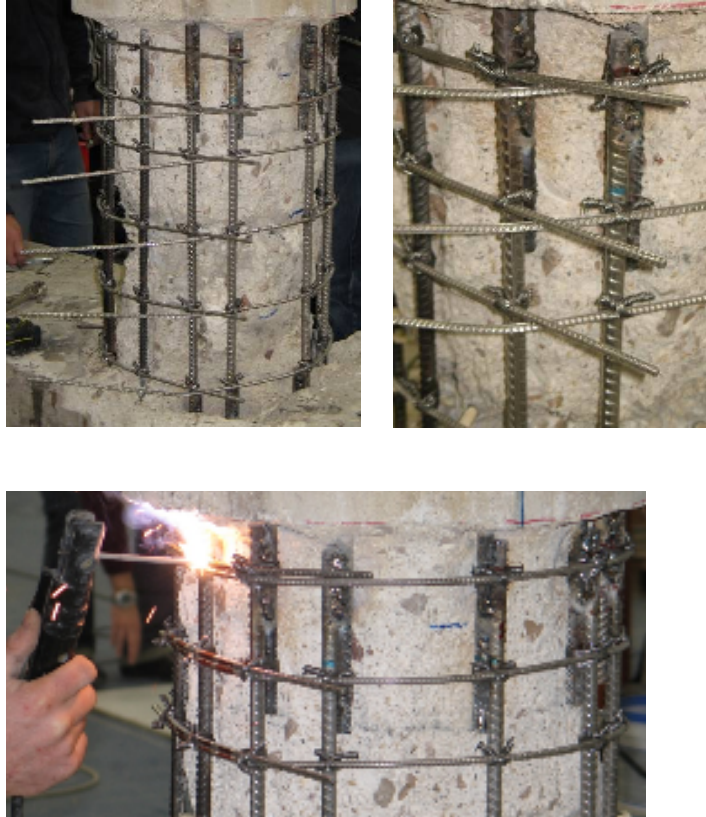
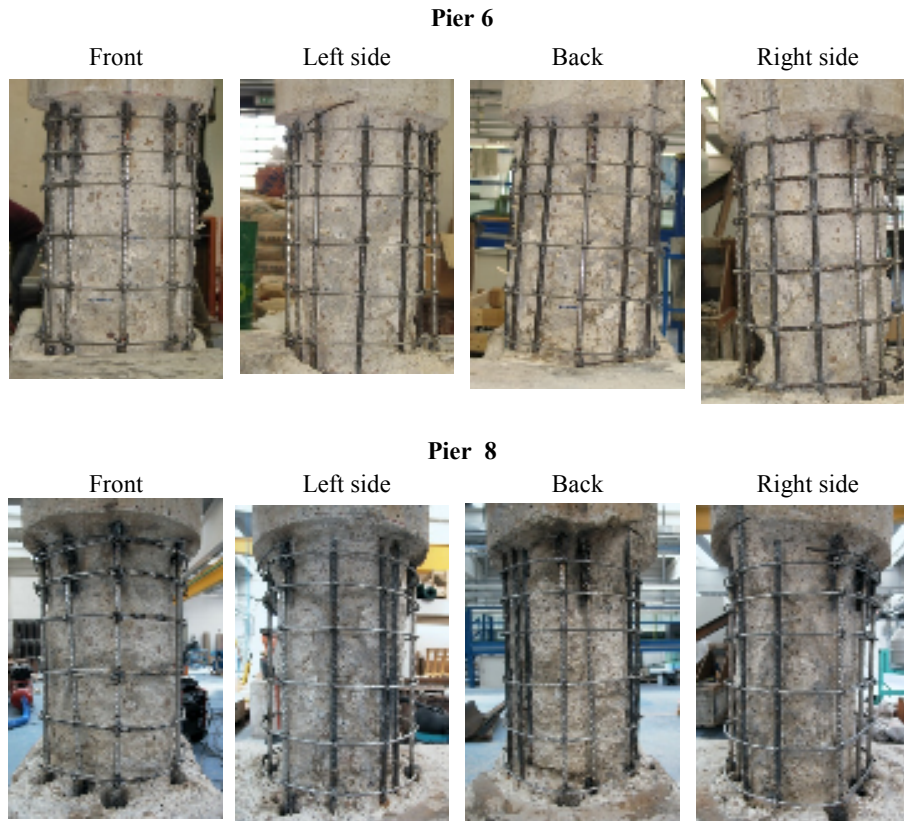


Figure17 Reinforcing bar restoration (phase 3)



8.4. Concrete restoration

Good workability and resistance to segregation and remarkable filling and passing ability make Self Compacting Concrete (SCC) an optimal material to restore damaged concrete parts thus restoring element continuity and homogeneity (crossing thick new and existing reinforcing bars without causing vacuums into the element and discontinuity at

contact surface). A restoring material should also have low shrinkage, high tensile strength and similar elastic modulus to that of the substrate in order to reduce tensile stresses due to shrinkage causing disjunction at interface and to guarantee continuity of the structural element after restoration. SCC with addition of an expansion anti-shrinkage agent is suitable to this purpose.

Generally used techniques for the application of restoring material are spraying or hand applied, casting and injection; they have different influence on the expansion of the new concrete since they affect material homogeneity and reinforcing bar bond (Figure 21 b).

Environmental conditions are very important for concrete expansion and for its resistance against shrinkage. Ageing agents or plastic sheets are less effective solutions but worthwhile

Cast-in-place SCC seemed the most adequate solution for the piers under consideration; it includes, in addition to substrate preparation, formwork construction, concrete production (Figure18), its application and ageing. Formwork originally used to build the specimens was opportunely modified to include a metallic groove (Figure18) allowing SCC pouring without interruptions from a single hole in the formwork (Figure18). The final result was generally good although superficial imperfections were present after formwork stripping (Figure3: phase 4). SCC filled up all available spaces even the upper part, opposite to pouring position. Concrete restoration results in a SCC jacket 50-90 mm thick and 550 mm high. A 35 MPa mean cubic strength is required as the most similar value to that of the original piers achievable with SCC. The main aims of the SCC mix design were: high fluidity, small diameter (<12 mm) aggregate (to easily fill up the space between reinforcement and concrete core), shrinkage offset adding conveniently measured out expansive agent (Figure 21). The latter was essential to guarantee complete filling and thus continuity at the interface between existing and new material. Resulting SCC mix was made of grit, sand, calcareous filler, cement expansive agent, superplasticizing and water with water-cement content equal to 0.48.

In case of pier 6, SCC was formed with the same mix design but required more water and superplasticizing to get acceptable slumps due to possible filler humidity now under investigation. SCC compressive cubic mean strength at failure, measured over six standard cubes, resulted in 48.19 MPa (1.60 MPa standard deviation) Table 2. Tests were carried out on fresh material to verify Code UNI 11040 (2003)[68] prescriptions

Figure 4, Table 3. Shrinkage behavior with time (Figure 4) was measured at the Laboratory of the Research Center BUZZI UNICEM in Guidonia (Rome).

In Figure 20, Figure 21 the hydraulic shrinkage of SCC is shown and is also presented a comparison with the hydraulic shrinkage of other materials.

The SCC concrete develops high mechanical resistance very quickly after it is poured and the framework can be removed just 24 hours after pouring. The SCC surface is uninterrupted without ridges and compact: occlusions or vacuums are not detected.

(a) SCC production



(d) formwork



SCC jet

SCC jet



Figure18 Concrete restoration (phase 4) (a) SCC production (b) formwork (c) SCC jet process

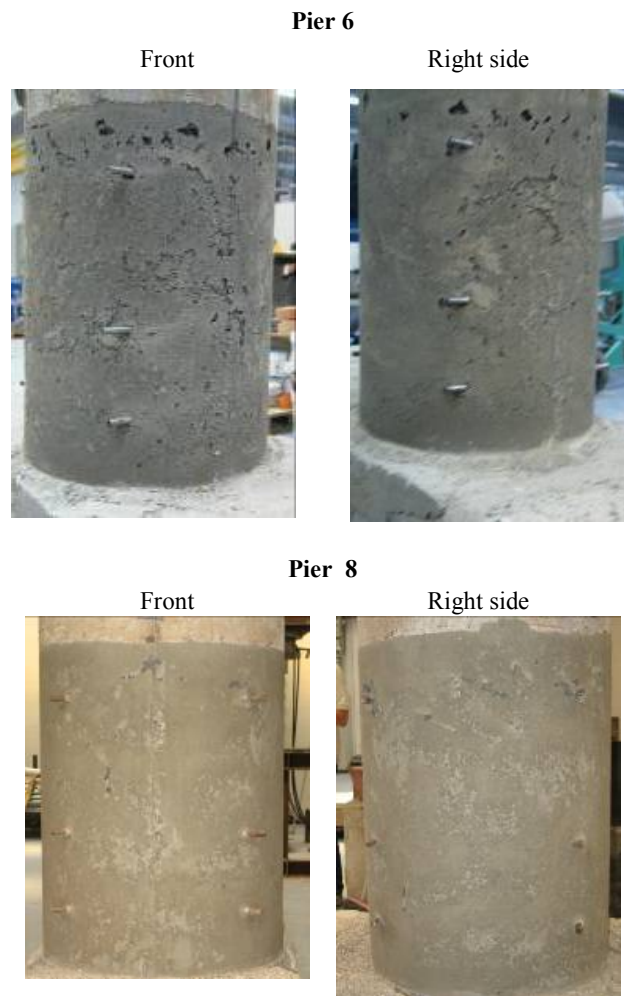


Figure19 Concrete restoration (phase 4). After removing the formwork, the SCC surface is smooth, compact and regular

<i>specimens</i>	R_c [MPa]
1	45,43
2	48,83
3	49,55
4	48,22
5	49,72
6	47,40
Mean value [MPa]	48,19
standard deviation [MPa]	1,60

Table 2 SCC standard cubic strength- Mean value and Standard deviation



Figure 5. Tests were on fresh material to verify Code UNI 11040 (2003) (a) Slump flow test, (b) V funnel

Test	code	Parameter measured	UNI 11040 (code limits)	pier	
				6	8
Slump flow	UNI 11041	D_m [mm]	>600	760	860
		T_{50} [s]	≤ 12	3,04	4,00
V funnel	UNI 11042	T_e [s]	(4÷12)	5,5	6,5
		T_{e5} [s]	$< T_e + 3$	5,5	7,5

Table 3 Testing fresh self compacting concrete: D_m = the largest diameter of the flow spread, T_{50} = the period between the moment the cone leaves the base plate and SCC first touches the circle of diameter 500 mm, T_e = the V-funnel flowtime, T_{e5} = the V-funnel flowtime after 5 minutes

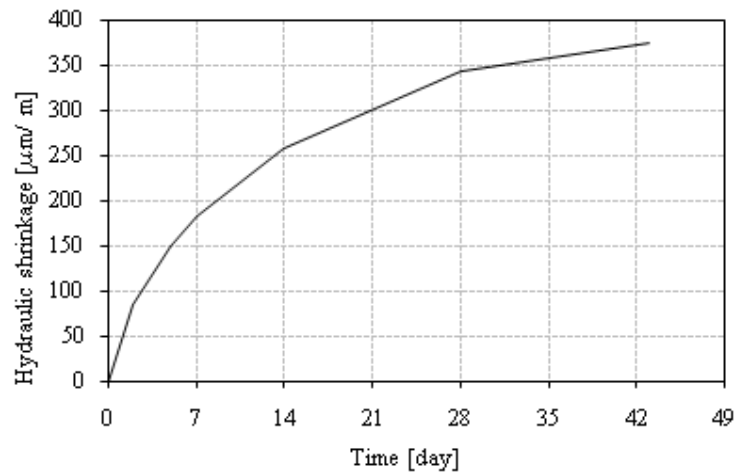


Figure 20: hydraulic shrinkage-time diagram for SCC.

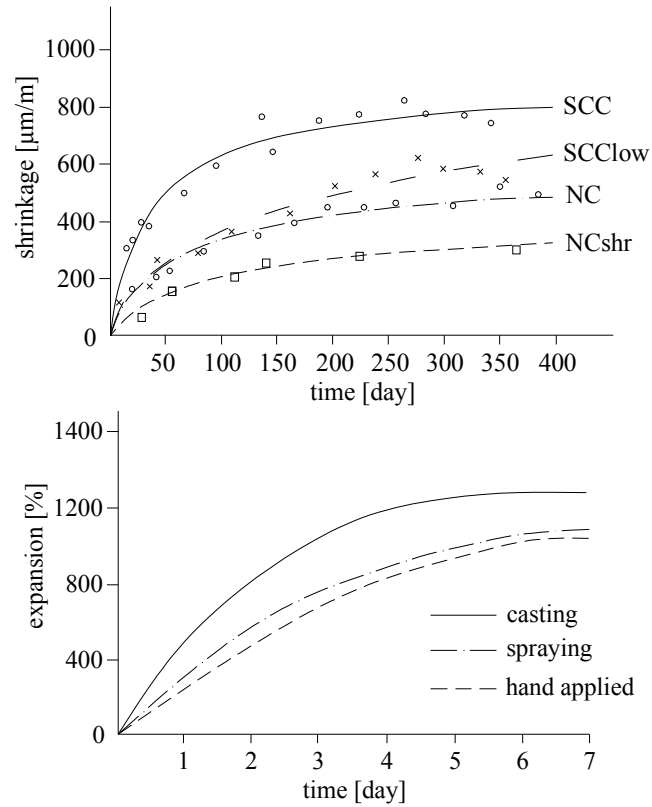


Figure 21: (a) Shrinkage of different Concretes (NC=normal C., NCshr=shrinkage offset C., SCC=self compacting C., SCClow=SCC with low cement content) (b) Preparation technique effect on concrete expansion

8.5. Seismic retrofitting

Seismic retrofitting is the modification of existing structures that are vulnerable to serious damage during an earthquake, to make them more resistant to earthquakes.

This protection strategy consists to assess the seismic vulnerability of existing structures and to recognize the inherent capacity within the existing structures.

Increasing the local capacity of structural elements is one possible solution to improve the seismic behavior of existing bridges that are vulnerable to serious damage during an earthquake.

Next, it will describe design procedures and techniques required to improve the seismic capacity of the above described specimens.

Among the possible solution to achieve such goal, the application of fiber reinforced polymers (FRP) wrapping on columns results is a very interesting solution.

The lightweight, high strength and corrosion resistance of FRP are some of the characteristics that make them ideally suited for quick and effective structural repairs and leads to a reduction in transport and assembly costs. Therefore, they have been preferred for conducting emergency bridge repairs.

In this research project, the specimens are reinforced with a discontinuous FRP wrapping that is placed on the surface of the concrete specimen.

8.5.1. Design procedure

The above results of visual inspection of damaged specimens showed that tested italian squat and tall piers suffered shear and flexural failure respectively.

Therefore, retrofitting designs aim to increase the ductility of the tall piers and the shear strength of the squat pier. C-FRP wrapping, as above said,

may be used to wrap columns to enhance the seismic capacity of the piers. The thicknesses of C-FRP wrapping are taken as the design variables. In particular the thickness of the C-FRP wrapping were determined according to CNR (CNR-DT 200 2004)[50] and EC8 [56]. The CFRP discontinuous wrapping are used because of the original transversal bars used to support the displacement transducer that exit from the surface of the specimen. Moreover, it allows to observe the cracking pattern on the surface of the concrete. The distance between the strips is of about 20mm within the most critical zone. The critical zone includes the repaired portion of the column. No partial coefficient was considered in the adopted capacity models. Commercial 0.169 mm thick C-FRP (Tenax HTS 300/10 with ultimate strain $\epsilon_{fu}=1.0\%$ and elastic modulus $E_f=240$ Gpa) was wrapped in 100 mm wide unidirectional fiber strips.

8.5.1.1. Squat piers

Detected damage state clearly shows that tested squat specimens 6 and 8 are suffered shear failure. These failure mechanisms were also analytically proved by comparing shear strength with shear at resisting bending moment. The deficiencies in seismic shear resistance may be attributed to the insufficient reinforcement of hoops for shearing force. It is important to remind that the inox stirrups spacing is calculated on the base of the above consideration in order to guarantee that the original shear contribution of stirrups is equal to the original one. In fact current code requirements for the design of transverse reinforcement in columns of bridges in high seismic regions result in severe reinforcement congestion. Moreover, the spaces in which are placed the reinforcement (new inox bars and the original ones) are narrow and closer stirrups can obstruct the flow of concrete which is used to restore the concrete cover and the damaged or removed parts of the core and could create voids. An alternative solution is to use C-FRP wrapping which can improve the shear resistance and confine the repaired portion of column. The latter is

particular important given the fact that the confining could improve the bond between the original concrete and the repair material.

It is possible evaluate the shear resistance of pier according to EC2 and EC8 BRIDGE and Italian code NUOVE NORME TECNICHE PER LE COSTRUZIONI (NNT) [87].

$$1 \leq \cot \theta \leq 2.5$$

(equ. 4.1.16 , NNT)

$$V_{Rsd} = 0.9d \frac{A_{sw}}{s} f_{yd} (\cot \alpha + \cot \theta) \sin \alpha$$

(equ. 4.1.18 , NNT)

$$V_{Rcd} = 0.9d b_w \alpha_c f'_{cd} (\cot \alpha + \cot \theta) / (1 + \cot^2 \theta)$$

(equ. 4.1.19 , NNT)

In the above expression it is assumed that:

d , effective depth of section (depth to the tension reinforcement)

- $d = d_e$

The effective depth (d_e) is equal to:

- $d_e = r + 2 \frac{r_s}{\pi}$

(equ. 7.9.11 NNT)

For circular concrete sections of radius r in which the longitudinal reinforcement is distributed over a circle with radius r_s , (2) 5.6.3.3 Shear resistance of elements outside the region of plastic hinges, EC8 Bridge. Note that the dimensions of the confined concrete shall be used in lieu of the section dimension d (3) P 5.6.3.4 Shear resistance of plastic hinges, EC8 Bridge.

- A_{sw} , cross-sectional area of stirrup
- s , centerline spacing of stirrups
- f_{yd} , design value of yield strength of (longitudinal) reinforcement
- θ , strut inclination angle in shear design
- α , is the inclination of stirrups (it is assumed equal to 90°)

For members with solid or hollow circular cross sections, the web width b_w shall be defined as the side length of the square with the same area as solid circular cross section

$$b_w = \sqrt{\frac{D_p^2}{4} \pi}$$

- D_p , pier diameter

Coefficient α_c is equal to:

$$\alpha_c = 1 + \frac{\frac{N_e}{\frac{D_p^2}{4} \pi}}{f_{cd}}$$

Where:

- N_e , compressive load applied (it is equal to 258kN for the squat piers)
- f_{cd} , concrete compressive strength

and the reduced concrete compressive strength

$$f'_{cd} = 0.5f_{cd}$$

It is important to remind that shear resistance of plastic hinges is calculated assuming θ equal to 45° whereas this angle outside the region of plastic hinges can be calculated by making equal the expressions equ. 4.1.18 , NNT and equ. 4.1.19 , NNT. Then the angle is calculated using the below expression:

$$\text{sen}\theta = \frac{A_{sw} f_{yd}}{s b_w \alpha_c 0.5f_{cd}}$$

Table 4 shows the above shear resistances of the as-build Italian squat piers.

Zone	$\cot\theta$	V_{RSd} [kN]
Plastic hinge	1	69
Out of plastic hinge	2.5	147

Table 4 Shear resistance of plastic hinges and Shear resistance outside of plastic hinges of the as-build Italian squat piers.

The CFRP contribution to the shear capacity ($V_{Rd,f}$) for completely wrapped elements having circular cross section when the fibers are placed orthogonal to the axis of the member is calculated by equation below:

$$V_{Rd,f} = \frac{1}{\gamma_{Rd}} D f_{eff} \frac{\pi}{2} t_f \cot \theta$$

(4.27 CNRDT200/2004)

γ_{Rd} is the partial factor for resistance models

$$D = D_p$$

t_f is the thickness of FRP system

The effective FRP design strength can be calculated as:

$$f_{eff} = E_f \varepsilon_{f,max}$$

(4.33 CNRDT200/2004)

Where E_f is the FRP Young modulus of elasticity and $\varepsilon_{f,max}$ is the FRP maximum allowable strain.

θ is the strut inclination angle in shear design

Note that the above expression for discontinuous wrapping can be written as:

$$V_{Rd,f} = \frac{1}{\gamma_{Rd}} D f_{eff} \frac{\pi}{2} t_f \cot \theta \frac{b_f}{p_f}$$

Where b_f is the width of FRP reinforcement and p_f is the spacing of FRP strips.

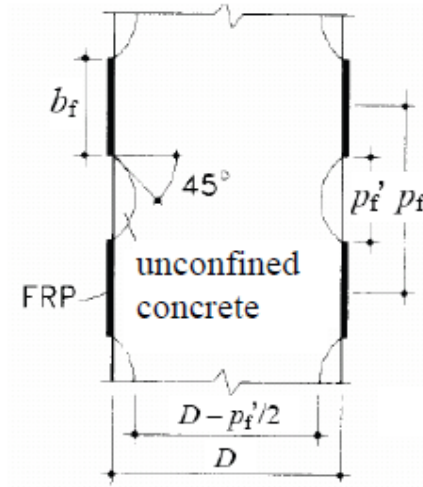


Figure 22 Elevation view of circular element confined with FRP strips
(Figure 4_11 CNRDT200/2004)

For the above consideration, it is assumed that :

- $\epsilon_{f,max}$ is assumed to be equal 1% (ϵ_{ju}) and no reduction coefficient is applied
- E_f is assumed to be equal 240 Gpa, no reduction coefficient is applied
- γ_{Rd} the partial factor for resistance models is equal to 1.2 (TABLE 3-3 CNRDT200/2004)
- t_f is equal to the C-FRP commercial thick
- b_f is equal to the C-FRP commercial width

- p'_f , the distance between the strips is assumed to be equal to about 20mm in the critical zone whereas it is assumed to be equal to the maximum allowed according to 4.5.2.2 Confinement lateral pressure (7), CNRDT200/2004 outside the critical region.
- $p_f = p'_f + b_f$
- The specimen is wrapped with one layer of CFRP (minimum number of layers)
- The total shear capacity (V_{tot}) can be evaluated as:

$$V_{tot} = V_{Rd,f} + V_{Rds}$$

- The total shear capacity has to be greater than the shear corresponding to the maximum moment.
- It is assumed that the shear capacity is equal to the shear capacity of the as-build Italian squat pier

After these assumptions, the CFRP contribution to the shear capacity is given by:

$$V_{Rd,f} = \frac{1}{\gamma_{Rd}} D_p E_f \varepsilon_{ju} \frac{\pi}{2} t_f \cot \theta \frac{b_f}{p_f} \quad (4.27 \text{ CNRDT200/2004})$$

Table 5 shows the above CFRP contribution to the shear capacity.

Zone	P'_f [mm]	$\cot \theta$	V_{RSd} [kN]
Plastic hinge	20	1	185.8
Out of plastic hinge	200	2.5	185.8

Table 5 The CFRP contribution to the shear capacity in plastic hinges and outside of plastic hinges

The shear corresponding to the moment strength can be calculated using the results of the analytical model. The analytical model of the repaired squat pier is described in detail and discussed in Chapter.... It is a fiber model in which the cross-section is modeled to take account of:

- “standard” longitudinal reinforcement bars
- longitudinal inox reinforcement bars
- new repairing material (SCC)
- original repaired concrete
- CFRP confinement

Moment curvature analysis is been performed to accurately determine the load deformation behavior of a reinforced concrete section using nonlinear material. The shear corresponding to the moment strength (T_{max}) is given by:

$$T_{MAX} = \frac{M_{MAX}}{H_p}$$

Where

- H_p is the pier height (1170mm)
- M_{max} is the maximum moment obtained by analysis (.....)

The shear corresponding to the maximum moment is equal to about 190kN. The comparison between the CFRP contribution to the shear capacity Table 4 and Table 5 the shear resistances shows that the shear strengthening can result effective to carry the maximum shear. In addition it is important to remind that there are uncertainties about the effectiveness of the repairing techniques. Then CFRP reinforcement assures reliability.

8.5.2. Tall piers

The confinement of concrete with CFRP enhanced strength and ductility of the concrete columns. The stirrups spacing have a remarkable influence on the curvature ductility of the pier.

It is evident from the table that stirrups spacing of the EC8 piers spacing (30mm) is larger than that of the DM piers (100mm).

Note that all of the tall specimens (EC8 and DM) have the same geometry and longitudinal reinforcement.

In addition all of the tall specimens have practically the same materials characteristics and the vertical loads applied at the top of the piers, is equal for each tall pier.

Therefore, it does not surprise that the EC8 tall piers show more ductile behavior than that of the DM tall piers. Moment curvature analysis is performed to accurately determine the curvature ductility of the tall piers.

In this research, the enhancement of deformation capacity (ultimate curvature) of the as-build Italian tall piers is achieved through concrete confinement by means of FRP jackets.

Discontinuous CFRP wrapping is applied around the pier to strengthen the element.

The strips are placed on the pier surface and displaced successively along the height of the specimen. In particular, it is assumed that:

- the number of CFRP layers that are necessary to increase the ductility are placed with spacing (p'_f) of about 20mm along the height of the specimen that is equal to the portion of the EC8 piers where the stirrups spacing is narrower.
- The CFRP strips that are used to increase the shear capacity are placed with maximum allowable spacing outside the critical zone

The thickness of FRP jackets is calculated according to the above codes.

For the above consideration, it is assumed that:

- $\epsilon_{f,max}$ is assumed to be equal 1% (ϵ_{ju}) and no reduction coefficient is applied
- E_f is assumed to be equal 240 Gpa, no reduction coefficient is applied
- t_f is equal to the C-FRP commercial thick
- b_f is equal to the C-FRP commercial width
- p'_f , the distance between the strips is assumed to be equal to about 20mm in the critical zone
- $p_f = p'_f + b_f$

The equation below are used to calculate the optimal thickness of FRP jacket. According to the Mander et al. model, the stress in the confined concrete (f_{cc_st}) by steel stirrups or spirals is determined by the following

Confinement effectiveness coefficient

$$k_e = \frac{(1 - \frac{(s - \phi_{st})}{2D})^2}{1 - \rho_{cc}}$$

Where:

ρ_{cc} is the ratio of the longitudinal reinforcement area to section core area

$$\rho_{st} = \frac{4A_{sw}}{sD_{st}}$$

The effective lateral confining pressure is:

$$f_{l,st} = 0.5k_e \rho_{st} f_{yst}$$

$$f_{cc_St} = (-1.254 + 2.254 \sqrt{1 + \frac{7.94f_l}{f_{c0}} - 2 \frac{f_l}{f_{c0}}}) f_{c0}$$

(8.5.2-1)

the concrete ultimate strain

$$\varepsilon_{cu} = 0.004 + \frac{1.4 \rho_{St} f_{ySt} \varepsilon_{su}}{f_{cc_St}}$$

(8.5.2-2)

f_{ySt} is the yield stress of the transverse reinforcement

ε_{su} the steel strain at maximum tensile stress

f_{c0} unconfined compression strength

$$f_l = 0.4 I_\gamma^2 \frac{f_c \varepsilon_{cu}^2}{\varepsilon_{ju}}$$

(A34 EC8 Part3)

(8.5.2-3)

Where:

f_l is the C-FRP confinement pressure

I_γ is the ratio between the target curvature ductility and the available curvature ductility.

f_c is the concrete strength

ε_{cu} is the concrete ultimate strain

ε_{cu} is the adopted FRP jacket ultimate strain,

For the case of wrapping applied through strips with spacing p'_f , the coefficient of vertical efficiency k_v can be obtained using:

$$k_v = \left(1 - \frac{p'_f}{2D_{\min}}\right)^2$$

(8.5.2-4)

In which:

D_{\min} is the pier diameter

$$t_f = \frac{\frac{f_l}{k_v}}{2E_f \varepsilon_{ju}} D \frac{p_f}{b_f}$$

(8.5.2-5)

This equation can be obtained by assuming that:

The effective confinement lateral pressure $f_{l,eff}$ is equal to

$$f_{l,eff} = K_v f_l$$

(4.42 CNRDT200/2004)

$$f_l = \frac{1}{2} \rho_f E_f \varepsilon_{fd,rid}$$

(4.43 CNRDT200/2004)

The geometric strengthening ratio ρ_f :

$$\rho_f = \frac{4t_f b_f}{D p_f}$$

(4.48 CNRDT200/2004)

D is the pier diameter

Number of layers is equal to:

$$n = \frac{t_f}{t_{com}}$$

Where t_{com} is the commercial CFRP thickness

The design procedure can be summarized as follows:

1	The concrete strength and the concrete ultimate strain are evaluated according to (8.5.2-1) and (8.5.2-2)
2	Moment curvature analysis is performed to accurately determine I_{χ}
3	The necessary amount of CFRP confinement pressure is calculated according to (8.5.2-3)
4	The coefficient of vertical efficiency k_v is calculated (8.5.2-4)
5	The optimal thickness of CFRP jackets is calculated (8.5.2-5)
6	The number of CFRP layers (n) is calculated on the base of the commercial CFRP thickness

Table 6 CFRP Discontinuous wrapping for Italian tall pier. Design procedure

Pier	I_{χ} [-]	f_{cc_st} [MPa]	ε_{cc_st} [-]	f_l [MPa]	t_f [mm]
1	1.918	20.4	0.0122	4.467	0.492
3	1.911	20.3	0.0126	4.699	0.518

Table 7 Discontinuous CFRP wrapping of the tall piers. Design parameters

The comparison between the shear strength of the EC8 tall piers and the DM tall pier shows that it is necessary to improve the shear strength of the Italian piers. Table 8 shows the shear strength of the piers

code	V _{rsd} (p.h.) [kN]	V _{rsd} (o.p.h.) [kN]
DM	58	158
EC8	166	227

Table 8 Shear resistances of the specimen; outside plastic hinge (o.p.h.) and in plastic hinge (p.h)

The CFRP contribution to the shear capacity is given by (4.27 CNRDT200/2004) It does not necessary to repeat the calculation to obtain the CFRP contribution. The CFRP material, the wrapping geometry, and the piers diameter are the same used for the squat piers.

The CFRP wrapping that is placed in the critical zone to increase the curvature ductility, is sufficient to increase the shear capacity whereas it is necessary to place CFRP discontinuous wrapping with one layer and maximum allowable spacing outside the critical zone.

Then, by proper design, CFRP wrapping can also ensure that the shear capacity of the retrofitted Italian piers is comparable with that of the EC8 tall piers

8.5.3. FRP wrapping

FRP strip configurations for squat and tall piers are shown in Figure 7-8. The CFRP reinforcing systems are placed on the concrete surface using the wet lay-up system. This system consists of dry unidirectional carbon fibers that are impregnated on-site with a saturating resin in order to provide a binding matrix for the fiber and bond the strips to the concrete surface.

The concrete surface must be properly prepared prior to remove bonding spalling or delamination in the case of concrete. The area of FRP strips

application was brushed with a metallic brush to remove the very superficial concrete substrate.

Next, the adhesive resin (EPR320+EPH550) is directly applied onto surface of the concrete using a roller or brush. When the concrete surface is saturated, the layers of fabric (1.700 m strips to guarantee 300-350 mm lap splice) were hand-placed with fibers direction perpendicular to pier axis. The sheet is unrolled and rolls onto the structural element being strengthened. In case of more layers, distinct overlapped FRP strips were applied. It is important to maintain tension to minimize intrusion of air entrainment behind sheet during the application. The reinforcement is placed one layer at a time applying pressure to wrap using a roller (hard rubber roller with ridges). Subsequently a layer of epoxy resin can be applied to the sheet to fully saturate the material.

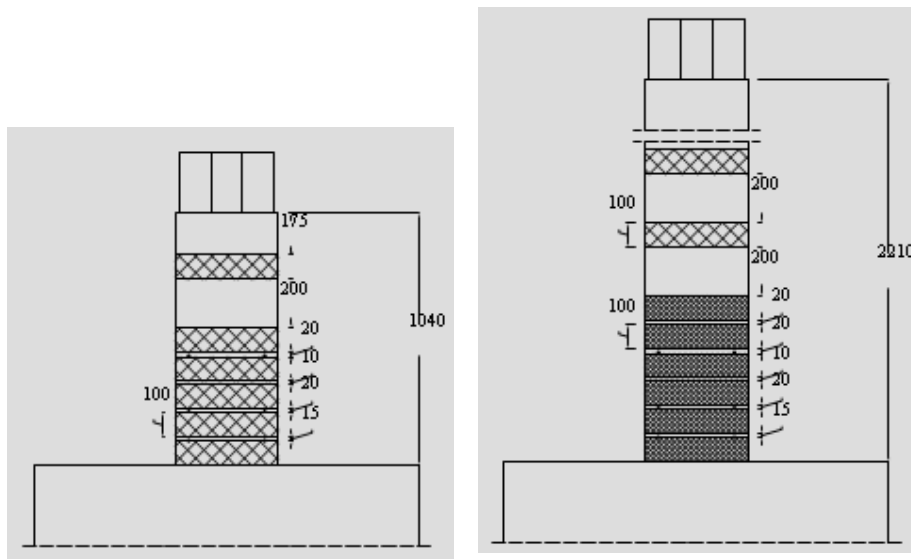



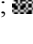

Figure 23 FRP strips configuration designed for squat piers 6, 8;  1 layer, [mm] and for tall piers FRP strips configuration designed for tall piers 2, 4, 5;  3 layers,  1 layer, [mm]



Figure 24 FRP strips application. Tall and squat piers.

9. Pseudo-dynamic test

The substructure testing methodology is an advanced dynamic testing technique in structural engineering, which was developed in the 80's and formulated by various researchers (Shing et al 1985, Nakashima 1985, Mahin et al 1985,).

The pseudo-dynamic testing method (PDTM) is a traditional form of substructure testing technique and was developed in the early 1970s, having a history of nearly thirty years.

This experimental technique simulates the seismic response of structures and structural components in the time domain and reproduces seismic effects by combining quasi-static experimental tests with numerical integration procedures.

In this test, the structural system is represented as a discrete spring-mass system and the PDTM models and solves the dynamic portion of the structural response to earthquakes, the velocity and acceleration dependent terms, numerically using numerical integration schemes.

The static, or displacement dependent, response of a substructure, the portion of the structure that cannot be described by using a numerical model, is determined using an experimental specimen. The pseudo-dynamic testing (PDT) program calculates the position of degree of freedom of the test specimens and applies the calculated displacement to the specimens. Thus, the restoring force of specimen is directly measured from an experimental test conducted in parallel.

The combination of numerical and experimental techniques allows to determinate the complete response of complex structures without applying experimental loads dynamically.

The pseudo dynamic test with a real-time control was developed in the 1990s and it is an extension of this testing technique (Nakashima et al. 2003)

9.1. Pseudo-dynamic testing software

Results from previous studies have established that the pseudo-dynamic test, which requires conventional basic test equipment and specific software solutions, is very effective in predicting the dynamic response of structures.

However, the correct choose of the pseudo-dynamic software is a key of the success of a pseudo-dynamic test.

Therefore, it is possible to decide more precisely between purchasing commercially available software, or undertake internal software development efforts.

The test software must by design be flexible and modifiable to accommodate unknown future needs.

The previous considerations can very well justify the decision to develop an in-house pseudo-dynamic test program.

This software may be designed to provide a complete solution accounting data acquisition, mechanical actuator control and dynamic integration software functionalities in one.

For this reason, in this research to implement an in-house pseudo-dynamic test program, MATLAB 7 and LabVIEW 8.2 developed by MathWorks and National Instruments respectively, were chosen as the programming languages.

The current version of the software is based on previous FORTRAN version that has been used with success in previous pseudo-dynamic test (rif).

In a first phase of implementation MATLAB has been used to create the integration algorithm with the aim of making use of efficient available tools.

More specifically MATLAB provides mathematical libraries and tools for analyzing results, data acquisition, control, graphics and visualization tools.

Afterwards, to be able to use a National Instruments data acquisition and control board the pseudo-dynamic main program is written in LabVIEW.

LabVIEW, developed by National Instruments in 1986, is a graphical programming environment based on the G or graphic programming language, suitable for interfacing computers with the instruments, data acquisition and control, data analysis, data presentation, collecting, storing, analyzing, transmitting measured data, developing program in a graphical environment, providing an effective user interface.

However, LabVIEW uses graphical programming language to create programs called "Virtual Instruments" or VI's due to the instrumentation-related origin, allowing the program to be in a "Block Diagram" form. This allows creating GUI capabilities built-in in LabVIEW programs. If structured properly, this graphical code represents directly the program flow chart.

However, Labview can call MATLAB to execute m-scripts using a MATLAB script nodes, which invoke the MATLAB software script server (installed on the same pc) to execute scripts written in the MATLAB language syntax.

In this way it is possible use MATLAB to solve the integration equations and Labview to control the actuator and to acquire the data.

The main program, a virtual instrument, includes three programs with different functions: controller, optimal numerical solvers, and physical tester and acquisition system.

The current version of program is designed to test a multi degree of freedom system, in which one substructure, for example a column specimen, may be either actual test or numerical model. The implicit alpha method is used in the main program as the step-by-step integration technique. This program can be easily modified to allow enabling multi-degree of freedom experimental test of substructure.

A pseudo-dynamic test requires both real-time support and accurate coordination of various simultaneously running tasks (data acquisition and actuator controller).

In order to do this the main program communicates with the control program, which allows to receive data by acquisition program in real time, and to transfer data (specimen degree of freedom position and reaction), whenever needed, to integration routine.

Accuracy certification, performance reliability and software capability enhancement are all checked individually and adjusted if necessary with all references traceable in previous FORTRAN version of pseudo-dynamic software.

The numerical results of new software version are directly confronted with previous version and show that new software version assures the same accuracy.

Finally the user can design a personal interface, which permits to communicate with the test equipment, to monitor the response and to control the actuator in an easy way. User interface may be the one most important part of a LabVIEW application.

In fact, it is the only part of the application the end-user is directly in contact with and must be intuitive to facilitate easy setup.

The user interface consists in a succession of explicit menus, which are easy to use and. The test equipment consists of:

- a PC computational machine,
- a controller and data-acquisition systems,
- an actuator used to control the displacements of a test structure

- test equipment used to restrain the specimen and to apply vertical loads

9.2. Acquisition program

The data acquisition program (DAQ) reads continuously data from the multi-channel acquisition system and does the data collection passively from instruments during the test. This program allows acquiring various settings like potentiometer positions (displacement transducers) and load cell loads.

However, in order to optimize the data acquisition and recording, it is possible to use a memory buffer to allow much faster data acquisition.

Moreover using a special file format TDM Streaming (.tdms LabVIEW format) for storing binary data, is one way to make faster writing performance in LabVIEW.

This format provides an easy way to describe the data information stored in the file (channel type, acquisition rate, number of acquisition point, etc) without having to write your own header label.

This program communicates with the control program (CP) of the PDT software to allow the actuator control.

The DAQ program communicates with the National instruments acquisition modules to retrieve and records specimen response and to plot time histories on the computer video to monitor the applied displacements and loads during the test.

The synchronization and communication between the main program, the control program and the acquisition program are usually one of the greatest difficulties to achieve good PDT program performance.

In fact, it is necessary to find a tool which allows exchanging response values at the right time. An important benefit of using LabVIEW is the availability of Notifiers, which permit to communicate between two independent parts of a program or between two virtual instruments running on the same PC.

In order to explain their functioning, it is possible to assume that Notifiers are similar to mailboxes for data: one subprogram sends data to the mailbox and another subprogram which receives necessary data. The

latter program completely pauses the execution while waiting data, and starts again only when new data becomes available.

The program is divided in two parts:

- a first part to reset to zero the instruments the at the beginning of a test using the mean values previously acquired and recorded for a time interval of few minutes.
- a second part to display data on the user interface, to record the data and to send the notification of displacement of the specimens free end and horizontal load.

Conceptually the choose of using for each channels the means value of data measured for that channel for several minutes before the test , is mainly related to the variation of instruments reading due to the noise.

The user interface is designed for easy and flexible use and it is realized using a tab control. A tab control consists of pages and tabs, which allow to an user to quickly perform the basic program functions. More precisely, he following tab defines and controls all the menu entries and associated information:

- the mean value for each channel is shown and the user , if it necessary , can reload a new file to reset to zero
- several windows allows interactive visualization of all channels entries and the user can control the initial value of each channel and checks the correct functioning of each instruments. The program is stopped and restarted by the user if a malfunctioning is detected.

In the case when the user needs to save the measured data to different files, the modular flexibility of the program allows it without stopping (or example if you would separate measured data during the pauses).



Figure 25 Acquisition user interface

9.3. Control program

Control program is a program designed to make it easier the interaction between acquisition subprogram and the main program, to manage and to monitor the electro-mechanical actuator.

The first task is to receive the target position of the degree of freedom of specimen used in the simulation and the velocity to move it.

The position of the free end of specimen is monitored in real time by using a displacement transducer.

So the control subprogram compares continuously the target position with the actual position of the pier free end and if the target position is reached, it will ask the acquisition program to retrieve actual load values of restoring force of the specimen.

The response of the specimen (restoring force as a function of displacement) is monitored in real time by plotting it on screen of controller's monitor.

The control program checks if the actual position is smaller than the maximum acceptable position and stops the execution if the actual position is beyond the maximum acceptable position.

Clearly the tolerance to displacement error is set up on the base of the instruments noise, the rate of acquisition as a function of actuator speed, and the expected response of specimens. In the latter case, tuning of actuator speed is needed.

The actuator is moved without stopping and its velocity is a function of the pseudo-dynamic velocity: the actuator decrease its velocity when the target position changes direction and increases its velocity when it approaches to zero position.

The control program receives the displacement and the load values by means of Notifier function implemented in Labview.

The experimental setup is composed of a system to impose a displacement to the free end of the specimen that consists of:

- a actuator that is employed to impose the displacement commands on the SDOF system.
- an inverter which provides the needed current to drive the motor (horizontal actuator velocity is a function of the frequency of alternative current; the inverter changes the main frequency of 50 Hz to increase or to decrease the actuator velocity)
- a National Instruments board that is used to acquire samples and provide a control signal to an external inverter

For the precise control of velocity and position, an input-output feedback system is used: a speed-closed loop control drive using a encoder sensor provides an efficient velocity control.

Therefore, the actuator velocity is known at each time interval and it is possible to predict the position of the actuator.

In this way the control program can remove almost any kind of noise due to inverter from instruments reading.

Finally the control program passes the load cell value to main program if the target displacement is reached.

The inverter is controlled using two analog voltage inputs (board analog outputs): an input trigger signal to activate the motor (on/off) and a voltage changeable from 0 to 10 to control the velocity of electromechanical actuator.

Thus, if the voltage changes in a range from 5V up to 10V, the velocity increases linearly in positive direction while if the voltage changes in a range from 5V up to 0V the velocity increases in negative direction. If the voltage is equal to 5V, the actuator stops.

9.4. Main program: pseudo-dynamic testing program

Different implicit or explicit integration schemes can be used to execute a pseudo-dynamic test.

In this research study, the α -method an implicit and unconditionally stable integration scheme with Second-Order Convergence has been selected.

The reason to choose this procedure is motivated by the fact that in previous study several authors have examined the accuracy, and error-propagation of the method.

The principal equation contains some terms that are either prescribed or to be determined by other equations defining the problem.

In this method, the time-discretized equations of motion and the displacement and velocity approximations can be written as:

$$Ma_{i+1} + (1+\alpha)Cv_{i+1} - \alpha Cv_i + (1+\alpha)r_{i+1} - \alpha r_i = (1+\alpha)f_{i+1} - \alpha f_i$$

$$d_{i+1} = d_i + \Delta t v_i + \Delta t^2 \left[\left(\frac{1}{2} - \beta \right) a_i + \beta a_{i+1} \right]$$

$$v_{i+1} = v_i + \Delta t \left[(1-\gamma)a_i + \gamma a_{i+1} \right]$$

where M and C represent the mass and damping matrices of the test structure that is modeled numerically while d_i , v_i , a_i , and r_i are the degree of freedom displacement, velocity, acceleration, and restoring force vectors at time integration step i . Moreover, Δt is the integration time interval and f_i is the vector of applied forces.

The numerical properties of the integration scheme are controlled by means of α , β , γ prescribed parameters. To obtain unconditional stability and second-order convergence, it is necessary that:

$$-\frac{1}{3} \leq \alpha \leq 0$$

$$\gamma = \frac{1}{2}(1-2\alpha)$$

$$\beta = \frac{1}{4}(1-\alpha)^2$$

The equations of motion are solved using a Newton-type iterative procedure in order to investigate nonlinear structure response. This procedure requires computing the actual tangent stiffness of a structure at each iteration.

However, it is too expensive to calculate the tangent stiffness of a structure during a test.

Hence, a modified Newton approach is used here which uses the initial structural stiffness K_{ini} , in place of the tangential stiffness.

Hereinafter it is assumed that $d_{i+1}^{m(k)}$ and $r_{i+1}^{m(k)}$ denote the actually imposed displacements and corresponding restoring forces measured directly from the specimen at the beginning of iteration k in time step $(i+1)$. The nonlinear restoring forces measured from the specimen are feedback to the numerical algorithm for determination of the next displacement step.

In order to describe briefly some basic features of the system, it is convenient to indicate below the basic equations which are used in numerical solution procedure.

It is appropriate therefore to begin by reminding the reader the expression to calculate the effective stiffness K^* and residual vector $R_{i+1}^{(k)}$

$$K^* = \frac{\bar{M}}{\Delta t^2 \beta} + (1+\alpha)K_{ini}$$

(9.4-1)

$$R_{i+1}^{(k)} = \frac{\bar{M}}{\Delta t^2 \beta} \left[\hat{d}_{i+1} - d_{i+1}^{m(k)} - (1+\alpha)r_{i+1}^{m(k)} \right]$$

(9.4-2)

In which parameters \bar{M} and \hat{d}_{i+1} are given by the following expression:

$$\bar{M} = M + (1+\alpha)\gamma\Delta t C$$

(9.4-3)

$$\begin{aligned} \hat{d}_{i+1} = & d_i + \Delta t v_i + \Delta t^2 \left(\frac{1}{2} - \beta \right) a_i + \\ & + \Delta t^2 \beta \bar{M}^{-1} \left[(1+\alpha)f_{i+1} - \alpha f_i - C v_i - (1+\alpha)(1-\gamma)\Delta t C a_i + \alpha r_i \right] \end{aligned}$$

and $\Delta d_{i+1}^{(k)}$ is calculated using:

$$K^* \Delta d_{i+1}^{(k)} = R_{i+1}^{(k)}$$

(9.4-4)

and then, the displacement at step k+1 is determined as:

$$d_{i+1}^{(k+1)} = d_{i+1}^{m(k)} + \Delta d_{i+1}^{(k)}$$

(9.4-5)

At each iteration, the Equation (9.4-4) is solved for the $\Delta d_{i+1}^{(k)}$ explicitly and the displacements $d_{i+1}^{(k+1)}$ is calculated with equation(9.4-5)

Afterward these displacements are sent as target positions to an actuator controller to apply the displacements to the specimen by means of an actuator.

When the target position is reached, the actually displacements $d_{i+1}^{m(k)}$ and the resulting restoring forces $r_{i+1}^{m(k)}$ are measured. Note well that the actually displacements are usually different from $d_{i+1}^{(k+1)}$ because of control errors.

If at this point all the already mentionated parameters are known, a new residual $R_{i+1}^{(k+1)}$ is computed using the Equation(9.4-2) and it allows to update the response in the next iteration.

In this implementation, however, the iterative procedure is terminated if all the specified convergence tolerances for each degree of freedom have been attained.

Once convergence is reached, the new acceleration and velocity vectors are computed using the equations (9.4-6) and (9.4-7) which are written below, and the solution is advanced to the next time step, where the process repeats.

$$a_{i+1} = \frac{1}{\Delta t^2 \beta} \left[d_{i+1} - d_i - \Delta t^2 (1/2 - \beta) a_i \right]$$

(9.4-6)

$$v_{i+1} = v_i + \Delta t \left[(1 - \gamma) a_i + \gamma a_{i+1} \right]$$

(9.4-7)

The problem solution procedure can be organized in steps, which are shown in Table 9. The main program is organized according to procedures in the flow chart shown in Figure 26.

1	<p>Set the number of integration points, n</p> <p>Evaluate \bar{M} and K^* with equations (9.4-3) and (9.4-1)</p> <p>Choose the tolerances for each degree of freedom $\Delta d^{(n)}$</p> <p>Initialize $d_0, d_0^C, d_0^{EX}, v_0, r_0$ and a_0</p>
2	Set the integration counter to zero
3	Read the input excitation f_i
4	Compute $\bar{M}\hat{d}_{i+1}$
5	Set $k = 0$ (Newton-type iterative procedure counter)
6	<p>Set $r_{i+1}^{(k)} = r_i$</p> <p>Set $d_{i+1}^{C(k)} = d_i^C$</p> <p>Set $d_{i+1}^{EX(k)} = d_i^{EX}$</p>
8	Calculate the error $\bar{M}e_{i+1}^{(k)} = \bar{M}d_{i+1}^{EX(k)} - \bar{M}\hat{d}_{i+1} + \Delta t^2 \beta (1 + \alpha) r_{i+1}^{(k)}$
9	Solve the equation to obtain $\Delta d_{i+1}^{(k)}$
10	If $ \Delta d_{i+1}^{(k)} < \Delta d^{(n)}$ go to step 16
11	Calculate $d_{i+1}^{C(k+1)} = d_{i+1}^{C(k)} + \mathcal{G}\Delta d_{i+1}^{(k)}$
12	Impose $d_{i+1}^{C(k+1)}$ to the specimen
13	Acquire $r_{i+1}^{(k+1)}$ and $d_{i+1}^{EX(k+1)}$, measured from test specimen
14	Set $k=k+1$
15	Go to step 8
16	<p>Calculate $d_{i+1} = d_{i+1}^{EX(k)} + \Delta d_{i+1}^{(k)}$</p> <p>Calculate $r_{i+1} = r_{i+1}^{(k)} + K\Delta d_{i+1}^{(k)}$</p> <p>Calculate $d_{i+1}^C = d_{i+1}^{C(k)}$</p> <p>Calculate $d_{i+1}^{EX} = d_{i+1}^{EX(k)}$</p>
17	<p>Calculate $a_{i+1} = \frac{1}{\Delta t^2 \beta} [d_{i+1} - d_i - \Delta t^2 (1/2 - \beta) a_i]$</p> <p>Calculate $v_{i+1} = v_{i+1} + \Delta t [(1 - \gamma) a_i + \gamma a_{i+1}]$</p>
18	Set $i=i+1$ go to step 3

Table 9 Integration procedure

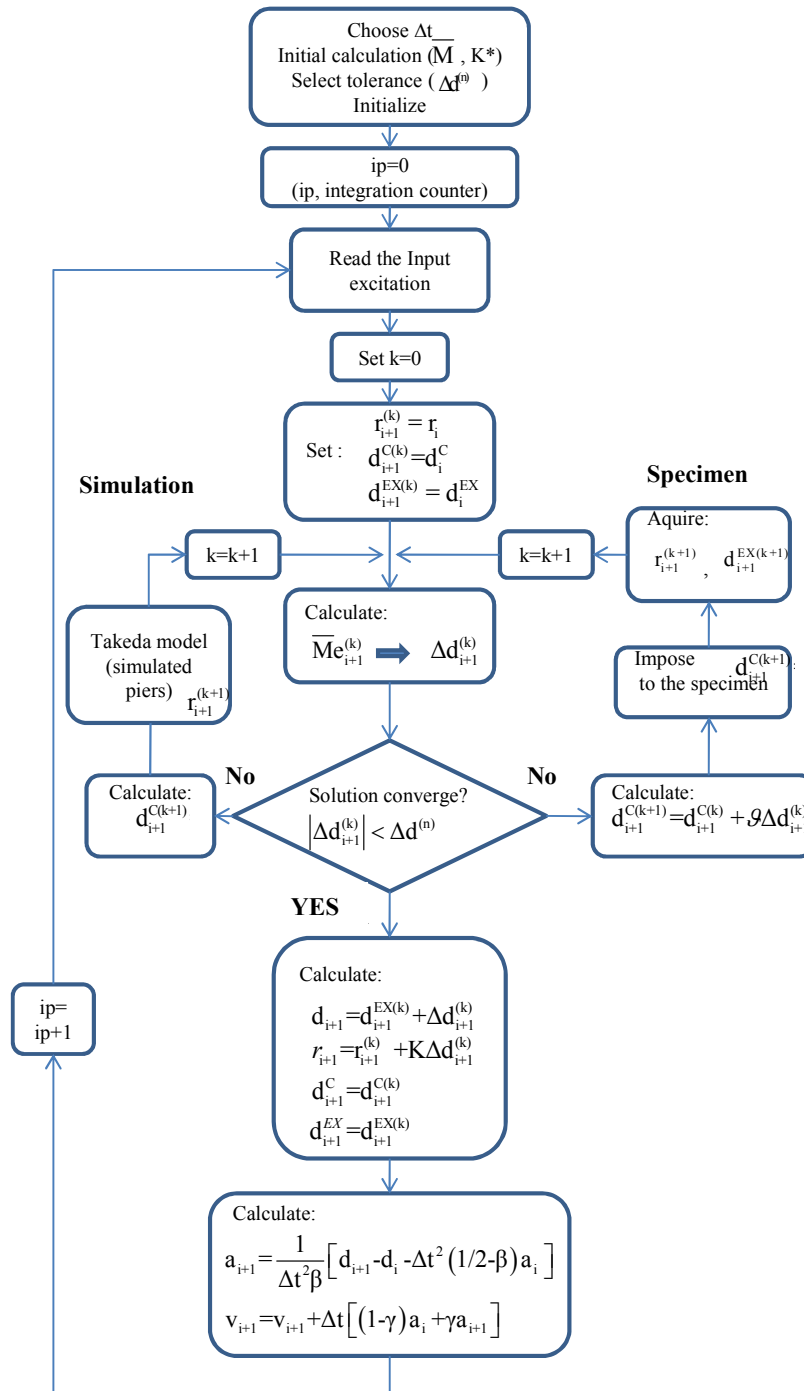


Figure 26 Procedure flow diagram

The tests here presented, were performed using an in-house software and the above method has been successfully implemented in Matlab and Labview.

In the software design phase, it is the general task to consider some important requirements of software such as:

- modularity, the software is composed by some independent components which are separately implemented and tested
- reliability, the software can execute a required task under stated conditions for a specific period of time
- extensibility, the user is able to add some new features to the software in easy way
- robustness, the software manages unpredictable input and can also perform the required task under stress
- usability - the user interface must be intuitive to user and it can provide quick interaction tools

The pseudo-dynamic software is designed to study the seismic response of a bridge structure. In this research a three degree-of-freedom model, one for each nodal point is studied. In particular in this model the degrees of freedom are all in horizontal direction.

The integration procedure described above is implemented using MATLAB while the LabVIEW graphical programming approach is used to communicate with National Instruments hardware of data acquisition device.

In the LabVIEW graphical environment, symbolic icons which represent subprograms, functions or applications are used to perform specific tasks as: to acquire and display data continuously, to compare variables, to generate output signals which are used to control the actuator, to pass the data to MATLAB.

For this later purpose the MATLAB Script Node allows to call upon the MATLAB software to run .m file scripts from LabVIEW.

The first part of the design procedure is clearly define the inputs and outputs.

The input data are loaded as text file and include: the structural model characteristics (masses, stiffnesses, and initial conditions), the integration parameters and the tolerances which are recorded in a specific file and the accelerograms points (temporal series of accelerations) which are stored in another text files.

Instead the selected relevant output include: the number of steps, pseudo-time, horizontal forces, displacements, velocities, accelerations, and restoring force for each degree of freedom which are calculated by numerical procedure and are saved in the output txt file. In particular we remind that the instrument measures are saved in different files in tdms format.

The software is organized in a modular way and the operations are as simple as possible.

First, several dialog boxes are displayed on the screen and prompt users to enter information as specifically required: the input file above and the file to set to zero the instruments patterns.

After the data are loaded, the data acquisition starts and the user can check if they are correct using several graphs which display continuously data in a graphical form. In this way it is sure that all the sensors are reading data correctly and are set to zero before taking reading.

Then if all is well the user pushes the “start” button in the graphical interface and so the numerical integration commences otherwise repeats the above steps or stops to adjust the sensors.

If the integration procedure begins a sequence of instruction blocks are executed in parallel and the pseudo-dynamic test can commence. A block is a list of statements that function as a single unit.

The numerical algorithm is implemented in LabVIEW using the Flat Sequence structure to ensure that an instruction block executes before or after another block

A Flat Sequence structure is divided in several sections or frames which are executed from left to right and only when all data values wired to a frame are available.

A first block sends to MATLAB the input file patterns and a sequence of statements in order:

- to import accelerogram (input seismic ground motion) points, structure data, integration parameter, initial condition, number of integration point, displacement tolerances into the MATLAB
- to compute \bar{M} and K^* with equations () and () and the integration time step Δt

Initial values of position and velocity must be applied to the test specimen before numerical integration commences

In a successive frame two Notifiers which are LabVIEW tools for communicating between two independent parts of a block diagram, send the initial position and velocity to control subprogram. The control program controls the actuator that imposes the displacement on the test specimen. The main program does not go on and waits until the target displacement is reached. In the same frame the reactions of other piers of structures are obtained using a Takeda's model routine written in MATLAB and invokes by Mathscript node.

The Takeda's model is a hysteresis model that is developed by Takeda, Sozen and Nielsen (1970) and used in several nonlinear programs to describe the hysteretic behavior of concrete element.

This model here used to simulate the force-displacement relationships of the piers which are modeled numerically and yielding, hysteresis rules for inner hysteresis loops inside the outer loop, and unloading stiffness degradation with deformation.

Only when the obtain Notifier placed in this code frame, receives the restoring force measured at the target position and MATLAB receives also the reaction of the test specimen, the program goes on.

At this point the initial conditions are imposed at time $t=0$ on the displacement and velocity of the two degree of freedom of bridge model and on the test specimens and the restoring forces are measured for each pier (two Takeda reactions and one actual restoring force of specimens)

Subsequently, in the following frame the integration procedure begins:

- the external excitation force at time integration steps i and $i+1$ are calculated after that the accelerations at these time steps are computed to interpolate between available input data with different time intervals

- the error $\overline{M}e_{i+1}^{(k)} = \overline{M}d_{i+1}^{EX(k)} - \overline{M}\hat{d}_{i+1} + \Delta t^2 \beta (1 + \alpha) r_{i+1}^{(k)}$ is calculated
- the equation (9.4-4) is solved to obtain $\Delta d_{i+1}^{(k)}$

Thus the iterative correction procedure can be applied to minimize the error and to respect the tolerances. This procedure is implemented in next frame. In particular, two cases are considered:

if all the displacement tolerances are respected

$$|\Delta d_{i+1}^{(k)}| < \Delta d^{(n)}$$

the displacements, restoring forces are computed as follows:

$$\begin{aligned} d_{i+1} &= d_{i+1}^{EX(k)} + \Delta d_{i+1}^{(k)} \\ r_{i+1} &= r_{i+1}^{(k)} + K \Delta d_{i+1}^{(k)} \end{aligned}$$

and the acceleration and velocity vectors are calculated as:

$$\begin{aligned} a_{i+1} &= \frac{1}{\Delta t^2 \beta} [d_{i+1} - d_i - \Delta t^2 (1/2 - \beta) a_i] \\ v_{i+1} &= v_{i+1} + \Delta t [(1 - \gamma) a_i + \gamma a_{i+1}] \end{aligned}$$

Finally the integration counter is set to $i+1$ and the numerical integration goes on.

Otherwise set $k=k+1$, where k is the iterative counter and the iterative procedure is repeated. The steps of the iterative procedure are:

- the displacements are calculated using the equation

$$d_{i+1}^{C(k+1)} = d_{i+1}^{C(k)} + \theta \Delta d_{i+1}^{(k)}$$

in which θ is a reduction factor.

- the displacements are imposed on the physical test specimen by actuators and on the two degree of freedom of bridge model.
- the restoring force are measured from test specimen and calculated by Takeda's model for the numerically simulated piers
- the new error is computed and the iterative procedure stops when the tolerances are respected.
- and the acceleration and velocity vectors are calculated as:

$$a_{i+1} = \frac{1}{\Delta t^2 \beta} \left[d_{i+1} - d_i - \Delta t^2 (1/2 - \beta) a_i \right]$$

$$v_{i+1} = v_i + \Delta t \left[(1 - \gamma) a_i + \gamma a_{i+1} \right]$$

Finally the integration counter is set to $i+1$ and the numerical integration goes on.

The user interface is one of the most important parts of any program because it determines how easily it is possible to control the program running.

The interface is very easy to use and provides almost all the options you need and is organized using tab controls that consists of pages and tabs. This control allows overlapping front panel controls and indicators in a smaller area.

In this way several front panel objects are placed on each page of a tab control and the tab is the selector for displaying different pages during a pseudo-dynamic test.

Particular attention must be paid to the setting of this interface structure: some checks must be conducted to ensure that the input data are correct and all the sensors (load cell and position transducer) work correctly before the pseudo-dynamic test.

To organize it well, it is needed to pay particular attention to the applicability and sequence of pages to ensure the pattern is right for test procedure

When the program runs some message windows appear to prompt the user to enter input file name to initialize the integration procedure and to set to zero the sensors reading.

In the first page of tab control, the user can find information on the mean values which are used to set to zero the sensors reading. If the values are correct, the user clicks a control button to proceed or retries to load another input file.

In the second and third pages, several graphs are placed to display data in a graphical form in order to control and to ensure that all sensors are acquiring accurate data during the test. On these screen, the user can see the current reading and the data previously acquired.

During the test the acquired data are displayed on different real time graphs to monitor individually:

- the horizontal restoring force
- the horizontal displacement of the free end of the specimen
- the horizontal displacement of actuator and of two specimen sections in plastic hinge
- the loads for each tendon of the structure that is used to apply the vertical loads
- the footing rotation (vertical displacements of potentiometers placed on footing)
- the vertical displacements of potentiometers located in plastic hinge regions to measure the relative displacements of two section (Figure 67)

- the vertical displacements of potentiometers located in plastic hinge regions to measure the relative displacements of another two section (Figure 67)
- the vertical displacements of potentiometers located in plastic hinge regions to measure the relative displacements of section..... relative to footing
- the horizontal relative displacements between the support points for vertical potentiometers placed in plastic hinge zone.
- the diagonal relative displacements between the support points for vertical potentiometers placed in plastic hinge zone.
- the vertical displacement of actuator
- the horizontal strains of strain gauges placed on the first CFRP ring
- the horizontal strains of strain gauges placed on the second CFRP ring
- the horizontal strains of strain gauges placed on the third CFRP ring
- the horizontal strains of strain gauges placed on the fourth CFRP ring
- the horizontal strains of strain gauges placed on the fifth CFRP ring

The input data are shown in input page of the tab control. In this page the user find information about the mass, stiffness matrix of the structure, the initial condition (displacement and velocity), the displacement tolerances, the integration procedure parameters and the accelerogram is shown in a graphical way.

In a next page, six graphs show in real time the acceleration, the velocity, the applied horizontal force, the restoring force and the displacement which are calculated at each step of the integration procedure.

For convenience, the monitoring of specimen response during testing to check the respect of procedures (convergence tolerance), the velocity of actuator and the correct data transfer between the acquisition, control and main program is performed placing some numeric indicator, graph and led in a specific page of control tab.

Finally the tab structure includes one page to display the response of each degree of freedom (restoring force against lateral displacement).

The rest of the user interface consists in:

- files and folder name views
- indicators to display numeric data, which are acquired or generated (for example the number of integration point, the actual integration point, the number of current iteration to minimize the error at step i)
- the green round led indicator that turns on when the convergence is reached.
- The green square led indicator that turns on when the maximum displacement is reached
- the pause control button used to pause the pseudo-dynamic test at the step i.
- the red stop control button to interrupt pseudo-dynamic test at the step i
- the graphs to display all the accelerogram data and the current input acceleration

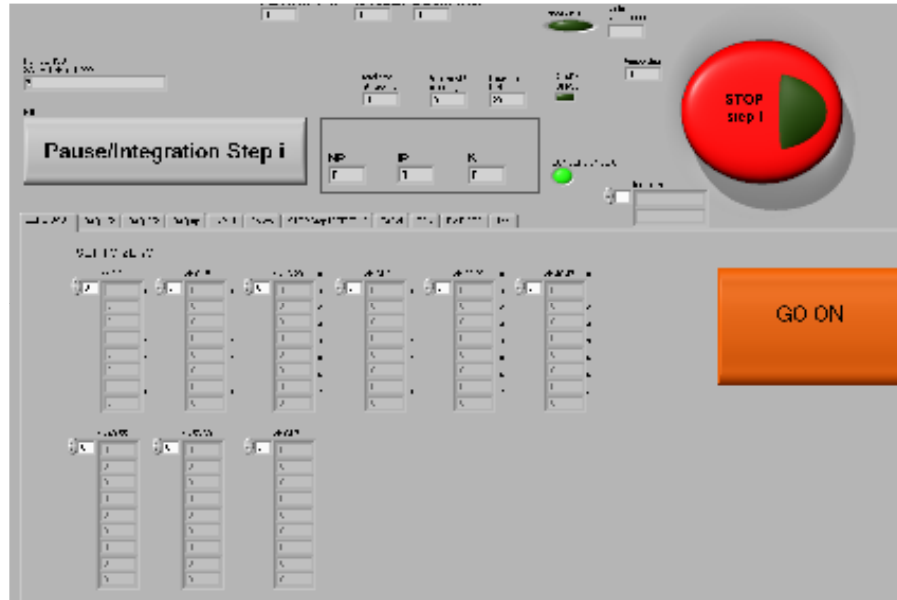


Figure 27 Pseudo-dynamic test software user interface

9.5. Software testing

Software testing is usually the first part of software development process. The software testing procedure is an activity aimed at evaluating capability of a program to perform the tasks for which it was designed. There are a lot of different ways to find software bugs.

So, despite the verification effort, software bugs exist in any software because the complexity of software is generally intractable.

To check if the software works properly the pseudo-dynamic software outputs obtained during a pseudo-dynamic test are compared with outputs of previous version.

The previous program is implemented in FORTRAN language (FORTRAN 77). This program performs numerical simulation of seismic response of bridge using for each pier a Takeda model. More specifically,

the Takeda model describes the lateral horizontal force-horizontal displacement relationship of each pier.

In the first one, the test specimen response to imposed displacements measured during the selected pseudo-dynamic test is sufficiently approximated by Takeda model

Then it is possible to obtain a sufficient approximation of specimen behaviour during the test using the various calibration curve options which are available for Takeda model (stiffness, yielding force, hardening, degradation stiffness factor). The good agreement achieved is the one presented in **Figure 28**.

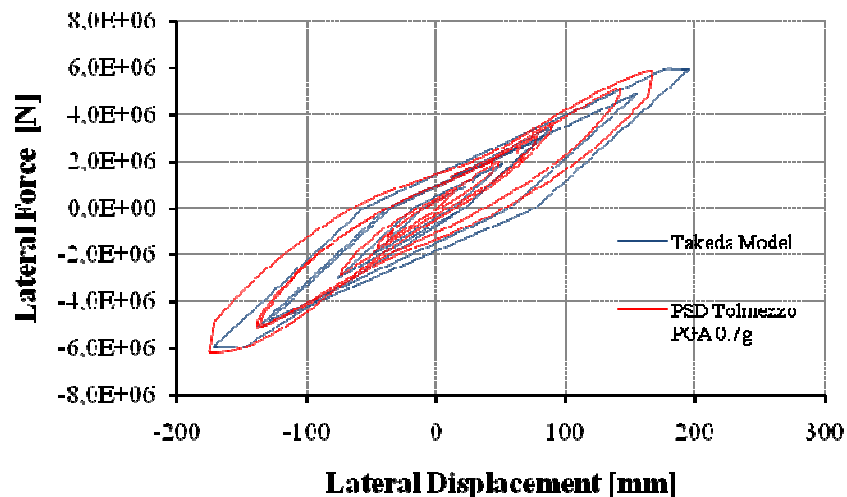


Figure 28 Comparison between the Force-Displacements cycles of the piers (7m) during pseudo-dynamic test and Takeda Model approximation.

Then nonlinear dynamic analyses were carried out for the analytical model of the bridge using the same input file (integration parameters, structure data...) and input ground motions in order to determine if the pseudo-dynamic test system works correctly.

Figure 29, Figure 30, Figure 31 show the comparison between the displacements of each degree of freedom of bridge obtained by the numerical simulation and by the pseudo dynamic test.

Finally, all three curves, one for each degree of freedom, obtained by numerical simulation give a general good agreement with the results of pseudo-dynamic test.

For sure, a better agreement can be achieved using a better numerical model to simulate the specimen response.

The close agreement of curves supports the consideration that the system provides reliable results and accurately describes the response of test structure.

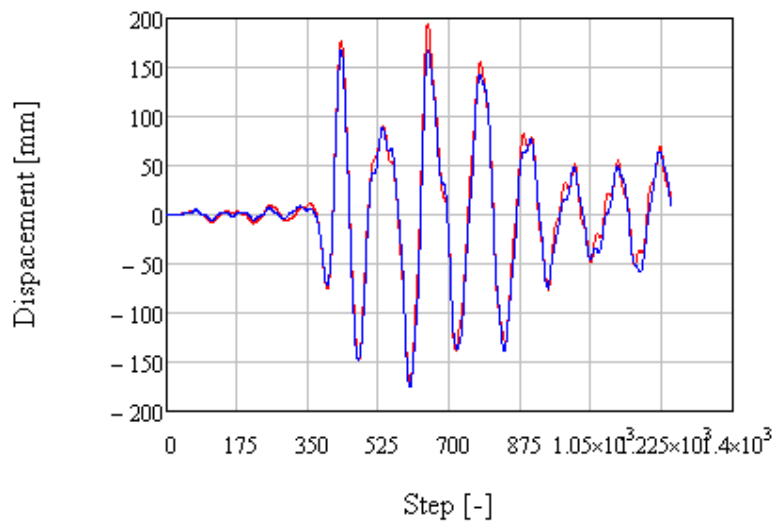


Figure 29 Displacement history of piers 7m; simulated by previous pseudo-dynamic test software (red line), during the pseudo-dynamic test

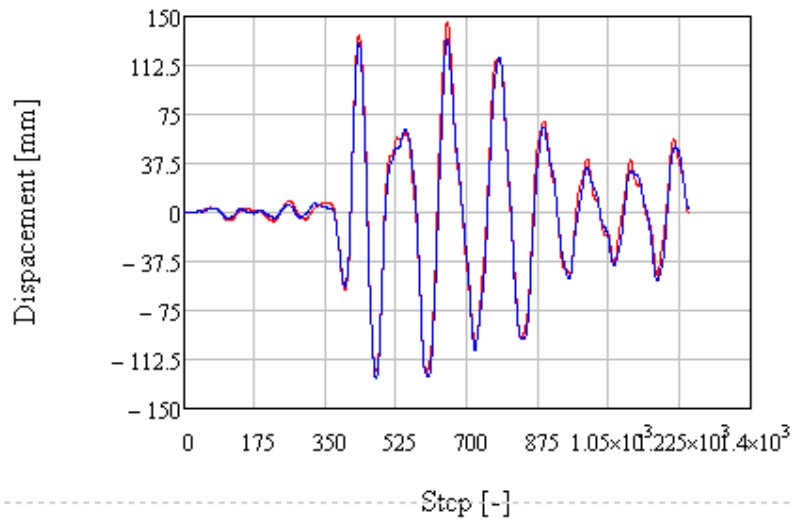


Figure 30 Displacement history of piers 14m; simulated by previous pseudo-dynamic test software (red line), during the pseudo-dynamic test

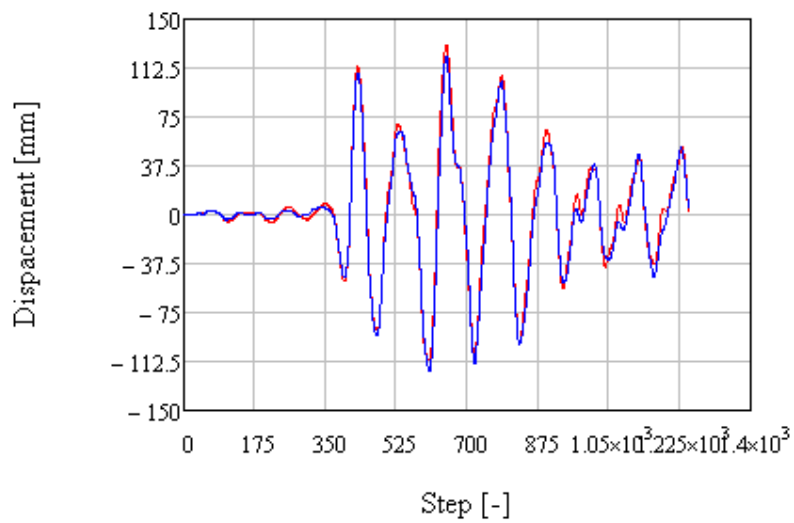


Figure 31 Displacement history of piers 21m; simulated by previous pseudo-dynamic test software (red line), during the pseudo-dynamic test

Moreover a comparison of force-deformation relationship measured by means of the pseudo-dynamic test equipment during a pseudo-dynamic test and the force-deformation relationship measured using different test equipment during a cyclic test on the same specimen is carried out to verify conformance and check correct functionality of the pseudo-dynamic test equipment. **Figure 32** shows good agreement between the experimental data.

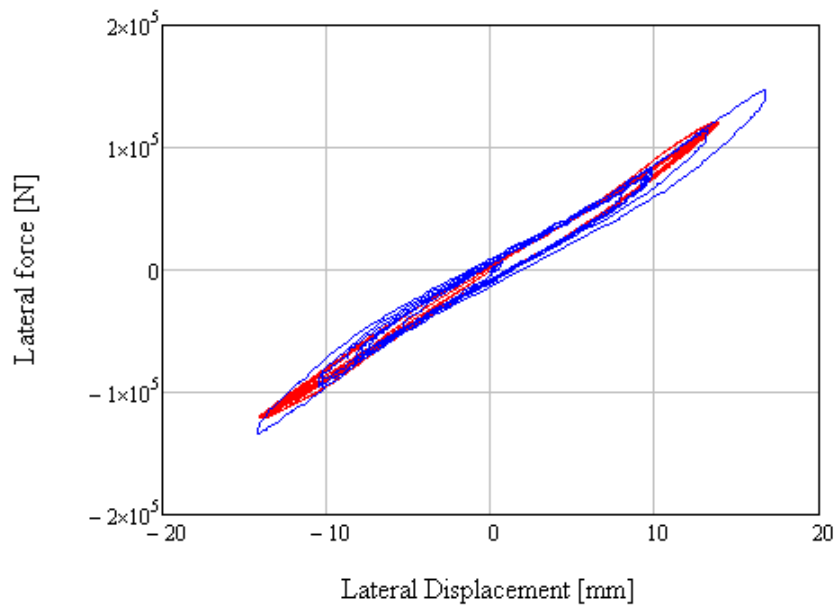


Figure 32 Behavior of the specimen 7 during a previous elastic test (red line) and during the pseudo-dynamic test (blue line)

10. Test equipment

The test equipment, schematically shown in Figure 33, Figure 34 is composed by:

#1: system for the application of vertical loads at the top of the specimen: the specimen is placed within a testing frame realized using a transverse spreader beam which is linked to the ground by means of two $\varnothing 47$ mm Dywidag rods, one on each side of the specimen, with hinged connections. The axial load is applied by prestressing the two rods by mean of two 1000 kN Hollow Plunger Cylinders, which are inserted in a cage bordered by four $\varnothing 26.5$ mm Dywidag rods and two hollows steel plates, the upper reaction one and the plate connected to the hinge.

#2: system for the application of horizontal loads and displacements: a 500 KN electromechanical actuator (stroke ± 200 mm), connected on one side to the top of the pier and on other side to a reaction wall, is used to impose displacements or loads to pier;

#3: ground anchorage system: the specimen footing is restrained to the laboratory strong floor using two transverse beams fixed to ground with steel tendons to avoid base horizontal displacements and rotations;

#4: control system and data acquisition: a closed loop control system governs the movement of the actuator by means of LVDT (stroke ± 200 mm), data acquisition system and control LabVIEW virtual instrument. The hardware of the data acquisition system is composed by the following components: NATIONAL INSTRUMENTS NI PCI 6281, High-Accuracy M series Multifunction DAQ 18-Bit, up to 625 kS/s, 9 modules NI SCXI 1520 Universal Strain Gauge Input Module with 8 Channels, ,with software LabVIEW Full System.

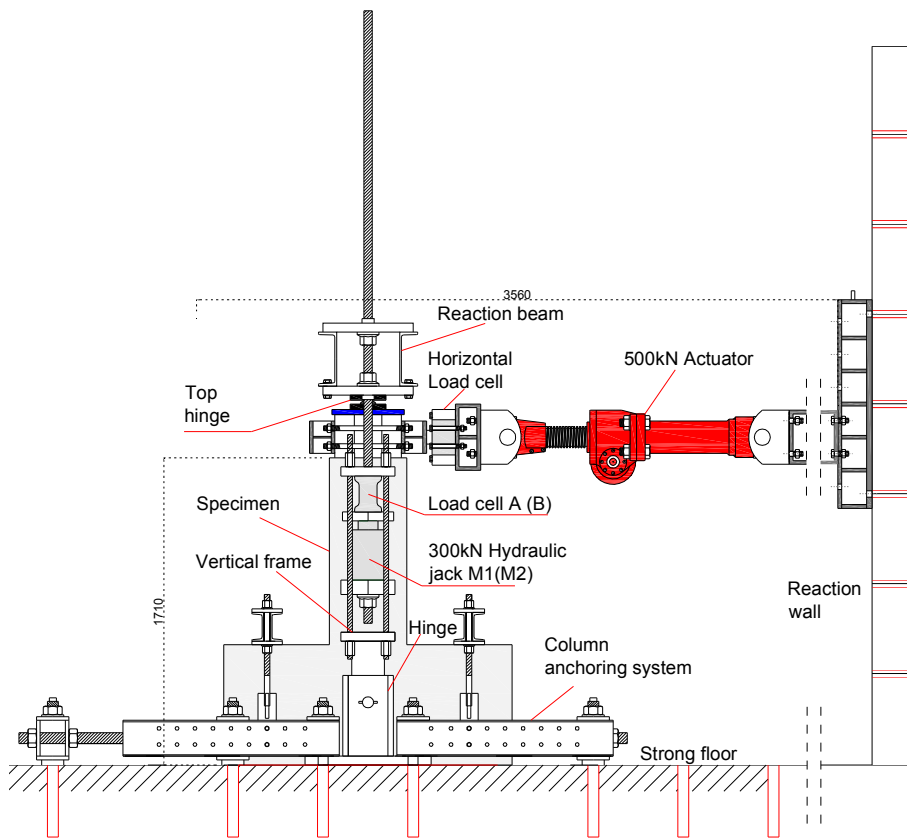


Figure 33. Test equipment

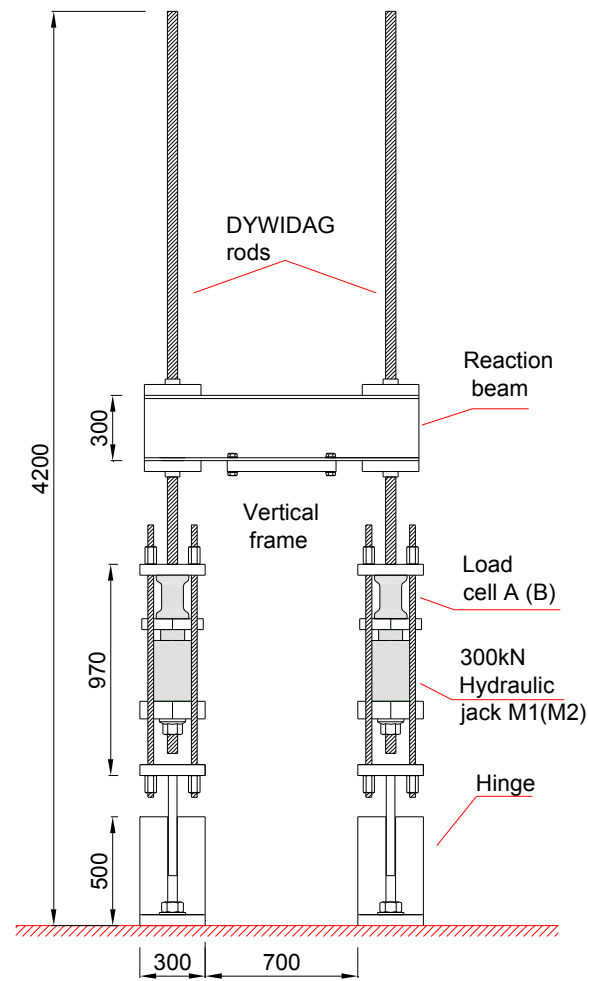


Figure 34. Test equipment: vertical frame (mm)

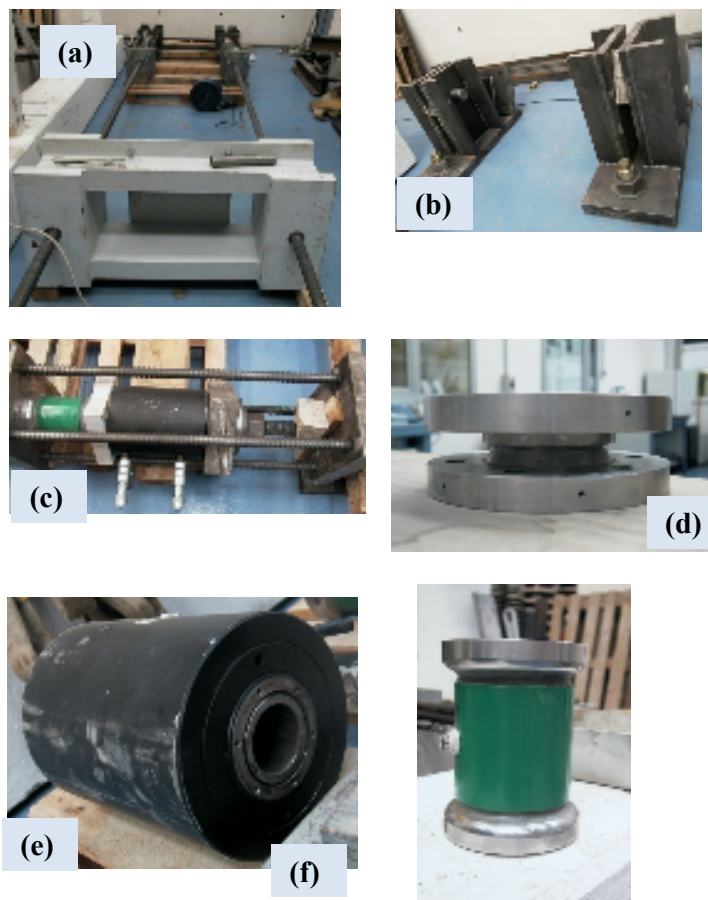


Figure 35. Test equipment: (a) vertical frame, (b) hinges constrains, (c) load system, (d) top hinge, (e) hydraulic jack, (f) load cell.

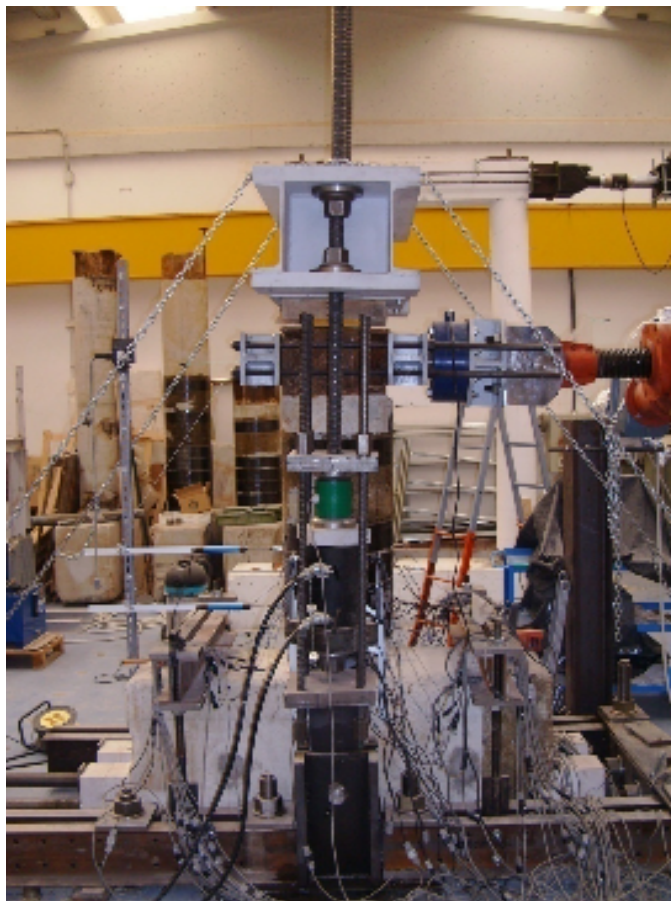


Figure 36. Test equipment real Side view

Extensive instrumentation, providing 72 channels of data, was used to monitor the response and the local deformations of the specimens

The instrumentation plan for the specimens included three basic types of instrumentation: load cell (load transducer), potentiometer (position transducer) and strain gauges (strain transducer).

In each test a total of 72 measurements were taken: on horizontal cell, two vertical cells, potentiometers and strain gauges.

The majority of the instrumentation was placed on the critical zone in one of four vertical instrumentation lines. From the base of the column up to 500mm in height it could be considered critical zone ("plastic hinge zone").

Most instrumentation was located along vertical instrumentation lines: twelve linear potentiometers are used for the acquisition of vertical displacements of three different pier sections (channels from 2 to 13) in order to estimate their curvature along the height.

The instrumentation included twelve diagonal potentiometers (six on each lateral side) to capture the shear deformation in plastic hinge zone. Two potentiometers were attached to the bottom footing to measure vertical displacement of the foundation. Additionally two horizontal potentiometers were located along the height of the specimens respectively at the height 230mm, 450mm. The loading point of each column was placed at 1170 mm and control displacement at the end of the pier was measured on opposite sides along the same horizontal line. However, it is also necessary to position a vertical transducer over actuator body to detect vertical movement. Figure 33, Figure 34, Figure 35, Figure 36 shows the test setup and instrumentation plan for specimens 8. One potentiometer was available to measure directly the screw translation.

Six horizontal potentiometers are used to measure the relative displacement between the supports of the above vertical transducer fig.

Two 1000kN(400bar) hollow load cells, between the axial load hollow jacks and the upper steel plate of the cage near the hinge end, measure the axial load in tendons. Finally, 1000kN pancake load cell was used to measure the horizontal load applied to the specimen at the load point. The instrumentation plan for specimens 6 and 8 was similar to specimen 7 but more extensive: strain gauges were attached on discontinuous CFRP strips and were used at various locations on the surface to monitor local strains and to capture the rupture strains. The horizontal load measured with a load cell was applied with variable velocity.

32 horizontal strain gauges are placed on the FRP wrapping to measure the longitudinal deformation of the FRP fibers. The disposition of the strain gauges is shown Figure 40 and Figure 41.

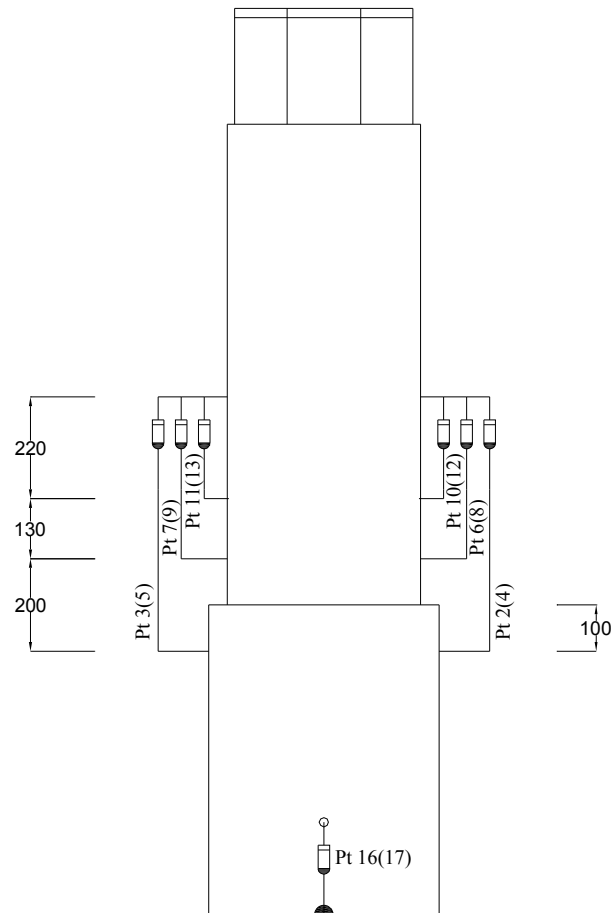


Figure 37. Disposition of the Vertical potentiometers (mm)

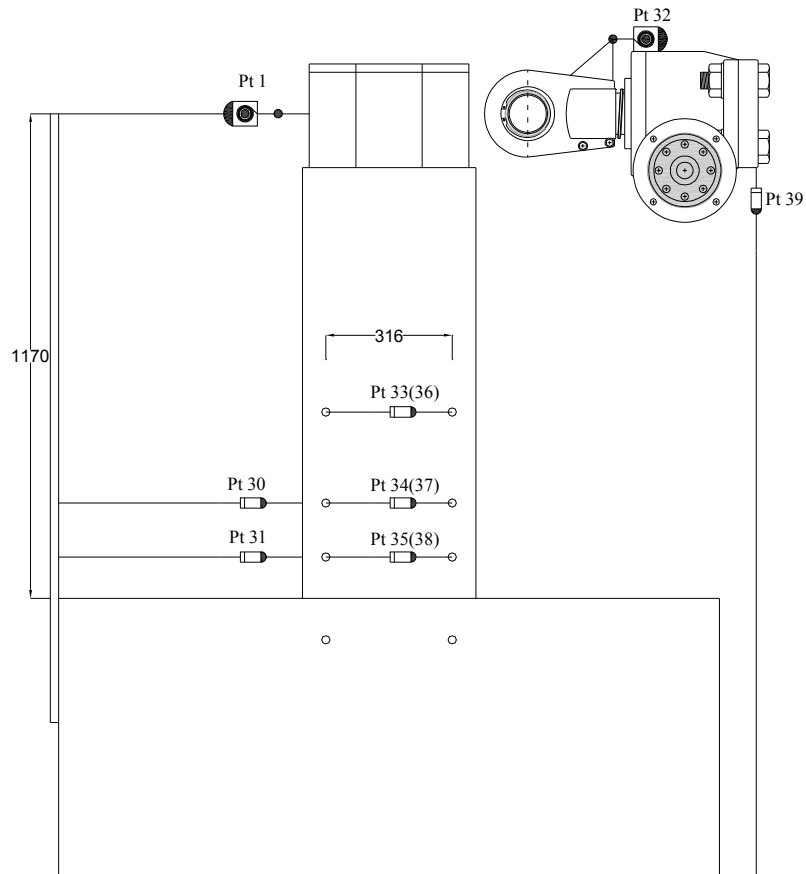


Figure 38. Disposition of horizontal potentiometers (mm)

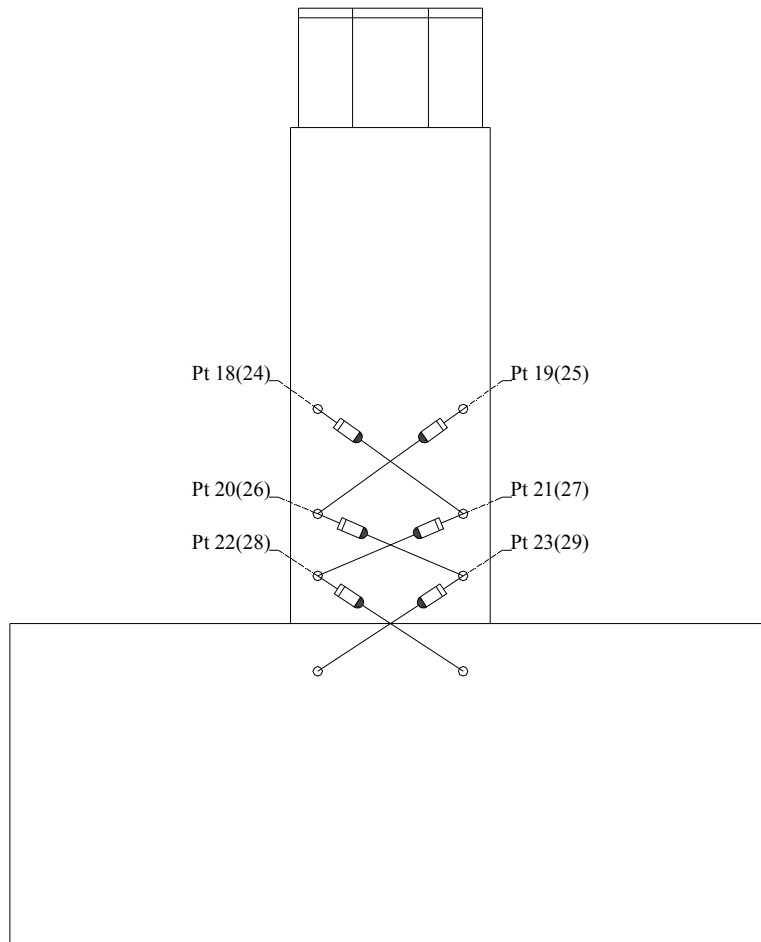


Figure 39. Disposition of diagonal potentiometers

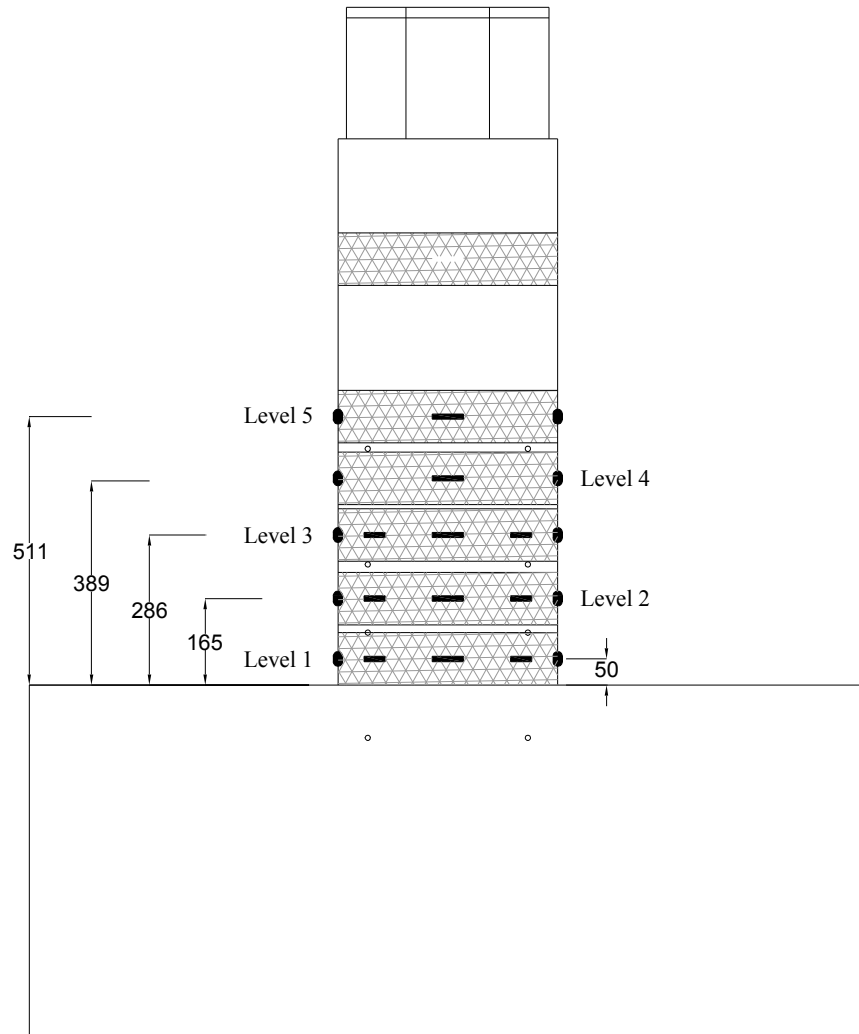


Figure 40. Disposition of strain gauges on CFRP wrapping (mm); side view.

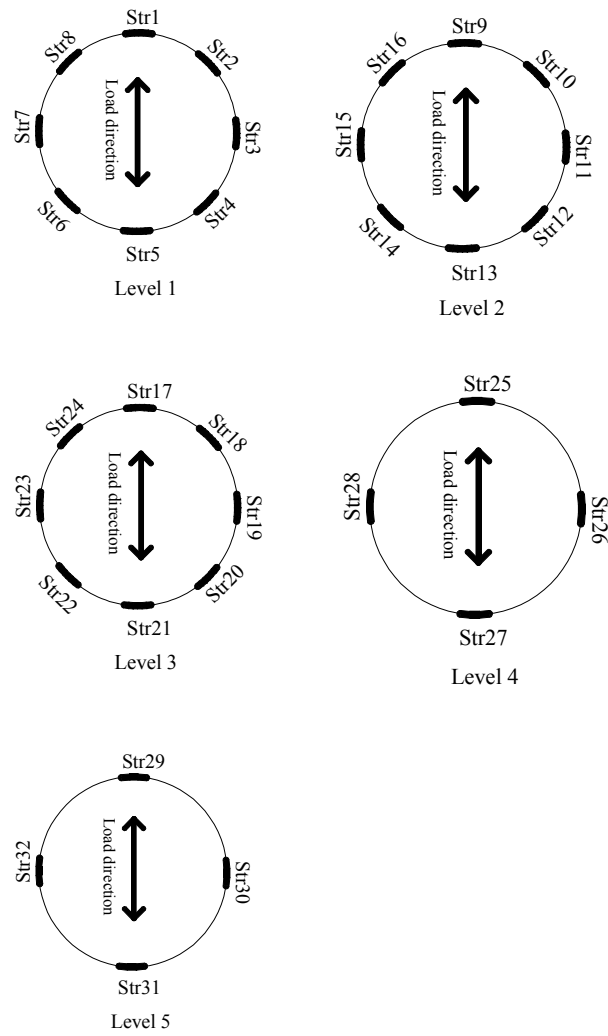


Figure 41. Disposition of strain gauges on CFRP wrapping; cross section view

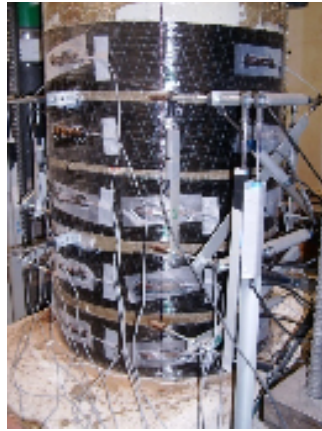


Figure 42. Disposition of strain gauges on CFRP wrapping.



Figure 43. Acquisition system

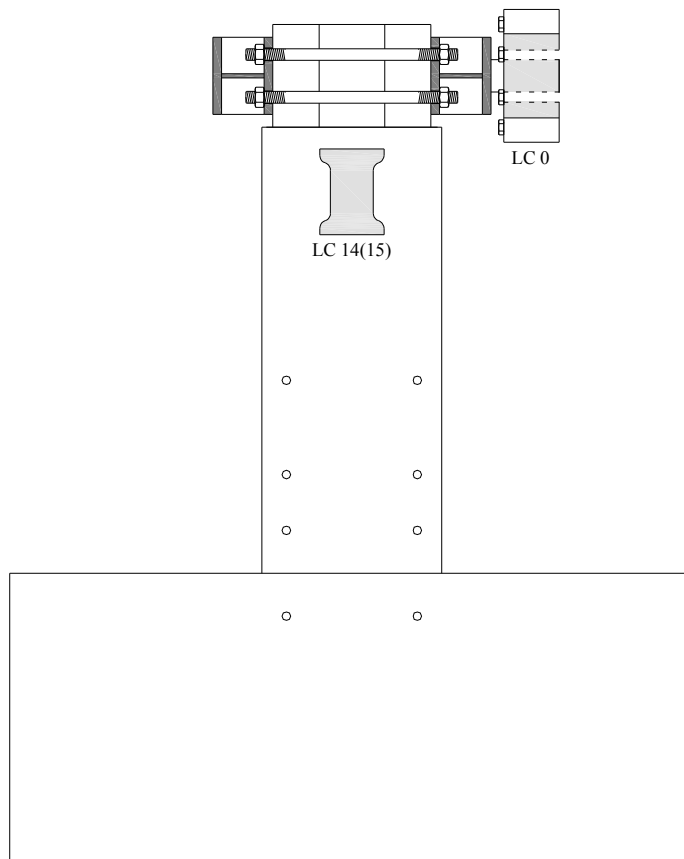


Figure 44. Load cells. The load cells Lc 14 and 15 measures the axial load applied at the top of the specimen whereas the load cell LC0 measures the horizontal restoring force.

11. Experimental results

In this section, experimental results of the present investigations are presented. These results are obtained performing:

- free oscillation tests to determine the specimen stiffness
- pseudo-dynamic tests to study the seismic response of specimen
- cyclic tests to evaluate the maximum response of specimen

In particular, this chapter describes the seismic response of a damaged specimen already tested in previous experiments [52] and the seismic behavior of a repaired and retrofitted specimen, the pier 8, using above techniques.

Next, it will report on some experimental results of the research project: the seismic response of the real scale bridge and the behavior of the test specimen.

It is important to remind that the geometry scale factor between the specimen and the real bridge is $1/6$ while the force scale factor is $1/36$.

The vertical axial load which is applied at the top of the squat specimen (specimen 7 and 8) is equal to 258kN during pseudodynamic and cycles test.

11.1. Free oscillations

First, a free oscillation test is performed to calculate the initial stiffness of the specimen.

This parameter value is necessary to carry out the pseudo-dynamic test. In fact it is used to initialize the stiffness matrix of the bridge and to execute the iterative procedure in order to minimize the error at the step i . Moreover, this test also provides information about the system damping. The test is carried out using the pseudo-dynamic software.

In particular a dynamical system with only one degree of freedom is considered and the initial conditions are selected to impose displacements on the specimens of less than 4mm. The integration parameters are the same used in pseudo-dynamic test.

The pier mass is concentrated at the top and is equal to the mass concentrated at deck level that results from the lumping of the bridge mass to the nodes.

Finally elastic test can be used to check the sensors reading and to complete the equipment setup.

11.1.1. Observations

The discussion explains the observations about the equipment setup and the measured results during preliminary test. These preliminary tests can provide some useful information which can be used to improve the test equipment without damaging the specimen. It is possible to check the sensors reading and to verify the restraint system.

In addition the unwanted load and/or displacement can be compensated successfully.

11.1.1.1. Pier 7

Some preliminary tests are carried out to evaluate the difference in the displacement measures of the top of the specimen by means of a potentiometer which is constrained to independent support structure near the specimen or to specimen footing. To eliminate the footing rotation contribution to the horizontal displacement of the top of the pier is used the latter solution for each test.

11.1.1.2. Pier 8

The foundation footing is irregular. A new footing is cast directly against the laboratory floor in order to eliminate the surface irregularity. The construction process comprising the steps of:

- creating a mold on laboratory floor
- pouring wet concrete into the mold
- positioning the specimen
- letting the concrete harden

11.1.2. Horizontal-Force Drift-Deformation Response

This chapter describes the relationship between the restoring force and the horizontal displacement of the specimens.

11.1.2.1. Pier 7

Figure 45 shows the force-displacement relationship of real scale pier 7 during free oscillations elastic test. It is clear that the behavior of the specimen is essentially elastic. The maximum displacement is equal to about 23mm while the maximum force is of about 1320kN. The calculated initial stiffness is of about 60000 N/mm. This value is in accordance with the value calculated using the results of previous elastic test and is a better approximation considering both the direction of load application.

The previous elastic tests are executed by means of different test equipment. The equivalent damping is calculated using the following expression:

$$\xi = \frac{1}{2\pi n} \ln \left(\frac{u_i}{u_{i+1}} \right) \quad (0.1)$$

In which n is the number of cycles, u_i the value of the maximum displacement at cycli i and $i+1$ respectively. The damping is of about 4%-6%. It is the only damping of the system

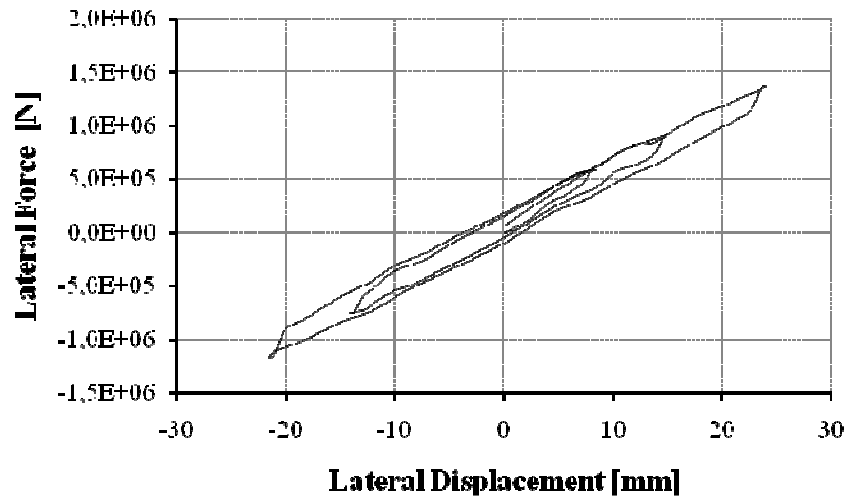


Figure 45 Irregular bridge central pier – free oscillations – Force-Displacement cycles (real scale)

11.1.2.2. Pier 8

The results plotted in Figure 46 show the force-displacement relationship of real scale pier 8 during free oscillations elastic test. These plots bring out the general elastic behavior of the specimen.

It is observed an initial value of force of about 700kN at horizontal displacement zero. This compression force applies a horizontal displacement in positive direction and is sufficient “to translate” the curve in positive direction. At the end of the test a residual displacement of about 11mm is observed. The maximum displacement is equal to about 43,7mm while the maximum force is of about 2900kN in positive direction. The restoring force increases until to reach an approximately value around 1870kN at about 14mm toward the negative direction. The equivalent damping is calculated using the above expression and it is of about 8%. Finally, the calculated initial stiffness is of about 77000 N/mm.

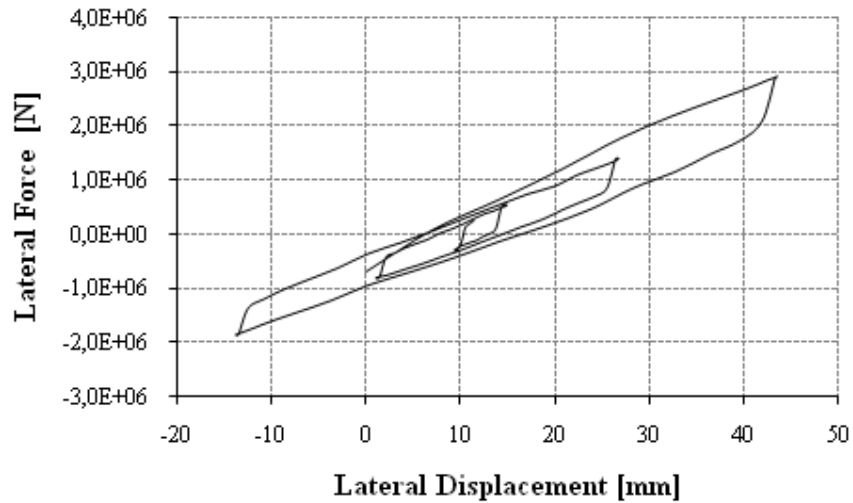


Figure 46. Repaired irregular bridge central pier – free oscillations – Force-Displacement cycles (real scale)

11.2. Pseudo-dynamic test

Since repairing and retrofitting technique used in this research program aims to improve the global seismic behavior of bridge, it is of particular interest to see how it will affect the bridge system response. To answer the question, a series of pseudo-dynamic tests were conducted to investigate the system response of a bridge under transverse earthquake excitations. The test were performed using the same accelerogram used previous test and using the same accelerogram scaled to 2 (2 times) with the objective of obtain large displacements.

11.2.1. Horizontal-Force Drift-Deformation Response

This chapter describes the relationship between the restoring force and the horizontal displacement of the specimens.

11.2.1.1. Pier 7

The dynamic response of specimen 7 is plotted in Figure 47. The ground motion of the 1976 Friuli earthquake recorded at Tolmezzo is used as input excitation. The maximum restoring force is equal to 5311kN and corresponds to the maximum displacement applies of 100mm in the positive direction. When the movement direction is opposite, the maximum force measured is 4819kN at a displacement of 85mm. The hysteretic behavior is then symmetric. The loops do not show degradation of stiffness. However, at a displacement of approximately 40mm the stiffness slightly increases in both directions. A few small diagonal cracks appear on the side of specimens. Although the specimen has already been damaged during a previous test, there is no evidence of plastic deformation.

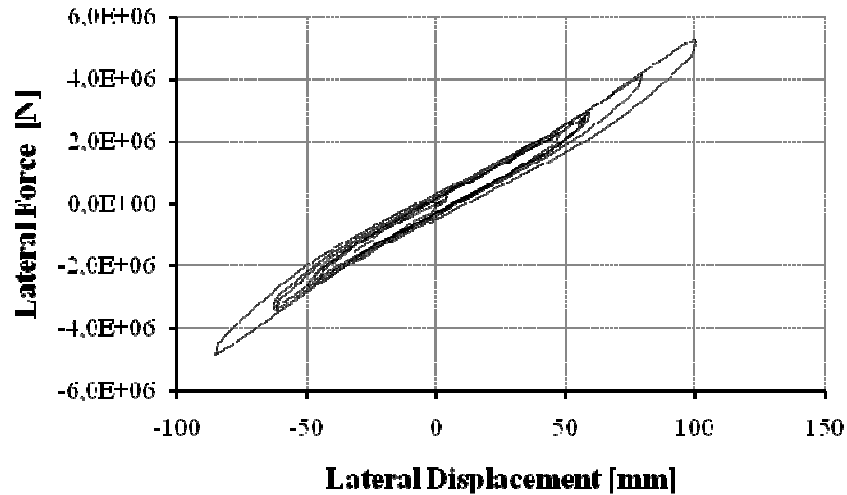


Figure 47 Irregular bridge central pier - pseudo-dynamic test Tolmezzo PGA=0.35g Force-Displacement cycles (real scale)

During the first test the specimen 7 exhibited moderate cracking. Refer to the pier base section the pre-existing crack width increased. However, there was no spalling. Rather new orthogonal cracking was apparent on the surface along the height of piers in the critical zone, which was probably due to flexural tension and compression. The preexistent cracks spread and reached the side surface. However the base crack quickly localized with moderate propagation of the other cracks. The failure was typical of a flexure-shear failure mode. Small diagonal cracks occurred on side.

Figure 48 shows the horizontal displacement of the top of the piers during the pseudo-dynamic test. The displacement history imposed on each pier can be divided in three parts:

- a first time interval of about 1,2s during which the displacements are modest
- a next time interval of about 3,5s, during which three successive cycles of displacements are imposed. The maximum displacement of 100mm is applied to central pier (pier height 7m) here.

- finally for about 3,6s, the displacement amplitude of the system is the same in all three cycles. However, during this time-interval the displacement is less than the maximum displacement and for the central pier is equal to about 50mm.

The displacement histories of each pier are always in phase

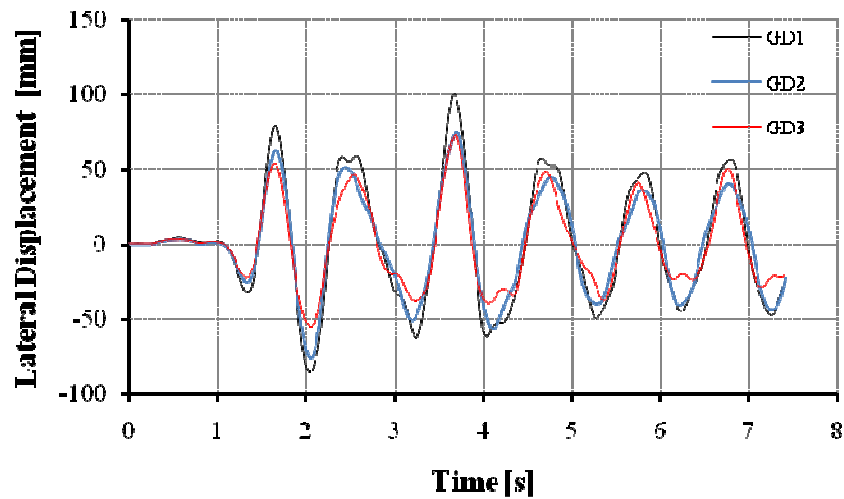


Figure 48 Irregular bridge, all piers - pseudo-dynamic test with Tolmezzo PGA=0.35g displacements time history; GD1 central pier (7m), GD2 lateral pier (14m), GD3 lateral pier (21m).

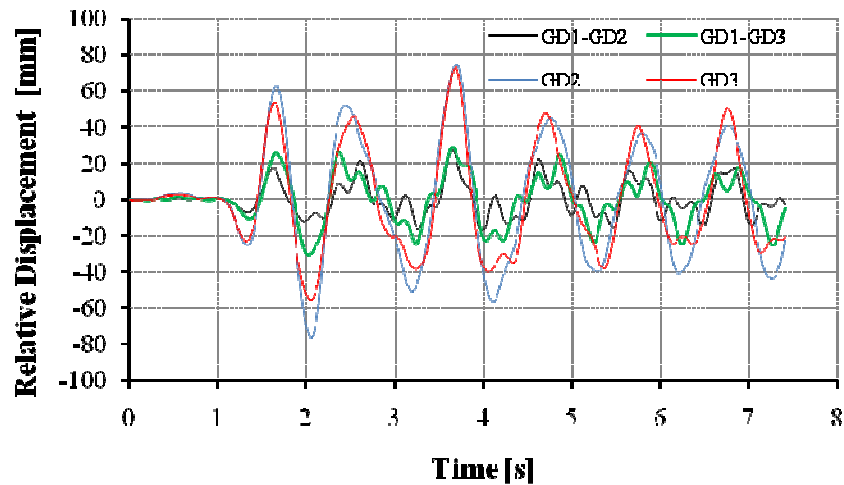


Figure 49 Irregular bridge, all piers - pseudo-dynamic test with Tolmezzo PGA=0.35g
Relative displacements time history: GD1-GD2 between the piers GD1 and GD2, GD1-GD3 between the piers GD1 and GD3, GD2 between the pier GD2 and the near abutment, GD3 between the pier GD3 and the near abutment.

Figure 49 shows the relative displacement between piers and between pier and abutment. In particular it is interesting to calculate the relative displacement between:

- the lateral pier (pier height 21m) and the central pier (pier height 7m)
- the lateral pier (pier height 21m) and the near abutment
- the lateral pier (pier height 14m) and the central pier (pier height 7m)
- the lateral pier (pier height 14m) and the near abutment

The maximum relative displacement was measured between the lateral pier (pier height 21m) and the near abutment. In the second pseudo-dynamic test the specimen was subjected to a new input excitation: the ground motion of the 1976 Friuli earthquake recorded at Tolmezzo scaled

up to two times is selected as input excitation. In Figure 50, the dynamic response of specimen 7 is plotted versus time.

The maximum restoring force is equal to 6274kN and corresponds to the maximum displacement applies of 167mm in the positive direction. When the movement direction is opposite, the maximum force measured is 6171kN at a displacement of 176mm. The hysteretic behavior is then symmetric.

The degradation of stiffness with lateral movement is observed during the test. After the test, the stiffness decreased to 67 percent of its initial stiffness.

As the amplitude of displacement increases beyond 100mm for both load directions, yielding is observed to occur.

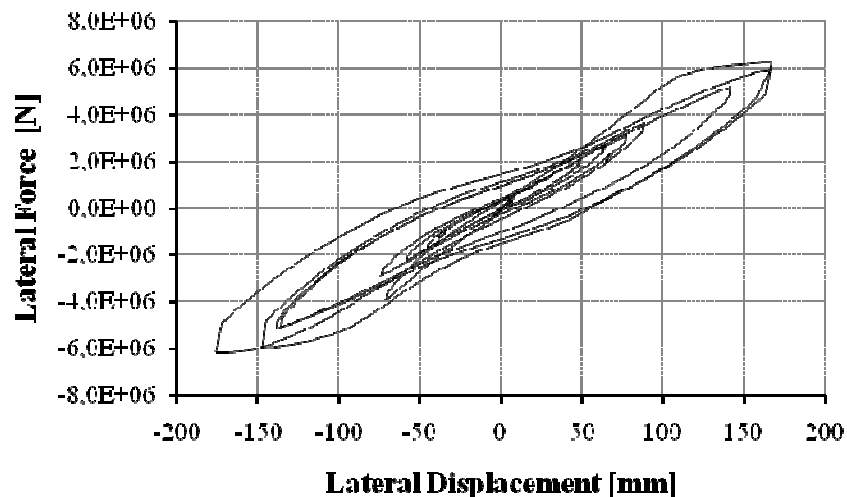


Figure 50 Irregular bridge central pier - pseudo-dynamic test Tolmezzo PGA=0.7g Force-Displacement cycles (real scale)

The majority of the cracking has been found at locations near the pier base where the localized main crack increased in width. Furthermore some vertical cracks initiated at the base of the specimen, propagate vertically. These vertical cracks could appear due to the instability of longitudinal bars.

During the test it is observed that lateral shear diagonal cracks spread continually and the shear cross cracks width on the right side increases

more than others. In addition the preexistent cracks spread and the dimensions of the forming cracks increase in the plastic hinge zone.

However, it can be seen that damage is concentrated at the base with moderate propagation of the other cracks. The failure was typical of a flexure-shear failure mode.

Figure 51 shows the horizontal displacement of the top of the piers during the pseudo-dynamic test (real scale). The displacement history imposed on each pier can be divided in three parts:

- a first time interval of about 3,6s during which the displacements are limited to about 9mm
- a next time interval of about 4,7s, during which four successive cycles of displacements are imposed. The maximum displacement of 167mm is applied to central pier here.
- finally for about 3,7s, the displacement amplitude of the system is similar during the cycles. However, during this time-interval the displacement is less than the maximum displacement and for the central pier does not exceed 72mm.

The displacement histories of each pier are always in phase.

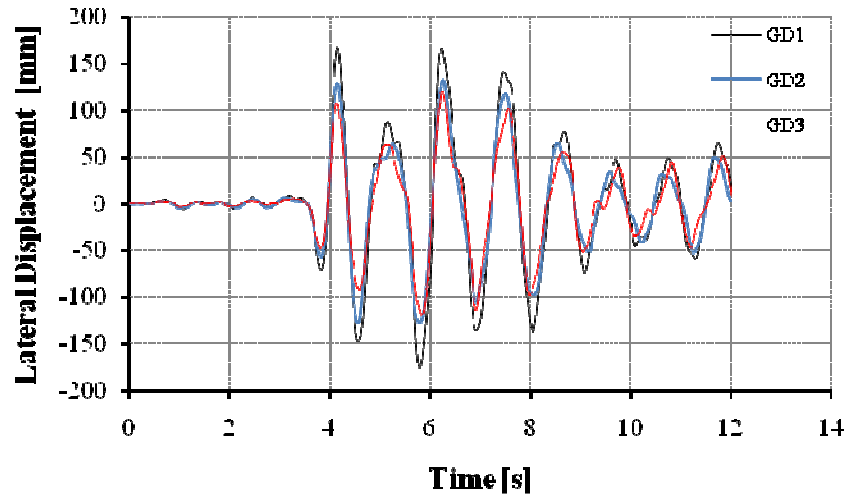


Figure 51 Irregular bridge, all piers - pseudo-dynamic test with Tolmezzo PGA=0.7g displacements time history; GD1 central pier (7m), GD2 lateral pier (14m), GD3 lateral pier (21m).

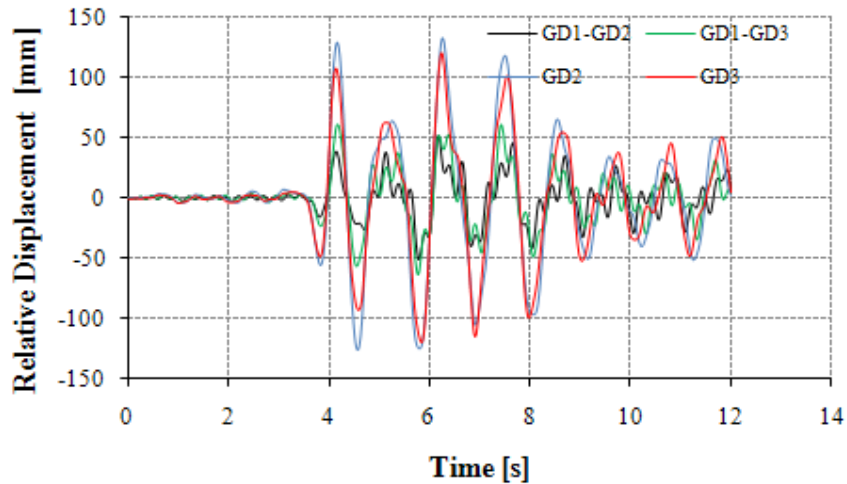


Figure 52 Irregular bridge, all piers - pseudo-dynamic test with Tolmezzo PGA=0.7g Relative displacements time history: GD1-GD2 between the piers GD1 and GD2, GD1-GD3 between the piers GD1 and GD3, GD2 between the pier GD2 and the near abutment, GD3 between the pier GD3 and the near abutment.

Figure 52 shows the relative displacement between piers and between pier and abutment. In this figure, the curves are plotted to focus attention on the relative displacement between abutment and pier and between adjoining piers.

The maximum relative displacement was measured between the lateral pier, (pier height 21m) and the near abutment.

11.2.1.2. Pier 8

The seismic behavior of specimen 8 during the first pseudo-dynamic test is plotted in Figure 53. The ground motion of the 1976 Friuli earthquake recorded at Tolmezzo is used as input excitation.

Unfortunately, it is necessary to keep in mind that the force reading from the horizontal load cell is set to zero during the initial setup of equipment whereas the load is already equal to about 18kN.

This initial load maybe is due to the eccentricity of the vertical force application. In fact the cap of the specimen is inclined slightly and even if it is used a hinge support system for holding the vertical system for the application of vertical loads, this load is introduced by the test equipment.

The maximum restoring force is equal to 5177kN and corresponds to the maximum displacement applies of 72,5mm in the positive direction.

When the displacement direction is in negative direction, the maximum force measured is 2843kN at a displacement of about 75,5mm while the maximum displacement reached is 107,8mm and the corresponding restoring force is equal to about 2600kN.

In particular it is evident as the stiffness decreases significantly after a displacement of about 30mm in negative direction. Then the restoring force reaches a plateau and the horizontal load drops of about 200kN at the displacement of 98mm in the same direction.

Immediately afterwards the response of the specimen is asymmetric in tension and compression. The stiffness of specimen changes in the negative direction and remains practically the same during the next cycles. The ratio between the stiffness of the pier in negative and in positive direction is equal to about 0.58.

Subsequently, the loops show only a slightly degradation of stiffness and cycles area is narrow.

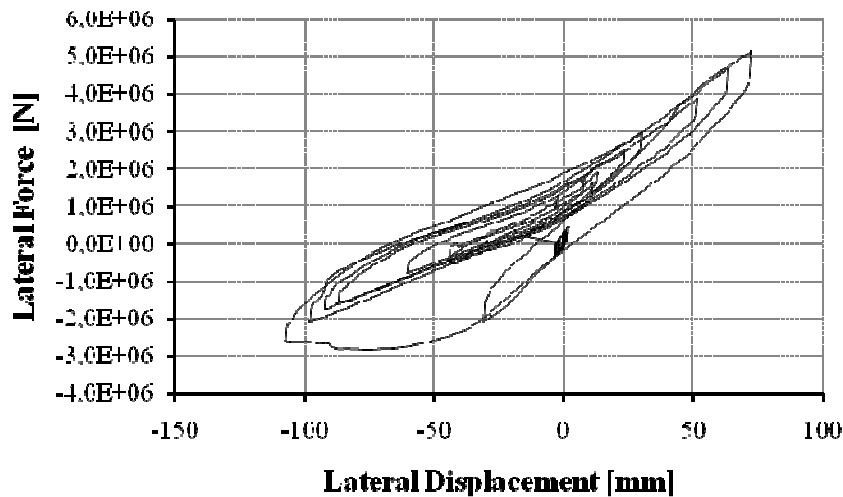


Figure 53 Repaired Irregular bridge central pier – first pseudo-dynamic test Tolmezzo PGA=0.35g Force-Displacement cycles (real scale)

It is noted that damage concentrated at the base of the specimen where the localized main crack increased in width during the test. Some portions of the concrete footing surface breaks away or raise up near the base of the specimen.

It is difficult to see other cracks on the surface of the specimen because of the FRP layers. However some narrow vertical cracks appear at the base of the specimens between the strips of FRP.

It is necessary to repeat the same test because of the above error. In fact the specimen does not undergo marked changes and the damage is modest, not serious.

For this test, the accelerogram of the 1976 Friuli earthquake recorded at Tolmezzo is selected again as input excitation.

At the beginning of the test, the specimen is constrained making attention to eliminate any unwanted loads from being applied to the specimen.

The seismic response of specimen 8 during the pseudo-dynamic test is plotted in Figure 54.

The maximum restoring force is equal to 4794kN and corresponds to the maximum displacement applies of 86,8mm in the positive direction.

When the displacement is in negative direction, the maximum force measured is 2808kN at the maximum displacement of about 92,7mm. The stiffness of specimen is different in the two directions and remains practically the same during the next cycles. The initial ratio between the stiffness of the pier in negative and in positive direction is equal to about 0,53.

It is evident as that a sequence of displacements applied to the specimen in positive direction produces degradation of stiffness whereas the stiffness does not decrease significantly in the negative direction even after several cycles of displacement.

It is possible to explain this by assuming that the damage at the base is more pronounced at the beginning on one side.

Note that the asymmetric disposition of new longitudinal bars primarily may influence the plastic range behavior while should have a very subdued effect on elastic range displacement. However it maybe is due to damage of anchorage where the welding is being done.

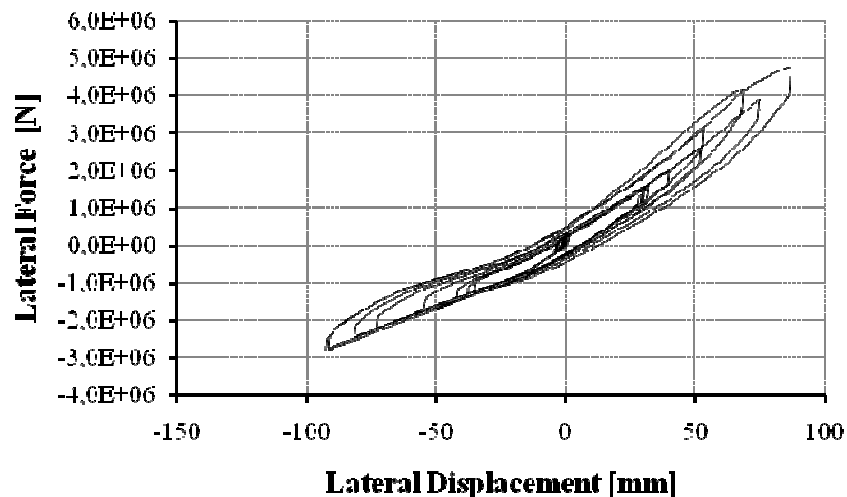


Figure 54 Repaired Irregular bridge central pier – second pseudo-dynamic test Tolmezzo PGA=0.35g Force-Displacement cycles (real scale)

Figure 55 shows the horizontal displacement of the top of the piers during the pseudo-dynamic test (real scale). The displacement history imposed on each pier can be divided in three parts:

- a first time interval of about 3,6s during which the displacements are limited to about 5 mm
- a next time interval of about 4,8s, during which four successive cycles of displacements are imposed. The maximum displacement of about 93mm is applied to central pier here.
- finally for about 3,7s, the displacement amplitude of the system is similar during the cycles. However, during this time-interval the displacement is less than the maximum displacement and for the central pier does not exceed 52mm.

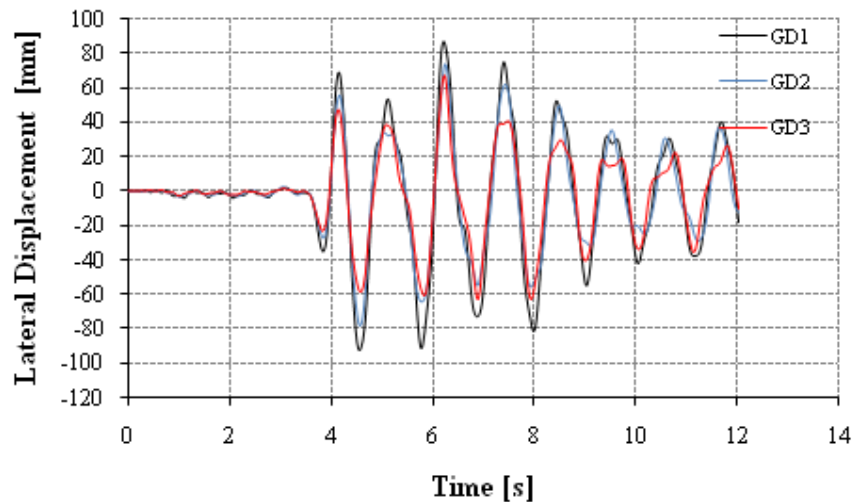


Figure 55 Repaired irregular bridge, all piers – second pseudo-dynamic test with Tolmezzo $PGA=0.35g$ displacements time history; GD1 central pier (7m), GD2 lateral pier (14m), GD3 lateral pier (21m)

Figure 56 shows the relative displacement between piers and between pier and abutment. In this figure, the curves are plotted to focus attention on the relative displacement between abutment and pier and between adjoining piers.

The maximum relative displacement was measured between the lateral pier (pier height 21m) and the near abutment.

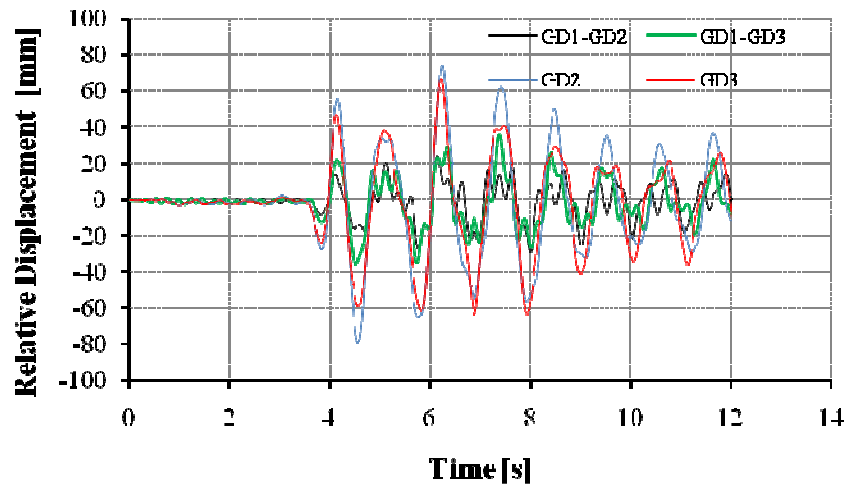


Figure 56 Repaired irregular bridge, all piers – second pseudo-dynamic test with Tolmezzo PGA=0.35g. Relative displacements time history: GD1-GD2 between the piers GD1 and GD2, GD1-GD3 between the piers GD1 and GD3, GD2 between the pier GD2 and the near abutment, GD3 between the pier GD3 and the near abutment.

Afterwards, a new pseudo-dynamic test is performed and the specimen is subjected to a: the ground motion of the 1976 Friuli earthquake recorded at Tolmezzo scaled up to two times. In Figure 57 the dynamic response of specimen 8 is plotted versus time.

The maximum restoring force is equal to 5654kN and corresponds to displacement applies of about 140mm in the positive direction while in the same direction the maximum displacement measured is equal to about 184,9mm and the corresponding force is of about 5525kN.

When the movement direction is opposite, the maximum force measured is 3768kN at a displacement of 189mm. In this direction, the maximum displacement is of about 218,3mm and the corresponding force is of about 3460kN.

The horizontal load reaches the yield point and the specimen undergoes plastic deformation in both directions. In particular the yield point is reached at a displacement of about 95mm in positive direction whereas it seems that the plastic deformations appear at the displacement of about 104mm in the negative direction.

The initial ratio between the stiffness of the pier in negative and in positive direction is equal to about 0,49. The stiffness of specimen is

different in the two directions and the difference remains during the next cycles.

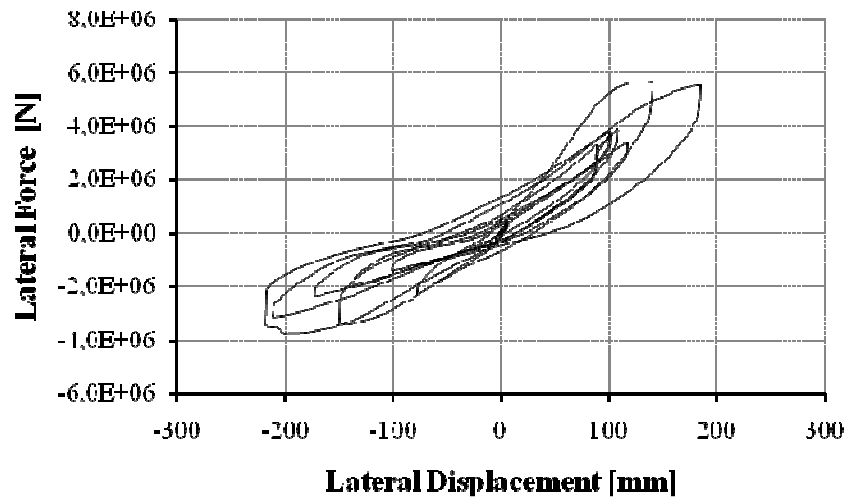


Figure 57 Repaired irregular bridge central pier - pseudo-dynamic test Tolmezzo PGA=0.7g Force-Displacement cycles (real scale)

Figure 58 shows. The displacement history imposed on each pier can be divided in three parts:

- a first time interval of about 3,6s during which the displacements are limited to about 4,8mm
- a next time interval of about 5,2s, during which four successive cycles of displacements are imposed. The maximum displacement of about 218mm is applied to the central pier here.
- finally for about 3,2s, the displacement amplitude of the system is similar during the cycles. However, during this time-interval the displacement is less than the maximum displacement and for the central pier does not exceed 52mm.

The displacement histories of each pier are always in phase

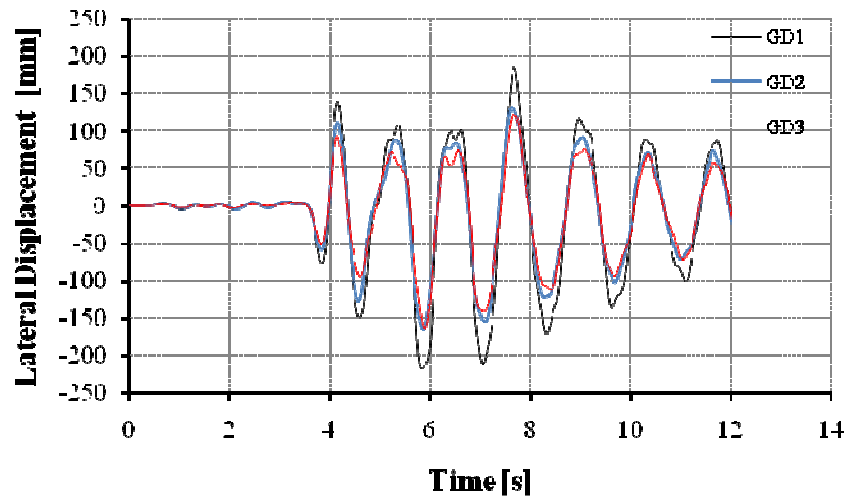


Figure 58 Repaired irregular bridge, all piers – second pseudo-dynamic test with Tolmezzo PGA=0.7g displacements time history; GD1 central pier (7m), GD2 lateral pier (14m), GD3 lateral pier (21m).

Figure 59 shows the relative displacement between piers and between pier and abutment. In this figure, the curves are plotted to focus attention on the relative displacement between abutment and pier and between adjoining piers.

The maximum relative displacement was measured between the lateral pier, (pier height 21m) and the nearest abutment.

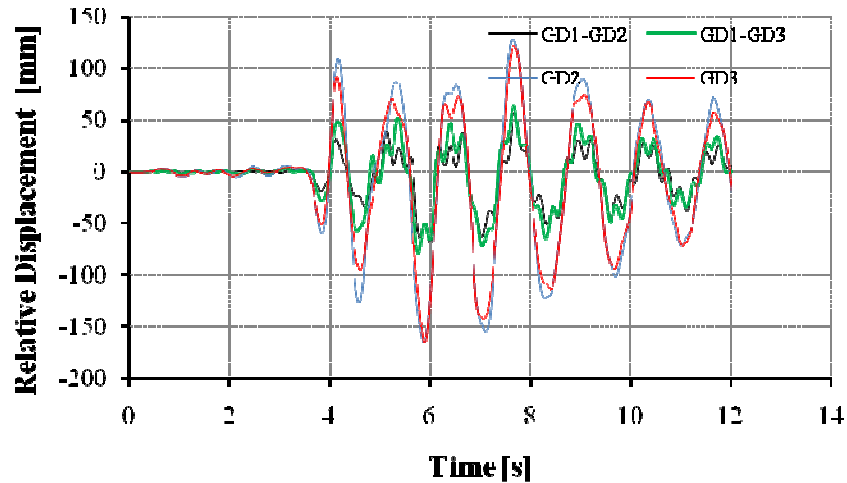


Figure 59 Repaired irregular bridge, all piers – second pseudo-dynamic test with Tolmezzo PGA=0.7g. Relative displacements time history: GD1-GD2 between the piers GD1 and GD2, GD1-GD3 between the piers GD1 and GD3, GD2 between the pier GD2 and the near abutment, GD3 between the pier GD3 and the near abutment.

11.3. Cyclic test

In order to investigate piers sufficiency as energy dissipating elements during severe earthquakes, cyclic inelastic tests were executed to determine the evolution of the specimen stiffness, ductility, strength during evolution of a deformation, after pseudodynamic tests.

The same test setup was used for the cyclic tests. The axial load value is the same as in previous pseudo-dynamic tests.

During cycling displacements, reactions, deformations were measured by means of the same instrumentations used in previous test.

The cyclic test was performed by applying cycles of increasing horizontal displacements to the top of specimens using slow cyclic loading.

The pier specimens were subject to displacement-controlled lateral loading, with displacement amplitudes ranging from 30 to 60mm at the top of the structural element. The results are shown in scale of specimen.

11.3.1. Observations

The secant stiffness corresponding at the maximum displacement in one direction (positive or negative) during a cycle is calculated as the slope of the line that connects the origin of the reference system with the point of maximum displacement.

11.3.1.1. Pier 8

To eliminate the above initial horizontal load on the load cell, some part of the test equipment are uninstalled and reinstalled several times. In fact it is necessary to modify the constraint system and follow a procedure to apply the vertical loads.

It is obvious that the initial deformation of the specimen enhances the effect of the eccentricity of the vertical loads and then a sequence of displacements is imposed in the same positive direction during the setup of equipment. So, the top specimen is deformed of about 16mm in the positive direction. This displacement is assumed as the zero position at the beginning of the test.

11.3.2. Horizontal-Force Drift Deformation Response

This chapter describes the relationship between the restoring force and the horizontal displacement of the specimens during the cyclic test.

11.3.2.1. Pier 7

The loading pattern began with three complete cycles in the push-and-pull direction to about 2.6% ($30/1170 \times 100$) drift ratio. The subsequent drift ratios were three cycles at about 3.4 and 4.3%. Testing was continued until a damage level occurred that was accompanied by a substantial drop-off in load (about 70-80% of maximum load capacity achieved in the first cycle).

The relationship between lateral-load and top-of-column lateral displacement is shown in Figure 60. Attained maximum load was 166kN in positive direction and 164.8kN in negative direction.

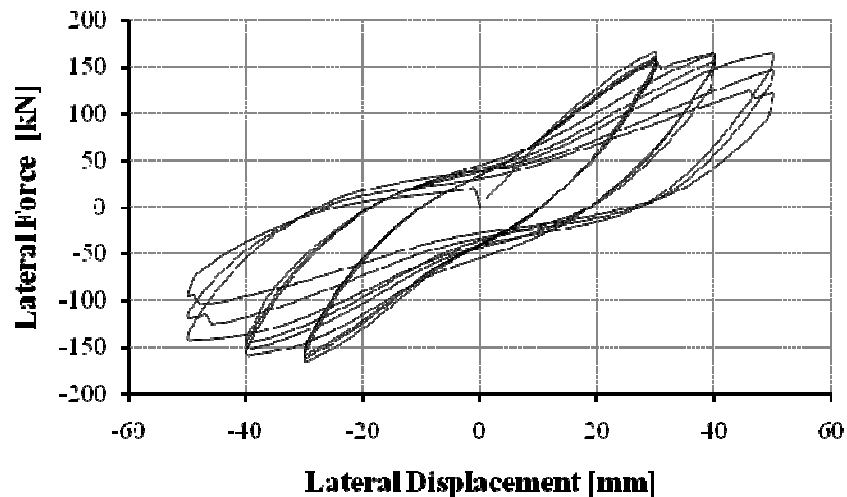


Figure 60 Cyclic test on specimen 7; force-displacement cycles (specimen scale)

It is noted that a significant reduction of lateral load capacity was not observed until specimen displacements reached approximately 50mm. After each audible rebar rupture, a fall-off of load of about 8kN occurred. These hysteresis loops show a nonlinear response, with hysteretic damping. The damage caused by shear has produced a reduction of the strength and pinching on the element hysteresis for displacement

amplitudes higher than the yield displacement. The maximum displacement achieved was 50mm.

At a drift ratio of 2.5% (30mm deflection case) the pre-existing cracks widened more but worsening degradation of concrete was not observed. Slight crushing of concrete localized at the footing region took place and tiny vertical cracks began to spread.

The restoring force, the stiffness and the hysteretic energy dissipation were stable during the entire duration of the first three cycles.

During the first displacement cycle the variation of energy dissipation at each cycle were negligible. The maximum restoring force is equal to about 166kN in the positive direction whereas the maximum negative force is 164.8kN.

However, a drop in load (about 9kN) took place after the displacement exceeded 30mm. At the end of the third cycle, the specimen was still capable to carry 158.5kN and -157.5kN in the push and pull directions respectively.

The stiffness had slightly variation during the entire duration of the first three cycles and was about equal in each loading direction (push and pull directions).

As the displacement reached a drift ratio of 3.4% (40mm deflection case), vertical cracks became evident and crushing was observed due to spalling of the cover concrete within a height of 150mm above the footing. The maximum restoring force is equal to about 165kN in the positive direction whereas the maximum negative force is -158kN.

The energy dissipated in each cycle is bigger and the variation of the maximum load is small and limited to about 10kN.

The degradation of the maximum load during loading cycles was gradual, and limited to about 10kN. At the end of the third cycle, the specimen was still able to carry 156.7kN and 144.5kN in the push and pull directions respectively.

Note also that in positive direction, the secant stiffness at the beginning of this group of cycles is about 75% of the secant initial stiffness and decrease to about 71% during the last cycle of this group. When the top of the specimen is moving in opposite direction, the secant stiffness is about 72% of the initial stiffness in this direction and decreases slightly during the cycles at this drift level.

At a drift ratio of 4.4% (50mm deflection case), compressive failure of the confined concrete, spalling of the cover concrete within a height of 300mm above the footing, the yielding of the spiral near the footing,

followed by buckling of the rebar, occurred. Also severe degradation in strength, stiffness is clearly visible as showed in Figure 60.

The maximum restoring force is equal to about 164.8kN in the positive direction whereas the maximum negative force is -141.6kN. It is seen that the load capacity of specimen is more rapidly decreased with an increase of about 25kN for each cycle.

It can be seen that rebar rupture causes a quick drop in load capacity and the fracture occurred that was accompanied by a substantial non-recoverable drop-off in load with the worst of the crushing near localized. At the end of the third cycle, the specimen was still able to carry 122.5kN and -95kN in the push and pull directions respectively.

It is evident that in positive direction, the secant stiffness at the beginning of this group of cycles is about 60% of the secant initial stiffness and decrease to about 44% during the last cycle of this group. When the top of the specimen is moving in opposite direction, the secant stiffness is about 52% of the initial stiffness in this direction and decreases to 34% during the cycles at this drift level.

The dissipated energy in each cycle was about the same and it is evident the effect of “pinching”, which has produced shear failure progressively formed on both sides of the pier.



Figure 61 Damages of the specimen 7 at the end of cyclic test

11.3.2.2. Pier 8

The loading pattern began with three complete cycles in the push-and-pull direction to about 2.6% ($30/1170*100$) drift ratio. The subsequent drift ratios were three cycles at about 3.4, 4.3% and 5.13%.

Testing was continued until a damage level occurred that was accompanied by a substantial drop-off in load (about 40% of maximum load capacity). The relationship between lateral-load and top-of-column lateral displacement is shown in Figure 62.

It can be seen that the curve shown is not symmetric. Attained maximum load was 148,2kN in positive direction and 87,3kN in negative direction.

It can be observed that the response of the specimen is nonlinear during the cycles. The maximum displacement achieved was 60mm

However, it is evident as the restoring force decreases relevantly only in positive direction. In fact the specimen is subject to bigger displacement in the positive direction because of the above initial deformation. The initial ratio between the stiffness of the pier in negative and in positive direction is equal to about 0.49.

It is noticing that the specimen oscillates around an initial position which was equal to a deflection (horizontal displacement) of about 16mm in the positive direction. Therefore the pier is more stressed in the positive direction.

However it is evident that the restoring force, the stiffness and the energy dissipation are bigger in the positive direction. It is observed that the cycles are narrower around the zero position.

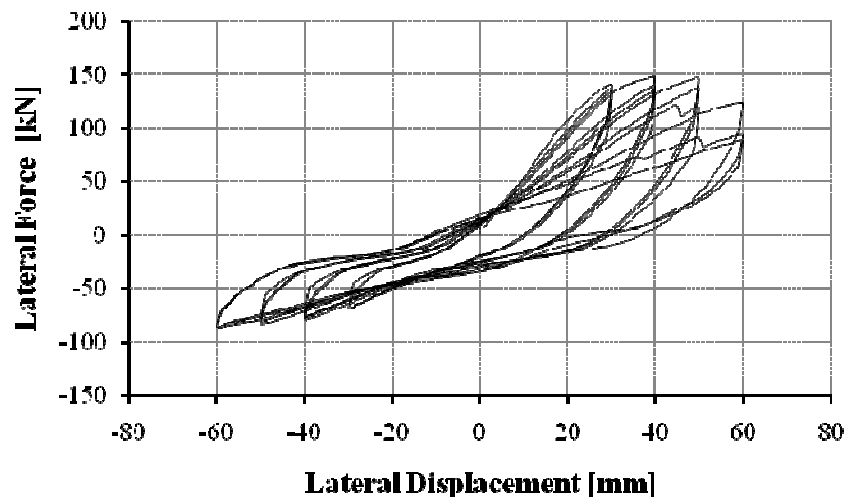


Figure 62 Cyclic test on specimen 8; force-displacement cycles (specimen scale)

At a drift ratio of 2.5% (30mm deflection case), the maximum restoring force is equal to about 141kN in the positive direction. When the movement is in the opposite direction, the maximum force is equal to 68,6kN.

The restoring force, the stiffness and the hysteretic energy dissipation have slightly variation during the entire duration of the first three cycles. The maximum positive force changes modestly with decrease of only 6kN.

At a drift ratio of 3.4% (at 40mm deflection case), the maximum restoring force is equal to about 148kN in the positive direction whereas the maximum negative force is 79kN.

The restoring force changes in positive direction during the cycles. It should be noted that, the maximum positive force drops to 139kN and then to 135kN during the cycles 5 and 6. The reduction of the restoring force is of about 3kN in the negative direction.

Note also that in positive direction, the secant stiffness at the beginning of this group of cycles is about 79% of the secant initial stiffness and decrease to about 72% during the last cycle of this group. When the top of the specimen is moving in opposite direction, the secant stiffness is about 86% of the initial stiffness in this direction and decreases slightly during the cycles at this drift level.

At a drift ratio of 4.3% (50mm deflection case), the maximum positive restoring force is equal to about 147kN. When the movement is in the opposite direction, the maximum force is 83kN. It is possible to see that, the maximum positive force drops to 138kN and then to 120kN during the cycles 8 and 9. The reduction of the restoring force is of about 3.2kN in the negative direction.

Important stiffness degradation is observed during the cycles 7, 8 and 9: the secant stiffness of the specimen is equal to about 63% of the secant initial stiffness during the first deflection in positive direction and then decreases to 51%.

It was also observed that when the top of the specimen is moving in opposite direction, the secant stiffness is about 72% of the initial stiffness in this direction and decreases slightly during the cycles at this drift level.

At a drift ratio of 5.13% (60mm deflection case), the maximum restoring force is equal to about 124kN in the positive direction while the maximum negative force is equal to -87kN. It is particularly evident that, the maximum positive force drops to 93kN and then to 88kN during the cycles 11 and 12. The reduction of the restoring force is of about 1.6kN in the negative direction.

It can be seen that considerable stiffness degradation takes place under cyclic loading: the secant stiffness of the specimen is equal to about 44% of the secant initial stiffness during the cycle 10 and then decreases to 30% during the last cycle.

Additionally, it should be observed that during negative deflection, the secant stiffness is about 64% of the initial stiffness in negative direction and decreases slightly during the cycles at this drift level.

The damage has produced a reduction of the strength and the stiffness of the specimen. The specimen shows a large localized crack at the base, some minor cracks between the FRP strips. In addition there is one hairline crack on the pier surface that is located at a height of 650mm above the base, outside the plastic hinge zone. Throughout the test, the preexisting crack at the base of the specimen continued to grow larger and spreads sideways into the specimen surface. After each audible rebar rupture, a fall-off of load of about 9kN occurred.

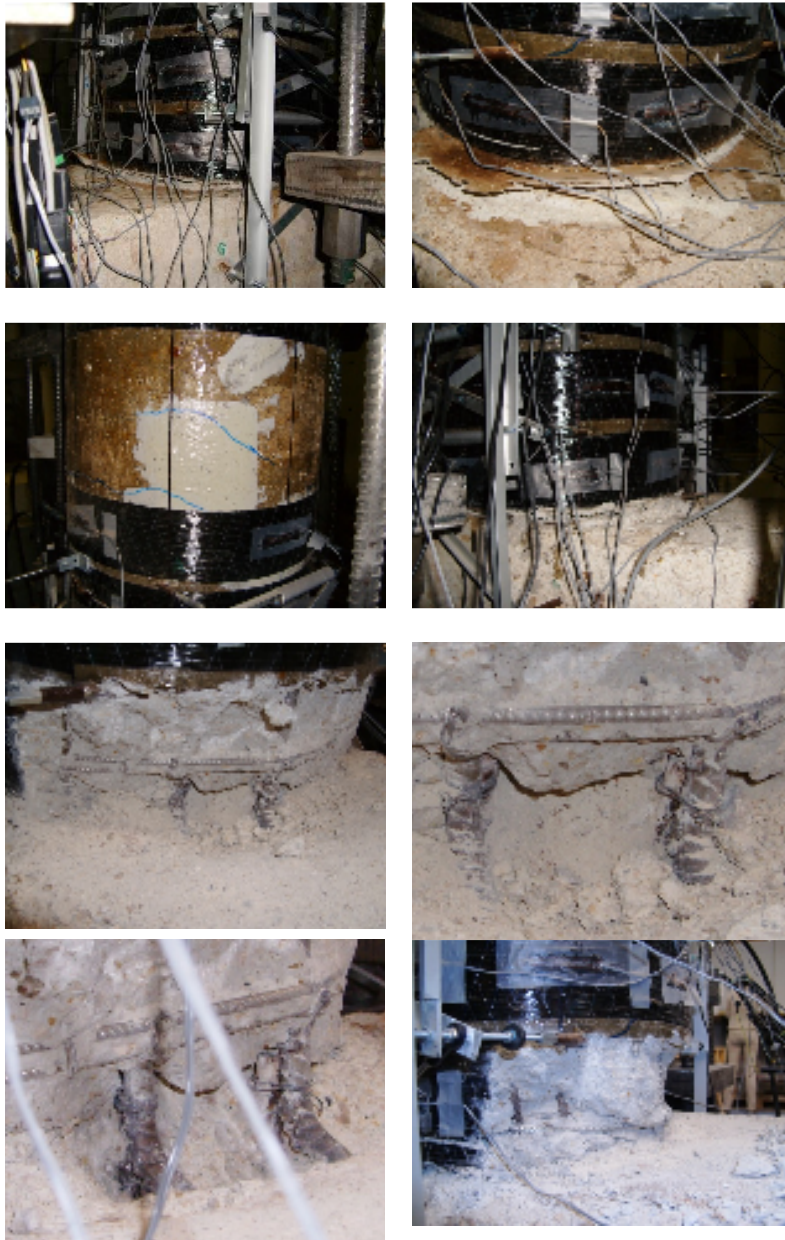


Figure 63 Damages of the specimen 8 during the loading sequence.

The Moment-curvature cycles can be calculated on the base of the displacements of the vertical transducers which are placed in the “critical zone near the base of the specimen.

Figure 64, Figure 65, Figure 66 show the moment-curvature relationships of the three section of the specimen. The position of these sections is indicated in Figure 67 by the series of horizontal lines.

The comparison between the moment-curvature relationships for the base section and the Force-Displacement relationships of the column shows that the behavior of the base section has much influence on the response of the columns.

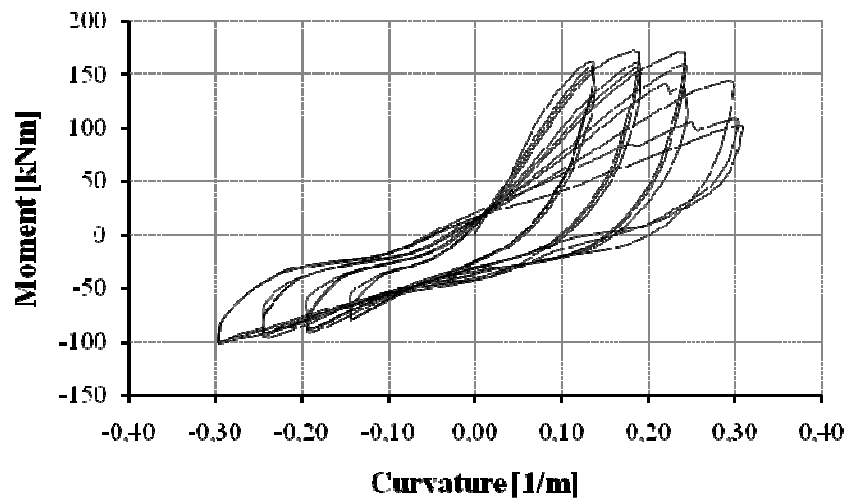


Figure 64 Specimen 8, Moment-Curvature cycles (base section).

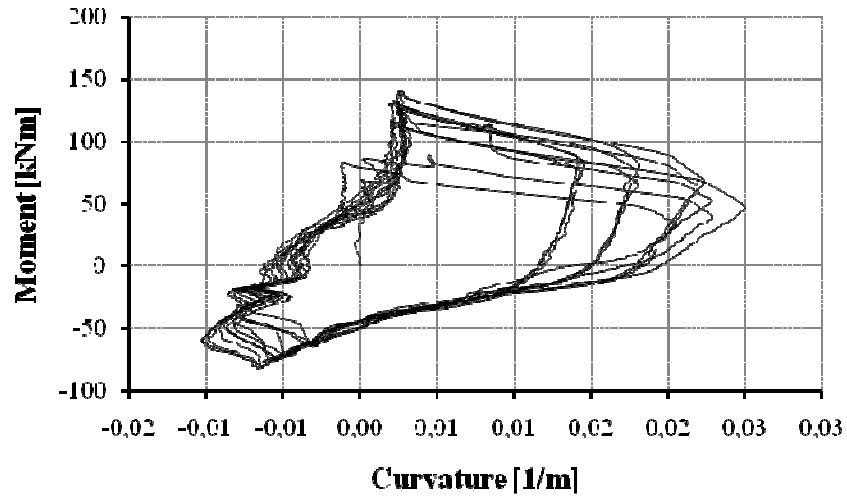


Figure 65 Specimen 8, Moment-Curvature cycles (section 1).

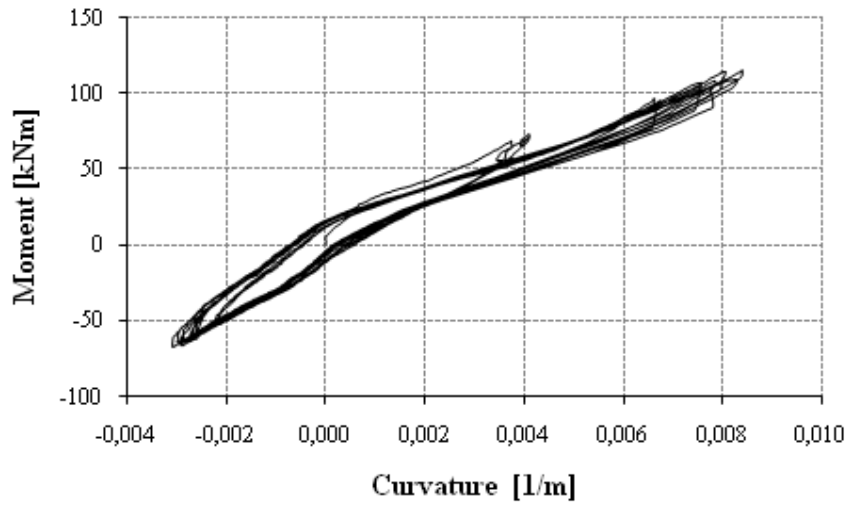


Figure 66 Specimen 8, Moment-Curvature cycles (section 2).

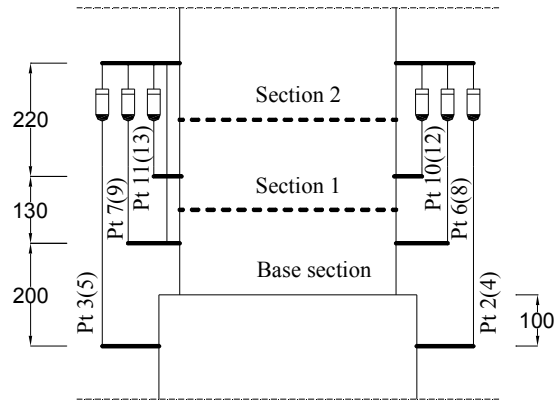


Figure 67 Moment-Curvatures cycles – Section for which the moment-curvature relationships are calculated.

Flexural displacements were computed by integrating curvatures along the height of the specimen and the contribution due to shear was then found as the difference between the pier top total displacement and the computed flexural one (Figure 68). Note that:

- the displacements due to the shear are small
- it is necessary to reflect about:
 1. the contribution of the yield penetration.
 2. the displacement due to the rotation of the base section of the specimen

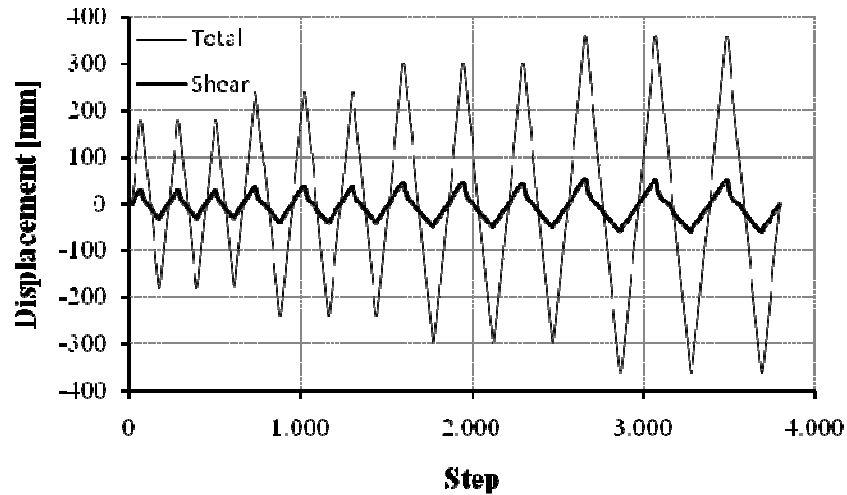


Figure 68 Repaired and retrofitted Pier (7m), evaluation of the displacement due to shear and flexure during cyclic test. Total: test response (real scale), Shear: displacement contribution due to shear.

1.1.1. Strain gauges

The local behavior of the CFRP fibers is measured through the use of strain gauges which are placed on the external surface of the CRP strips of the discontinuous wrapping in the direction of the fiber placement. The CFRP wrapping has to improve the shear resistance of the member.

The value of the deformations measured during the cyclic test, are shown for the base strips in Figure 69, Figure 70. These deformations are measured on the FRP strips at the base of the specimen and the strain gauges Str5 measured a deformation of about 4 mEpsilon but maybe it was broken or placed where the failure occurred. The strain gauges Str2 e Str5, show the same strange behavior even if for different deformation. In fact the amplitude of the minimum deformation of these strain gauges changes during the test. The local failure may be there.

The deformations of the lateral strain gauges are limited to about 1mEpsilon . The strain gauges Str6 has measured an initial deformation comparable to that of the strain gauges Str1, Str7 and then a deformation equal to that measured by Str4 and Str2.

The deformation measurements show that the strain gauges Str1, Str7, Str5 and Str6 have measured the maximum deformations at the base CFRP strips and then it seems that the left side of the specimen is more stressed at the base.

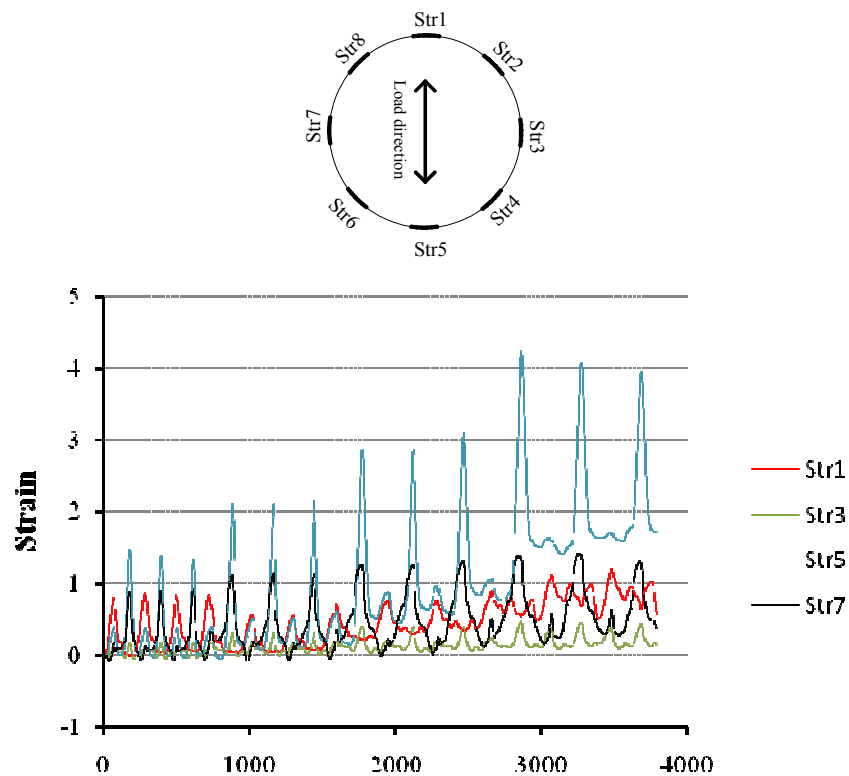


Figure 69 Jacket Strain (level 1); strain gauges (Str) 1-3-5-7, cyclic test [mEpsilon].

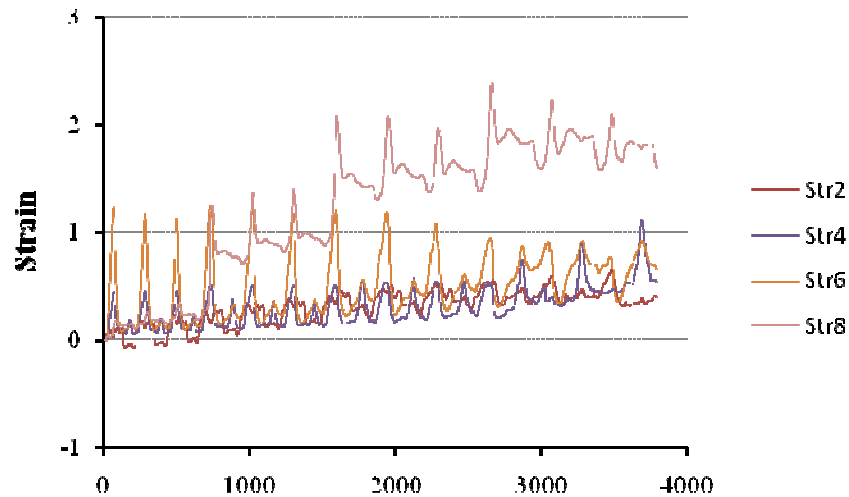
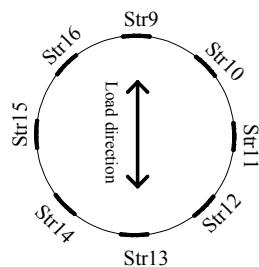


Figure 70 Jacket Strain (level 1); strain gauges (Str) 2-4-6-8, cyclic test [mEpsilon].

Figure 71, Figure 72 shows the deformations measured on the CFRP strip of the level 2 (Figure 40). This strip is located immediately above the above base CFRP strip. The deformations are more regular than those measured on the base CFRP strip. The strain gauges Str9 and Str13 are more stressed and the deformations are equal to about 2mEpsilon. The strain gauges Str10 and Str16 have measured deformations of about 1mEpsilon. Note that the strain gauges maximum deformations are in concordance with the load direction. However the deformation of the strain gauges Str10 and Str16 which are placed on the side towards the actuator are greater than those of the Str14 and Str12



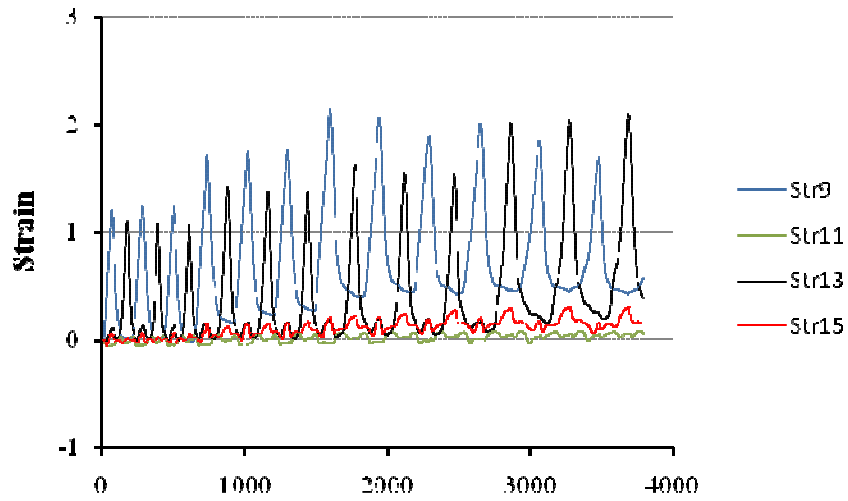


Figure 71 Jacket Strain (level 2); strain gauges (Str) 9-11-13-15, cyclic test [mEpsilon].

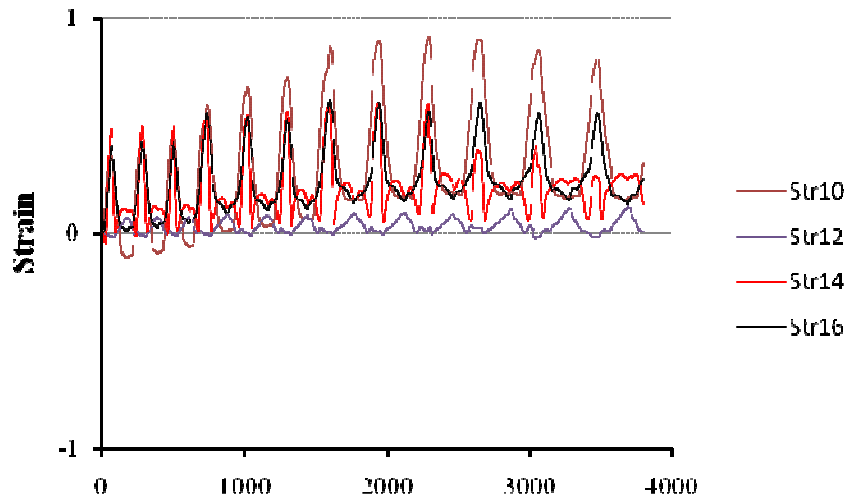


Figure 72 Jacket Strain (level 2); strain gauges (Str) 10-12-14-16, cyclic test [mEpsilon].

2. Comparison of previous experimental and recent tests

In this chapter a comparison between previous experimental results and actual experimental results is presented.

It is important to remind that the seismic performance of a group of piers of the same type is been studied during a previous research study [52].

The present study aimed to repair two damaged piers of that group. Unfortunately, we do not know precisely which of them is been repaired.

So, the comparison between the response of the repaired pier and the as build pier is been done using the available data of two original piers of the same type.

It is not possible to be sure that the comparison can help to find a correspondence because of the serious damage level of the piers.

In addition, the initial direction of loading could be different for the repaired and as-build specimens. However, the comparison can provide information on the efficiency of the repair techniques.

Finally, it is possible to select the most appropriate Force-Displacement cyclic response of the as-build piers between all the possible comparisons (see Appendix I).

In particular, the force-displacement cycles of two as-build piers (central pier of the Italian irregular bridge), specimen II71BN1 and II71BN2 are considered, which are measured during previous pseudo-dynamic test (Tolmezzo PGA=0.35g). These piers have the same longitudinal and transversal reinforcement, the same geometry (height, cross section) and the same materials. Two different possible initial horizontal load directions (D1, D2) are taken in account in the study.

First, the response of the repaired specimen 8 during the first pseudo-dynamic test is compared with the responses of an as-build piers of the same type in Figure 73. Unfortunately, it is important to remind that the force reading from the horizontal load transducer is been set to zero during the initial setup of equipment whereas the load was already equal to about 18kN (specimen scale). So the dynamic response of the bridge has to be study carefully and maybe the dynamic results must be adjusted to make them comparable.

Anyway, the response of the specimen can be adjusted including the amount of the initial horizontal load.

It can be observed that when the horizontal displacement of the top of the pier was equal to about -32mm, a quick variation of the stiffness occurs for loads equal to 2000kN. Next, the stiffness greatly decreases in the negative direction.

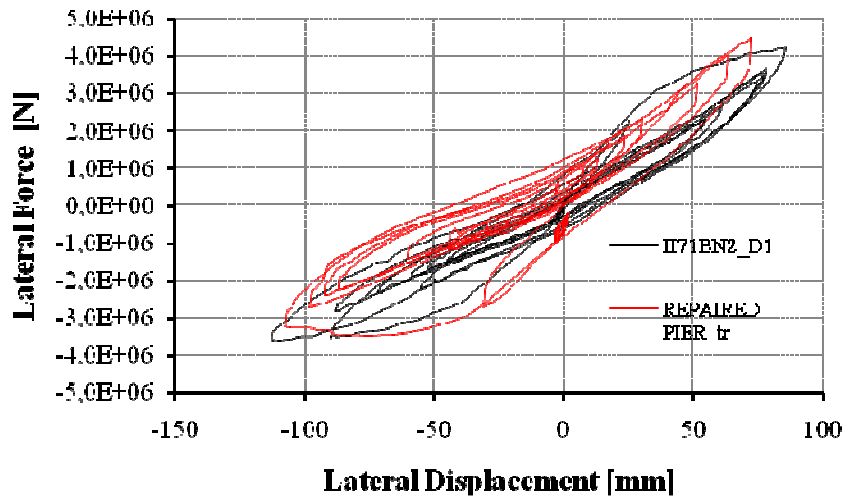


Figure 73 Repaired Italian irregular bridge and irregular Italian bridge – first pseudo-dynamic test with Tolmezzo PGA=0.35g. Comparison between the response of the repaired specimen 8 including the initial horizontal load (REPAIRED PIER_tr) and the as-built Italian pier II71BN2 if the initial displacements are imposed in the direction D1(II71BN2_D1). (real scale)

Then the performance of the repaired pier is compared with that of the as-built pier during the second pseudo-dynamic test (Tolmezzo, PGA=0.35g, without the initial horizontal load due to equipment). The bridge structure, the input excitation and the integration parameters are the same which are used during the previous test.

The repair techniques guarantees satisfactory seismic performance of the repaired specimen and have improved the strength and the stiffness of the damaged piers.

This comparison evidences that it is possible to recover the seismic performance of the as-built piers which show a severe damage state.

It becomes clear that the damage is concentrated near the base but the pier can hold the vertical load.

The maximum restoring forces are equal or bigger than that of the “as build pier” in the positive direction. It is also observed that the forces could be less than that of the “as build pier” in the opposite direction even if the difference is at the most of about 300kN. The initial stiffness of the repaired pier is better than that of the “as build pier” in each loading direction (and only in one case, it maybe is less). The dissipated energy is less than that of the as-build pier.

The different stiffness in the negative direction could be due to the anchorage failure during the first pseudo-dynamic test. It is evident that this great reduction of the stiffness is a problem about which it is necessary to reflect.

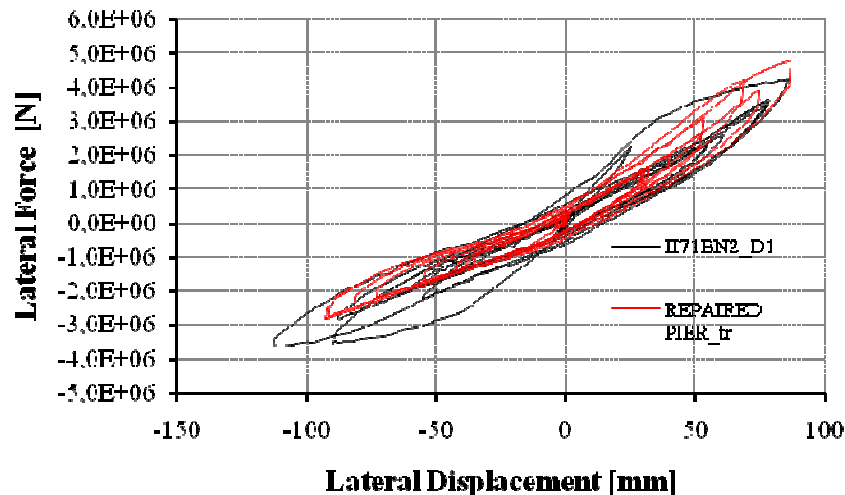


Figure 74 Repaired Italian irregular bridge and irregular Italian bridge – second pseudo-dynamic test with Tolmezzo PGA=0.35g. Comparison between the response of the repaired specimen 8 without the initial horizontal load (REPAIRED PIER_tr) and the as-built Italian pier II71BN2 if the initial displacements are imposed in the direction D1 (II71BN2_D1). (real scale)

Figure 75 shows the displacements time history of each pier of the Italian irregular bridge which are measured during pseudo-dynamic test with Tolmezzo PGA=0.35g

In particular, Figure 76 shows the comparison between the displacement time history of the as-build piers and that of the repaired one.

The maximum displacements of the as- build pier are greater than those of the repaired one in the positive direction, whereas the maximum displacements are about the same in the opposite direction. The difference is of about 25mm (real scale) in the positive direction.

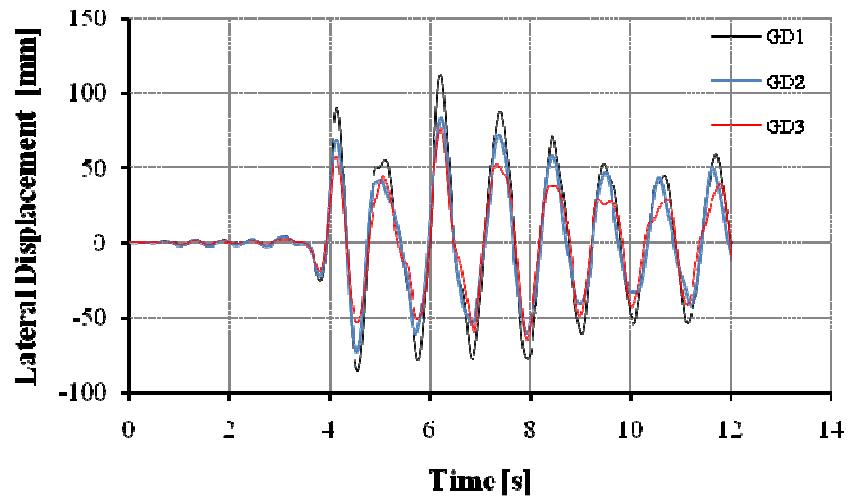


Figure 75 Italian irregular bridge, all piers –pseudo-dynamic test with Tolmezzo
PGA=0.35g displacements time history; GD1 central pier (7m), GD2 lateral pier (14m),
GD3 lateral pier (21m).

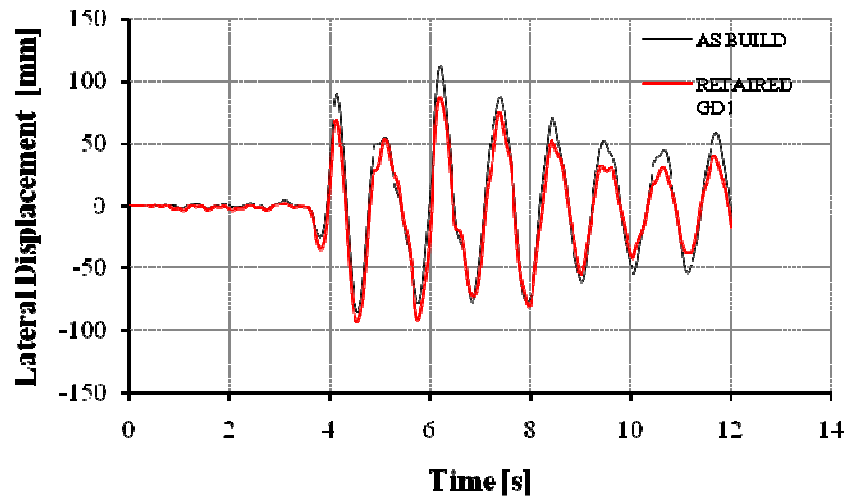


Figure 76 Italian irregular bridge–pseudo-dynamic test with Tolmezzo PGA=0.35g
Comparison between the displacement time history of the repaired central pier and the as build Italian central pier. pseudodynamic test (Tolmezzo)

3. Analytical studies

Recently, the use of detailed finite element models and analysis has become common for investigating the response of reinforced concrete (r.c.) elements.

The reason is easy to understand, since only recently the significantly increased computation power, reduced computer hardware cost and the developments software with increased accuracy of FE codes have made possible it.

The numerical simulation of the seismic response of concrete pier specimens may be carried out using an OpenSees Finite Element Model.

The OpenSystem for Earthquake Engineering Simulation (OpenSees) is “a software framework for developing sequential, parallel and grid-enabled simulation applications in earthquake engineering using finite element methods” [69].

This software provides a wide range of material and element models for nonlinear analysis, solution methods, data processing procedures for research and problem-solving to users interested in advanced simulation of detailed structural and geotechnical systems with realistic models of nonlinear behavior.

Moreover OpenSees is open-source software, and it has an application program interface (API) for users that allows extending the program capability for simulation applications.

In this thesis the first results of the analytical study on the behavior of tall and squat piers are shown. The analytical results can provide useful information to predict the seismic behavior of the piers and can be used to understand the influence of a particular physics phenomenon on the experimental response of the specimen. The seismic behavior of two specimens is investigated: the repaired and retrofitted pier and the as-build tall piers.

In this introduction a brief description of the fiber model is given: the description refers to the base fiber model that is modified to simulate the tall piers and the squat piers.

First, the material parameters of a detailed nonlinear fiber model were initially calibrated using the results of standard compressive test on cubic shaped concrete specimens ($15\text{cm} \times 15\text{cm} \times 15\text{cm}$) and tensile test on specimens of each bar diameter used to construct the pier specimens, and then fine tuned with pseudo-dynamic tests results conducted at the University of Roma, Sapienza in 1994-1996 [52].

The tuning of the model involved the investigation of the influence of: the loading history, the material properties, fiber discretization of the cross sections and the number of elements into which the member is discretized on the numerical results.

However, the model should be able to correctly simulate the response of specimens including some important phenomena in seismic response of specimens.

One important aspect to consider is concerning the reliability of numerical model to perform an accurate prediction of the hysteretic behavior and nonlinear performance of reinforced concrete structural specimen under seismic loads.

A complete model for reinforcing steel, that has additional capabilities and is able to more accurately simulate test data, it is successfully used in a reinforced concrete fiber section as the reinforcing steel material [77], [78], [79], [80].

Another very important consideration is whether it is possible to model the initial lateral stiffness and the stiffness degradation due to cracking of a reinforced concrete element, subject to lateral and gravity loads.

For the accurate prediction of stiffness evolution, a uniaxial Popovics [74] concrete material object with degraded linear unloading/reloading stiffness according to the work of Karsan-Jirsa [75] and tensile strength with exponential decay may be used.

In order to obtain an accurate response of specimen, it is most important to consider a fixed end rotation at the base of the pier due to strain penetration along reinforcing bars fully anchored in footings and bridge joints. In these circumstances only one large crack may open at the column-footing interface and lead to an increase in the inelastic axial strain in the longitudinal bar crossing the crack some distance into the footing.

These strains diminish gradually to zero over a length required to develop sufficient bond strength for anchoring the bars against ultimate tensile forces.

The column deformation due to strain penetration was modeled using a zero length fiber section in OpenSees combined with appropriate material model for longitudinal reinforcing steel [76].

The pier model is subdivided into two nonlinear fiber elements with different section to model the “as build section” concrete section and the repaired one.

The repaired concrete fiber section has a geometric configuration formed by sub regions of simpler, regular shapes, circular or ring: a new restoring unconfined concrete ring, a confined by stirrups and FRP concrete ring, a central circular region with repaired confined concrete.

The analytical model was subjected to a sequence of displacements that were recorded during the pseudo-dynamic test conducted at University at Sapienza [52].

3.1. Material models

Analytical techniques can be a useful tool used to predict the response of specimen under various load conditions. An essential precondition for this

task is an appropriately defined analytical model for the material of the section of the structural member. Recently different analytical, numerical techniques and several models have been developed to describe the physical behavior of materials.

The selection of the material models, which best describes the experimental response of the element, is essential to obtain accurate results.

Therefore, it is most important to determine and select which material properties can influence the elastic and inelastic response of the element.

Another important step is to choose the most appropriate value for the material properties.

Therefore for simplicity, if you are not sure whether the available material properties are correct, only an average value of the material properties can be introduced taking into account the range of possible variation of each parameter.

Parameters setting and tuning of the material model can subsequently improve the accuracy of the results. The comparison between the analytical predictions and the experimental data can provide help in calibration of the material parameters.

In the numerical model, concrete and steel bars are represented as nonlinear behavior materials and also nonlinear behavior for concrete and steel under cyclic loadings are included.

To assume a specific material model for steel allows simulating the element end rotation due to strain penetration.

3.1.1. Steel

In order to capture the structural response of concrete specimen and associated damage under cyclic loading, such as that which occurs during an earthquake, an accurate modeling of longitudinal reinforcing steel behavior is required.

In particular, the steel material model for longitudinal bars should incorporate important physics phenomena as buckling, strength deterioration, and failure resulting from low cycle fatigue.

The complete formulation for steel material has been implemented in OpenSees as a uniaxial material object. This material, namely Reinforcing Steel [77], [78], [79], [80]., can be efficiently used in a reinforced concrete fiber section as the steel reinforcing material.

The backbone curve is constructed using the experimental value of yield stress in tension, ultimate stress in tension, initial elastic tangent, tangent at initial strain hardening, strain corresponding to initial strain hardening, strain at peak stress and it is used as a bounding surface for the reinforcing bar simulation. This curve is shifted according to Chang and Mander (1994) [77] to account for Isotropic hardening.

The model can predict diminishing yield plateau when a reinforcing bar is subjected to plastic strain reversals within the yield plateau and isotropic hardening due to repeated strain reversals (accumulated plastic strain).

The Reinforcing Steel material includes two buckling models, Gomes and Appleton buckled curve [79] and Dhakal and Maekawa buckled curve [81] and cyclic degradation.

According to cyclic degradation model, if a bar has been determined to have fractured, the strength is rapidly degraded to zero and it describes loss in strength due to damage or other phenomenon resulting in softening due to plastic reversals.

In cyclic degradation model some parameters which are considered important, are: the number of half cycles to fracture, the half cycle plastic strain amplitude (they are used to define a cumulative damage factor), a degrade constant used to describe loss in strength caused by damage.

The Giuffrè-Menegotto-Pinto constitutive model [82] is adopted as the constitution of steel, which can simulate the behavior of stiffness degradation and buckling of steel well. This model was firstly put forward by Menegotto and Pinto and modified by Filippou, taking isotropic strain hardening into account. It is effective in calculation due to the explicit form of strain function. Meanwhile, it matches well with the results gained by cyclic loading test of steel. Fixed end rotation at the base of the pier due to the strain penetration effects, under seismic load, may be included in the model using the zero-length section element available in OpenSees and a model to describe the bar stress vs. loaded end slip response.

This model has been recently introduced on base of measured response of well-designed columns and pulls out test data of steel reinforcing bars that were anchored in concrete with sufficient embedment length (Zhao and Sritharan 2005)[76].

The monotonic bar stress -loaded-end slip (σ - s) relationship can be described using a straight line for the elastic region (3.1.1-1) and a curvilinear portion for the post-yield region (3.1.1-2).

In this model, the envelope of the bar stress vs. the slip response at the end of the flexural member is described using the function:

$$\sigma = Ks \quad (3.1.1-1)$$

$$\sigma = \bar{\sigma}(\sigma_u - \sigma_y) + \sigma_y$$

$$\bar{\sigma} = \frac{\frac{\bar{s}}{\mu - \bar{s}}}{\left[\left(\frac{1}{\mu b} \right)^{R_e} + \left(\frac{\bar{s}}{\mu - \bar{s}} \right)^{R_e} \right]^{1/R_e}} \quad (3.1.1-2)$$

$$\bar{s} = \frac{s - s_y}{s_y}$$

$$\mu = \frac{s_u - s_y}{s_y}$$

Whereas the hysteresis rule can be found in [76]. The slip when the bar stress reaches the yield (s_y) and ultimate strengths (s) are calculated using:

$$s_y = 0.4 \left(\frac{d_b}{4} \frac{f_y}{\sqrt{f'_c}} (2\alpha + 1) \right)^{1/\alpha} + 0.34$$

The yield slip (s_y) is a function of the concrete compressive strength (f'_c), the bar diameter (d_b), and the bar yield strength (f_y). The authors indicates that $s_u = 35s_y$ and $b = 0.3 \sim 0.5$ can be appropriate coefficients. The factor R_e should be slightly greater than one and α is the parameter used in the local bond-slip relation is taken as 0.4 in accordance with CEB-FIP Model Code 90 (MC90).³⁴

3.1.2. Concrete

In the work described here, constitutive models used for unconfined concrete are based on the Kent-Scott-Park stress-strain relation, as modeled in OpenSees.

A uniaxial material, namely concrete01, with degraded linear unloading and reloading stiffness according to Karsan-Jirsa [75] model and without tensile strength is implemented in OpenSees to simulate the monotonic envelope curve introduced by Kent-Scott-Park. The OpenSees concrete01 model requires four parameters:

- concrete compressive strength at 28 days
- concrete strain at maximum strength
- concrete crushing strength
- concrete strain at crushing strength

and the the initial slope for this model is $2 * f_{pc} / \epsilon_{psc0}$.

The transverse reinforcement (spiral or stirrups) confines the compressed concrete in the core region and provides higher compressive and strain values than the unconfined concrete. The transverse reinforcement is not modeled directly.

However, the effect of confinement may be taken into account by using appropriately a uniaxial model for concrete confined with transverse steel reinforcement but also with fiber-reinforced polymers (FRP) or with steel jackets. A Mander et al. (1988) [73] constitutive relation is used to model confined concrete by steel transverse reinforcement.

In OpenSees, a uniaxial material, namely concrete04, with degraded linear unloading and reloading stiffness according to Karsan-Jirsa [75] model and without tensile strength is used to simulate the monotonic envelope curve introduced by Popovics(1973) [74]and if the user sets

$$E_c = 5700 \sqrt{f_c} \quad (\text{in psi})$$

can be obtained as an envelope curve identical to that proposed by Mander et al. (1988) [73].

The concrete04 model requires seven parameters:

- floating point values defining concrete compressive strength at 28 days (compression is negative)
- floating point values defining concrete strain at maximum strength*
- floating point values defining concrete strain at crushing strength
- floating point values defining initial stiffness
- floating point value defining the maximum tensile strength of concrete
- floating point value defining the exponential curve parameter to define the residual stress (as a factor of f_t) at ϵ_{tu}

The following equation (Popovics 1973) [74] is adopted for the stress-strain envelope curve of confined concrete subjected to loading in compression.

This model is used to predict the stress-strain curves until the concrete crushing strength, and also for strains beyond that corresponding to the crushing strength.

$$f_{ci} = f'_{ci} \left(\frac{\varepsilon_{ci}}{\varepsilon_{ci}} \right)^{\frac{n}{n-1 + \left(\frac{\varepsilon_{ci}}{\varepsilon_{ci}} \right)^n}}$$

$$E_{sec} = \frac{f_{ci}}{\varepsilon_{ci}}$$

$$n = \frac{E_c}{E_c - E_{sec}}$$

where subscript i refer to the stress/strain at any load step and

- E_c is the Initial Modulus of Elasticity
- E_{sec} is the Secant Modulus of Elasticity determined at the peak stress
- f'_{ci} is the peak strength

The Karsan-Jirsa model (1969) [75] is used to evaluate the unloading and reloading paths (the slope of the curve). Finally, an exponential curve is used to define the envelope to the stress-strain curve of concrete in tension. The secant stiffness is used to define the path. and generally the value of β considered is 0.1.

Many studies have demonstrated that compressive behavior of concrete confined by carbon fiber composite jackets (FRP) is quite different from the compressive behavior of concrete confined by spiral or stirrups.

A constitutive model for concrete confined by FRP subjected to compressive loadings is proposed by Hosotani and Kawashima (1998) [84], [85].

In this model, the carbon fiber sheet ratio is an important parameter to evaluate the uniaxial behavior of confined concrete by FRP. The carbon fiber sheet ratio (volumetric ratio) ρ_{CF} is defined as **((3.1.2-1))**:

$$\rho_{CF} = \frac{4nt_{CF}b_{CF}}{d}$$

(3.1.2-1)

Where

- t_f is the thickness of a CFRP sheet
- n is the number of layers wrapped
- d diameter of the wrapped element

The stress-strain curves of confined concrete by FRP has a peak strength at spherical strains between 1,100 and 2,500 μ if the carbon fiber ratio ρ_{CF} is smaller than 0.167%, whereas the concrete stress f_c continues to increase in the confined concrete with a larger ρ_{cf} until rupture of the carbon fiber sheet. In the latter case, it is observed the stiffness gradually deteriorates from a pre-deterioration value to a post-deterioration value. The equations which describe the model for confined concrete by means of FRP, proposed by Hosotani and Kawashima (1998) [84], [85] are:

For circular section

$$E_g = -0.658 \frac{f_{c0}^2}{\rho_{CF} \varepsilon_{CFt} E_{CF}} + 0.078 \sqrt{\rho_{CF}} E_{CF}$$

Where:

- E_g is the post-deterioration stiffness

- f_{c0} concrete strength
- E_{fc} is the elastic modulus of CFRP
- ε_{CFt} is the spherical strain where the stiffness has shifted to the post-deterioration stiffness as

and if $E_g > 0$

$$f_c = E_c \varepsilon_c \left[1 - \frac{1}{n} \left(1 - \frac{E_g}{E_c} \right) \left(\frac{\varepsilon_c}{\varepsilon_t} \right)^{n-1} \right]$$

$$n = \frac{(E_c - E_g) \varepsilon_t}{E_c \varepsilon_t - f_t}$$

Or if $E_g < 0$

$$f_c = E_c \varepsilon_c \left[1 - \frac{1}{n} \left(\frac{\varepsilon_c}{\varepsilon_t} \right)^{n-1} \right]$$

$$0 < \varepsilon_c \leq \varepsilon_t$$

$$f_c = f_t + E_g (\varepsilon_c - \varepsilon_t)$$

$$\varepsilon_t < \varepsilon_c < \varepsilon_{cu}$$

$$n = \frac{E_c \varepsilon_t}{E_c \varepsilon_t - f_t}$$

Where:

f_t ε_t and the concrete stress where the stiffness has shifted to the post-deterioration stiffness and the corresponding strain.

The parameters required to determine the constitutive relation of concrete confined by CFS can be calculated using:

$$\frac{f_t}{f_{c0}} = 1.0 + 1.93 \frac{\rho_{CF} \varepsilon_{CFt} E_{CF}}{f_{c0}}$$

$$\varepsilon_t = 0.00343 + 0.00939 \frac{\rho_{CF} \varepsilon_{CF} E_{CF}}{f_{c0}}$$

$$\varepsilon_{cu} = 0.00383 + 0.1014 \left(\frac{\rho_{CF} f_{CF}}{f_{c0}} \right)^{3/4} \left(\frac{f_{CF}}{E_{CF}} \right)^{1/2}$$

Instead, for reinforced concrete specimens confined by stirrups or spiral, the confinement force is saturated at the yield of the transverse reinforcement. Only a small amount of residual strength is available after the failure. Lateral confinement of concrete by both CFRP and steel Ties can be included in a model which describes the behavior of confined concrete. Hosotani and Kawashima (1998) [84], [85] proposed:

For circular section

$$f_c = E_c \varepsilon_c \left[1 - \frac{1}{n} \left(\frac{\varepsilon_c}{\varepsilon_t} \right)^{n-1} \right]$$

$$0 < \varepsilon_c \leq \varepsilon_t$$

$$f_c = f_t + E_g (\varepsilon_c - \varepsilon_t)$$

$$\varepsilon_t < \varepsilon_c < \varepsilon_{cu}$$

$$n = \frac{E_c \varepsilon_t}{E_c \varepsilon_t - f_t}$$

$$\rho_s = \frac{4A_{sw}}{sd}$$

In which:

ρ_s is volumetric hoop reinforcement ratio

A_{sw} , f_{yk} , s sectional area, yield strength and interval of hoops,

$$\frac{f_t}{f_{c0}} = 1.0 + 1.93 \frac{\rho_{CF} \varepsilon_{CFt} E_{CF}}{f_{c0}} + 2.2 \frac{\rho_s f_{yh}}{f_{c0}}$$

$$\varepsilon_t = 0.003 + 0.00939 \frac{\rho_{CF} \varepsilon_{CFt} E_{CF}}{f_{c0}} + 0.0107 \frac{\rho_s f_{yh}}{f_{c0}}$$

$$E_g = -0.658 \frac{f_{c0}^2}{\rho_{CF} \varepsilon_{CFt} E_{CF} + 0.098 \rho_s f_{yk}} + 0.078 \sqrt{\rho_{CF}} E_{CF}$$

$$\varepsilon_{cu} = 0.00383 + 0.1014 \left(\frac{\rho_{CF} f_{CF}}{f_{c0}} \right)^{3/4} \left(\frac{f_{CF}}{E_{CF}} \right)^{1/2}$$

Moreover, most of the published FRP-confined concrete models are not implemented in finite elements software.

In particular the available model cannot be used to predict the response of the system when the strength of concrete continues to increase until it can no longer be confined by FRP and then the uniaxial material model suddenly gives very modest strength.

However, in order to approximate with a good accuracy by means of polygonal line, the stress-strain relationship of confined concrete by FRP, some points on or near the confined concrete stress-strain curve, can be used.

In OpenSees, compressive behavior of confined concrete by FRP can be simulated by using a uniaxial material, namely Pinching4 [86], that represents a 'pinched' load-deformation response and exhibits degradation under cyclic loading.

Present implementation of this material includes cyclic degradation of strength and stiffness (unloading stiffness degradation, reloading stiffness degradation, strength degradation).

The pinching4 model requires several floating point values:

- which defining force and deformation points on the positive and negative response envelope.
- which defining the ratio of the deformation at which reloading occurs to the maximum historic deformation demand, the ratio of the force at which reloading begins to force corresponding to the maximum historic deformation demand, the ratio of strength developed upon unloading from negative load to the maximum strength developed under monotonic loading
- which defining the ratio of the deformation at which reloading occurs to the minimum historic deformation demand, the ratio of the force at which reloading begins to the force corresponding to the minimum historic deformation demand and the ratio of the strength developed upon unloading from a positive load to the minimum strength developed under monotonic loading
- which controlling cyclic degradation model for unloading stiffness degradation, cyclic degradation model for reloading stiffness degradation, cyclic degradation model for strength degradation, used to define maximum energy dissipation under cyclic loading.
- type of damage

3.2. Fiber Models

The fiber method may be a very efficient method for predicting the flexural response of structural element, particularly when axial loads and bending moments control the element response.

There are some assumptions that are basic for fiber model: a plane section before bending remains plane after bending, fibers are fully bonded and have no relative slip and shear deformation is ignored.

The main idea of fiber model is to divide element section into small parts, fiber or layers.

Each fiber with resistance only effective in the direction of its length is under uniaxial state of stress. The stress-strain behavior of overall section is calculated according to uniaxial stress-strain relationship of the fiber. Each element is divided in “i” integration points, which are subdivided into several fibers (fiber section), by which stiffness matrix is calculated along longitudinal division in element of the structure. The integration points can be located at the element ends and at the midpoint in each element.

Take notice that calculation accuracy may be good enough so long as fine cross-section subdivisions and correct constitutive model of materials.

The materials of the reinforced concrete cross section are different (concrete, steel) and they have also different mechanical behavior due to different lateral restraints, such as the stirrup confinement or/and carbon fiber sheet confinement.

Then different uniaxial constitutive models are assigned to the fibers according to their location and area. A three-dimensional nonlinear model of the piers was developed using OpenSees.

The specimen is subdivided longitudinally into two Nonlinear Beam-Column Elements: the repaired and/or retrofitted part with height of about 550mm and the “as build” part with height of about 1790mm or 620 for tall and short specimen respectively as shows in Figure 77.

The Nonlinear Beam-Column Elements is based on the non-iterative (or iterative) force formulation, and includes the spread of plasticity along the element. The integration along the element uses Gauss-Lobatto quadrature rule.

To simulate the fixed-end rotation due to strain penetration along reinforcing bars fully anchored in footings, a zero-length section element is placed at the intersection between the flexural element that has been used to simulate the repaired portion of specimen, and the node on the foundation (fixed node).

The zero-length section element in OpenSees, have a unit length. With this in mind, the element deformations (elongation and rotation) are equal to the section deformations (axial strain and curvature). A zeroLength element connects two nodes that have the same, or almost position.

The two different type of circular reinforced concrete sections of the same diameter (repaired and as build section) are modeled using the same “complete” fiber model, defining and discretizing the concrete core and cover, and placing the longitudinal reinforcement, as shown in **Figure 77**. The “complete” fiber cross section is divided into two ring regions and one central circular region or patch (concrete core). The longitudinal reinforcement is modeled as single steel fiber of standard steel or inox: individual fibers are defined using the fiber command and they are located in the section.

The section is separated into different regions, for which different fiber discretizations may be generated. Patch object with a circular shape have a number of subdivisions (fibers) in the circumferential direction and number of subdivisions (fibers) in the radial direction such that the model can provide accurate response. The number of subdivisions is function of thickness of the different layer (patches).

Thus, for the “as build” reinforced concrete section the concentric ring regions begin with an innermost ring region having a concrete confined by steel stirrups different from the unconfined concrete of the external ring region. The core is built with the same confined concrete of the inner ring.

In case of the repaired and retrofitted concrete section the concrete core is built with repaired concrete confined by steel stirrups and discontinuous CFRP wraps, the innermost ring of the section is model by means of self compacting concrete confined by steel stirrups and discontinuous CFRP wraps and the external ring of the section is model with self compacting concrete confined by discontinuous CFRP wraps.

The only difference in the fiber section for the zero-length slip section and the column element is in the material models attributed to the section to simulate the strain penetration.

The vertical loads and displacements are applied at the node that is located at the free end of the column.

This software allows you to monitor and record different response parameters during the analysis, which could be the displacement history at a node or element at each step of the solution procedure. The node recorders are used to output the horizontal and vertical displacements at particular nodes during the simulation while the element recorder provides element resisting force in global or local coordinates or response quantities (section forces, deformations, stiffness) from a specific section along the member length (integration point).

Afterwards, the response of top node is discussed in detail followed by correlation studies on the experimental results. Furthermore, a very interesting and useful output is stress-strain relationship of steel and concrete fiber.

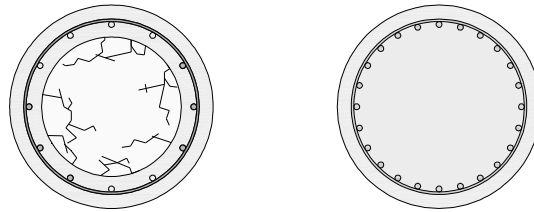


Figure 77 Piers cross section: (a) repaired squat pier, (b) as-build tall pier

```

      1
      2
      3
      4
      5
      6
      7
      8
      9
     10
     11
     12
     13
     14
     15
     16
     17
     18
     19
     20
     21
     22
     23
     24
     25
     26
     27
     28
     29
     30
     31
     32
     33
     34
     35
     36
     37
     38
     39
     40
     41
     42
     43
     44
     45
     46
     47
     48
     49
     50
     51
     52
     53
     54
     55
     56
     57
     58
     59
     60
     61
     62
     63
     64
     65
     66
     67
     68
     69
     70
     71
     72
     73
     74
     75
     76
     77
     78
     79
     80
     81
     82
     83
     84
     85
     86
     87
     88
     89
     90
     91
     92
     93
     94
     95
     96
     97
     98
     99
    100
    101
    102
    103
    104
    105
    106
    107
    108
    109
    110
    111
    112
    113
    114
    115
    116
    117
    118
    119
    120
    121
    122
    123
    124
    125
    126
    127
    128
    129
    130
    131
    132
    133
    134
    135
    136
    137
    138
    139
    140
    141
    142
    143
    144
    145
    146
    147
    148
    149
    150
    151
    152
    153
    154
    155
    156
    157
    158
    159
    160
    161
    162
    163
    164
    165
    166
    167
    168
    169
    170
    171
    172
    173
    174
    175
    176
    177
    178
    179
    180
    181
    182
    183
    184
    185
    186
    187
    188
    189
    190
    191
    192
    193
    194
    195
    196
    197
    198
    199
    200
    201
    202
    203
    204
    205
    206
    207
    208
    209
    210
    211
    212
    213
    214
    215
    216
    217
    218
    219
    220
    221
    222
    223
    224
    225
    226
    227
    228
    229
    230
    231
    232
    233
    234
    235
    236
    237
    238
    239
    240
    241
    242
    243
    244
    245
    246
    247
    248
    249
    250
    251
    252
    253
    254
    255
    256
    257
    258
    259
    260
    261
    262
    263
    264
    265
    266
    267
    268
    269
    270
    271
    272
    273
    274
    275
    276
    277
    278
    279
    280
    281
    282
    283
    284
    285
    286
    287
    288
    289
    290
    291
    292
    293
    294
    295
    296
    297
    298
    299
    300
    301
    302
    303
    304
    305
    306
    307
    308
    309
    310
    311
    312
    313
    314
    315
    316
    317
    318
    319
    320
    321
    322
    323
    324
    325
    326
    327
    328
    329
    330
    331
    332
    333
    334
    335
    336
    337
    338
    339
    340
    341
    342
    343
    344
    345
    346
    347
    348
    349
    350
    351
    352
    353
    354
    355
    356
    357
    358
    359
    360
    361
    362
    363
    364
    365
    366
    367
    368
    369
    370
    371
    372
    373
    374
    375
    376
    377
    378
    379
    380
    381
    382
    383
    384
    385
    386
    387
    388
    389
    390
    391
    392
    393
    394
    395
    396
    397
    398
    399
    400
    401
    402
    403
    404
    405
    406
    407
    408
    409
    410
    411
    412
    413
    414
    415
    416
    417
    418
    419
    420
    421
    422
    423
    424
    425
    426
    427
    428
    429
    430
    431
    432
    433
    434
    435
    436
    437
    438
    439
    440
    441
    442
    443
    444
    445
    446
    447
    448
    449
    450
    451
    452
    453
    454
    455
    456
    457
    458
    459
    460
    461
    462
    463
    464
    465
    466
    467
    468
    469
    470
    471
    472
    473
    474
    475
    476
    477
    478
    479
    480
    481
    482
    483
    484
    485
    486
    487
    488
    489
    490
    491
    492
    493
    494
    495
    496
    497
    498
    499
    500
    501
    502
    503
    504
    505
    506
    507
    508
    509
    510
    511
    512
    513
    514
    515
    516
    517
    518
    519
    520
    521
    522
    523
    524
    525
    526
    527
    528
    529
    530
    531
    532
    533
    534
    535
    536
    537
    538
    539
    540
    541
    542
    543
    544
    545
    546
    547
    548
    549
    550
    551
    552
    553
    554
    555
    556
    557
    558
    559
    560
    561
    562
    563
    564
    565
    566
    567
    568
    569
    570
    571
    572
    573
    574
    575
    576
    577
    578
    579
    580
    581
    582
    583
    584
    585
    586
    587
    588
    589
    590
    591
    592
    593
    594
    595
    596
    597
    598
    599
    600
    601
    602
    603
    604
    605
    606
    607
    608
    609
    610
    611
    612
    613
    614
    615
    616
    617
    618
    619
    620
    621
    622
    623
    624
    625
    626
    627
    628
    629
    630
    631
    632
    633
    634
    635
    636
    637
    638
    639
    640
    641
    642
    643
    644
    645
    646
    647
    648
    649
    650
    651
    652
    653
    654
    655
    656
    657
    658
    659
    660
    661
    662
    663
    664
    665
    666
    667
    668
    669
    670
    671
    672
    673
    674
    675
    676
    677
    678
    679
    680
    681
    682
    683
    684
    685
    686
    687
    688
    689
    690
    691
    692
    693
    694
    695
    696
    697
    698
    699
    700
    701
    702
    703
    704
    705
    706
    707
    708
    709
    710
    711
    712
    713
    714
    715
    716
    717
    718
    719
    720
    721
    722
    723
    724
    725
    726
    727
    728
    729
    730
    731
    732
    733
    734
    735
    736
    737
    738
    739
    740
    741
    742
    743
    744
    745
    746
    747
    748
    749
    750
    751
    752
    753
    754
    755
    756
    757
    758
    759
    760
    761
    762
    763
    764
    765
    766
    767
    768
    769
    770
    771
    772
    773
    774
    775
    776
    777
    778
    779
    780
    781
    782
    783
    784
    785
    786
    787
    788
    789
    790
    791
    792
    793
    794
    795
    796
    797
    798
    799
    800
    801
    802
    803
    804
    805
    806
    807
    808
    809
    810
    811
    812
    813
    814
    815
    816
    817
    818
    819
    820
    821
    822
    823
    824
    825
    826
    827
    828
    829
    830
    831
    832
    833
    834
    835
    836
    837
    838
    839
    840
    841
    842
    843
    844
    845
    846
    847
    848
    849
    850
    851
    852
    853
    854
    855
    856
    857
    858
    859
    860
    861
    862
    863
    864
    865
    866
    867
    868
    869
    870
    871
    872
    873
    874
    875
    876
    877
    878
    879
    880
    881
    882
    883
    884
    885
    886
    887
    888
    889
    890
    891
    892
    893
    894
    895
    896
    897
    898
    899
    900
    901
    902
    903
    904
    905
    906
    907
    908
    909
    910
    911
    912
    913
    914
    915
    916
    917
    918
    919
    920
    921
    922
    923
    924
    925
    926
    927
    928
    929
    930
    931
    932
    933
    934
    935
    936
    937
    938
    939
    940
    941
    942
    943
    944
    945
    946
    947
    948
    949
    950
    951
    952
    953
    954
    955
    956
    957
    958
    959
    960
    961
    962
    963
    964
    965
    966
    967
    968
    969
    970
    971
    972
    973
    974
    975
    976
    977
    978
    979
    980
    981
    982
    983
    984
    985
    986
    987
    988
    989
    990
    991
    992
    993
    994
    995
    996
    997
    998
    999
    1000
    1001
    1002
    1003
    1004
    1005
    1006
    1007
    1008
    1009
    1010
    1011
    1012
    1013
    1014
    1015
    1016
    1017
    1018
    1019
    1020
    1021
    1022
    1023
    1024
    1025
    1026
    1027
    1028
    1029
    1030
    1031
    1032
    1033
    1034
    1035
    1036
    1037
    1038
    1039
    1040
    1041
    1042
    1043
    1044
    1045
    1046
    1047
    1048
    1049
    1050
    1051
    1052
    1053
    1054
    1055
    1056
    1057
    1058
    1059
    1060
    1061
    1062
    1063
    1064
    1065
    1066
    1067
    1068
    1069
    1070
    1071
    1072
    1073
    1074
    1075
    1076
    1077
    1078
    1079
    1080
    1081
    1082
    1083
    1084
    1085
    1086
    1087
    1088
    1089
    1090
    1091
    1092
    1093
    1094
    1095
    1096
    1097
    1098
    1099
    1100
    1101
    1102
    1103
    1104
    1105
    1106
    1107
    1108
    1109
    1110
    1111
    1112
    1113
    1114
    1115
    1116
    1117
    1118
    1119
    1120
    1121
    1122
    1123
    1124
    1125
    1126
    1127
    1128
    1129
    1130
    1131
    1132
    1133
    1134
    1135
    1136
    1137
    1138
    1139
    1140
    1141
    1142
    1143
    1144
    1145
    1146
    1147
    1148
    1149
    1150
    1151
    1152
    1153
    1154
    1155
    1156
    1157
    1158
    1159
    1160
    1161
    1162
    1163
    1164
    1165
    1166
    1167
    1168
    1169
    1170
    1171
    1172
    1173
    1174
    1175
    1176
    1177
    1178
    1179
    1180
    1181
    1182
    1183
    1184
    1185
    1186
    1187
    1188
    1189
    1190
    1191
    1192
    1193
    1194
    1195
    1196
    1197
    1198
    1199
    1200
    1201
    1202
    1203
    1204
    1205
    1206
    1207
    1208
    1209
    1210
    1211
    1212
    1213
    1214
    1215
    1216
    1217
    1218
    1219
    1220
    1221
    1222
    1223
    1224
    1225
    1226
    1227
    1228
    1229
    1230
    1231
    1232
    1233
    1234
    1235
    1236
    1237
    1238
    1239
    1240
    1241
    1242
    1243
    1244
    1245
    1246
    1247
    1248
    1249
    1250
    1251
    1252
    1253
    1254
    1255
    1256
    1257
    1258
    1259
    1260
    1261
    1262
    1263
    1264
    1265
    1266
    1267
    1268
    1269
    1270
    1271
    1272
    1273
    1274
    1275
    1276
    1277
    1278
    1279
    1280
    1281
    1282
    1283
    1284
    1285
    1286
    1287
    1288
    1289
    1290
    1291
    1292
    1293
    1294
    1295
    1296
    1297
    1298
    1299
    1300
    1301
    1302
    1303
    1304
    1305
    1306
    1307
    1308
    1309
    1310
    1311
    1312
    1313
    1314
    1315
    1316
    1317
    1318
    1319
    1320
    1321
    1322
    1323
    1324
    1325
    1326
    1327
    1328
    1329
    1330
    1331
    1332
    1333
    1334
    1335
    1336
    1337
    1338
    1339
    1340
    1341
    1342
    1343
    1344
    1345
    1346
    1347
    1348
    1349
    1350
    1351
    1352
    1353
    1354
    1355
    1356
    1357
    1358
    1359
    1360
    1361
    1362
    1363
    1364
    1365
    1366
    1367
    1368
    1369
    1370
    1371
    1372
    1373
    1374
    1375
    1376
    1377
    1378
    1379
    1380
    1381
    1382
    1383
    1384
    1385
    1386
    1387
    1388
    1389
    1390
    1391
    1392
    1393
    1394
    1395
    1396
    1397
    1398
    1399
    1400
    1401
    1402
    1403
    1404
    1405
    1406
    1407
    1408
    1409
    1410
    1411
    1412
    1413
    1414
    1415
    1416
    1417
    1418
    1419
    1420
    1421
    1422
    1423
    1424
    1425
    1426
    1427
    1428
    1429
    1430
    1431
    1432
    1433
    1434
    1435
    1436
    1437
    1438
    1439
    1440
    1441
    1442
    1443
    1444
    1445
    1446
    1447
    1448
    1449
    1450
    1451
    1452
    1453
    1454
    1455
    1456
    1457
    1458
    1459
    1460
    1461
    1462
    1463
    1464
    1465
    1466
    1467
    1468
    1469
    1470
    1471
    1472
    1473
    1474
    1475
    1476
    1477
    1478
    1479
    1480
    1481
    1482
    1483
    1484
    1485
    1486
    1487
    1488
    1489
    1490
    1491
    1492
    1493
    1494
    1495
    1496
    1497
    1498
    1499
    1500
    1501
    1502
    1503
    1504
    1505
    1506
    1507
    1508
    1509
    1510
    1511
    1512
    1513
    1514
    1515
    1516
    1517
    1518
    1519
    1520
    1521
    1522
    1523
    1524
    1525
    1526
    1527
    1528
    1529
    1530
    1531
    1532
    1533
    1534
    1535
    1536
    1537
    1538
    1539
    1540
    1541
    1542
    1543
    1544
    1545
    1546
    1547
    1548
    1549
    1550
    1551
    1552
    1553
    1554
    1555
    1556
    1557
    1558
    1559
    1560
    1561
    1562
    1563
    1564
    1565
    1566
    1567
    1568
    1569
    1570
    1571
    1572
    1573
    1574
    1575
    1576
    1577
    1578
    1579
    1580
    1581
    1582
    1583
    1584
    1585
    1586
    1587
    1588
    1589
    1590
    1591
    1592
    1593
    1594
    1595
    1596
    1597
    1598
    1599
    1600
    1601
    1602
    1603
    1604
    1605
    1606
    1607
    1608
    1609
    1610
    1611
    1612
    1613
    1614
    1615
    1616
    1617
    1618
    1619
    1620
    1621
    1622
    1623
    1624
    1625
    1626
    1627
    1628
    1629
    1630
    1631
    1632
    1633
    1634
    1635
    1636
    1637
    1638
    1639
    1640
    1641
    1642
    1643
    1644
    1645
    1646
    1647
    1648
    1649
    1650
    1651
    1652
    1653
    1654
    1655
    1656
    1657
    1658
    1659
    1660
    1661
    1662
    1663
    1664
    1665
    1666
    1667
    1668
    1669
    1670
    1671
    1672
    1673
    1674
    1675
    1676
    1677
    1678
    1679
    1680
    1681
    1682
    1683
    1684
    1685
    1686
    1687
    1688
    1689
    1690
    1691
    1692
    1693
    1694
    1695
    1696
    1697
    1698
    1699
    1700
    1701
    1702
    1703
    1704
    1705
    1706
    1707
    1708
    1709
    1710
    1711
    1712
    1713
    1714
    1715
    1716
    1717
    1718
    1719
    1720
    1721
    1722
    1723
    1724
    1725
    1726
    1727
    1728
    1729
    1730
    1731
    1732
    1733
    1734
    1735
    1736
    1737
    1738
    1739
    1740
    1741
    1742
    1743
    1744
    1745
    1746
    1747
    1748
    1749
    1750
    1751
    1752
    1753
    1754
    1755
    1756
    1757
    1758
    1759
    1760
    1761
    1762
    1763
    1764
    1765
    1766
    1767
    1768
    1769
    1770
    1771
    1772
    1773
    1774
    1775
    1776
    1777
    1778
    1779
    1780
    1781
    1782
    1783
    1784
    1785
    1786
    1787
    1788
    1789
    1790
    1791
    1792
    1793
    1794
    1795
    1796
    1797
    1798
    1799
    1800
    1801
    1802
    1803
    1804
    1805
    1806
    1807
    1808
    1809
    1810
    1811
    1812
    1813
    1814
    1815
    1816
    1817
    1818
    1819
    1820
    1821
    1822
    1823
    1824
    1825
    1826
    1827
    1828
    1829
    1830
    1831
    1832
    1833
    1834
    1835
    1836
    1837
    1838
    1839
    1840
    1841
    1842
    1843
    1844
    1845
    1846
    1847
    1848
    1849
    1850
    1851
    1852
    1853
    1854
    1855
    1856
    1857
    1858
    1859
    1860
    1861
    1862
    1863
    1864
    1865
    1866
    1867
    1868
    1869
    1870
    1871
    1872
    1873
    1874
    1875
    1876
    1877
    1878
    1879
    1880
    1881
    1882
    1883
    1884
    1885
    1886
    1887
    1888
    1889
    1890
    1891
    1892
    1893
    1894
    1895
    1896
    1897
    1898
    1899
    1900
    1901
    1902
    1903
    1904
    1905
    1906
    1907
    1908
    1909
    1910
    1911
    1912
    1913
    1914
    1915
    1916
    1917
    191
```

3.2.1. Tall Piers

The tall specimen is representative of the lateral pier (14m height) of the regular bridge (**Figure 1**). The applied dead axial load due to the deck is equal to 10800kN.

The OPENSEES model is a fiber model in which the cross-sectional area of a flexural member is divided into a number of longitudinal fibers. A description of the cross section (fibers subdivisions) can be found in the [3.2] The OPENSEES model represents the scaled 1:6 tall specimen. The displacements history of the top of the lateral piers that was imposed on the specimen during the pseudodynamic test (Kobe accelerogram) and the constant axial load are applied to the node that corresponds to the top of the model. The real scale results are shown in Figure 79.

The comparison between the Force-displacement cycles of the OPENSEES model and the actual response of the tall specimen during the pseudo-dynamic test shows that the model can predict with good agreement the behavior of the tall specimen.

In particular the model provides good predictions of the reloading and unloading stiffness during the cycles in the positive direction and the maximum force are practically the same.

The restoring forces and the stiffness are different in the negative direction. In particular the specimen shows greater restoring forces than those of the model whereas the stiffness of the OPENSEES is greater than that of the specimen.

Some differences between the cycles of the specimen and of the model are also evident around the zero position.

Note that the difference can be due to:

- Non symmetric disposition of the longitudinal bar in the section that was already detected for the squat piers
- The mean values of the material property which are calculated on the base all the available data for the tall piers, are used because of the uncertainty in the identification of the specimen.

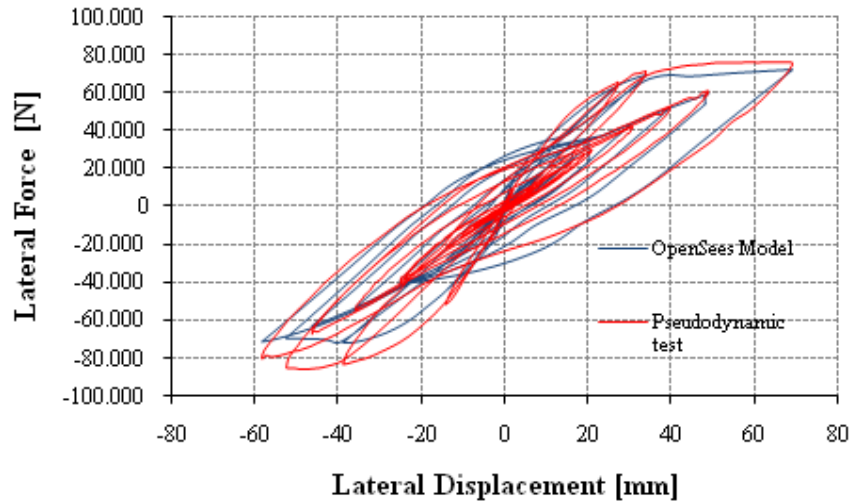


Figure 79 Comparison between the Force-displacement cycles of tall pier (14m) of the regular bridge and the OpenSees model response during the pseudodynamic test.

This analysis was performed to test the effectiveness of the OPENSEES fiber model to predict the seismic response of the tall specimen. First the tall specimen is chosen to be modeled because of the experimental results show that the column exhibited a typical flexural failure that usually is simple to model. Then the model can be refined to include the effects of other physical phenomena such as the shear contribution or in the case of the repaired squat piers the damage of the specimen base.

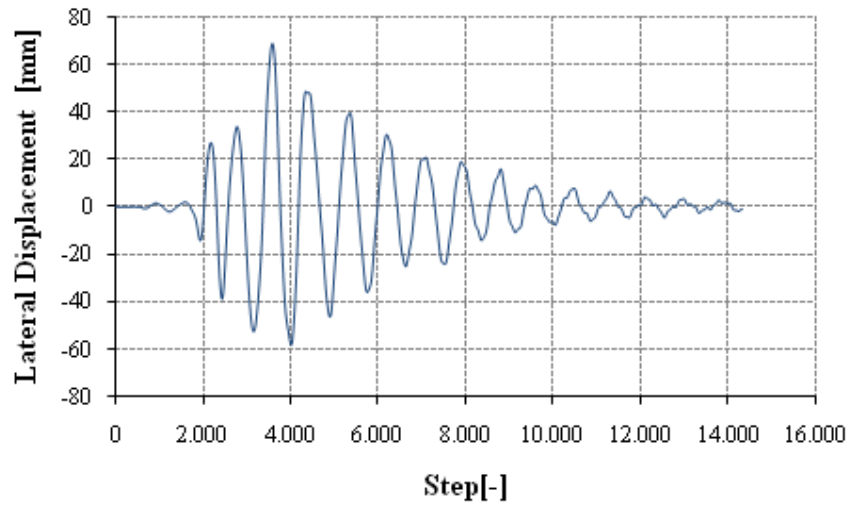


Figure 80 EC8 regular bridge lateral piers – pseudodynamic test with Kobe Displacements history. This displacements History is applied on the Top of the Opensees Model

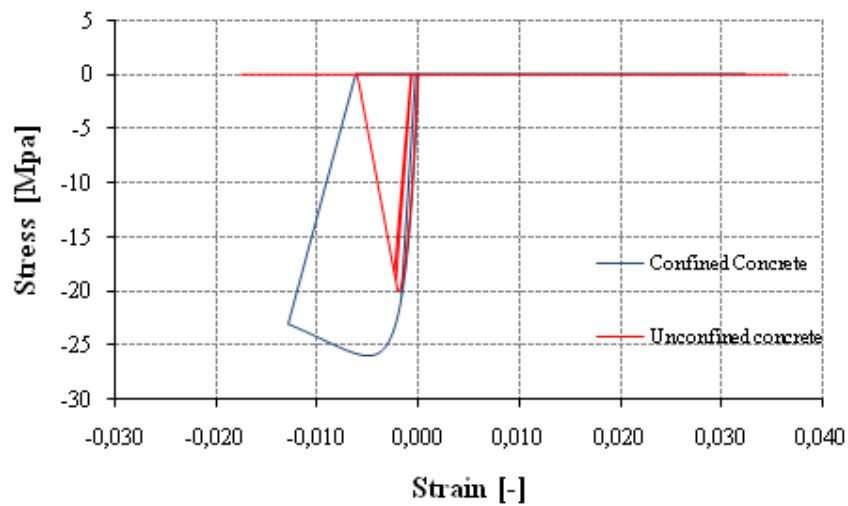


Figure 81 Confined (core) and unconfined concrete (cover) of the cross section of the as-build tall pier.-cyclic behavior of the model during the analysis (Displacements history applied at the top of the specimen during the pseudodynamic test (Kobe accelerogram)

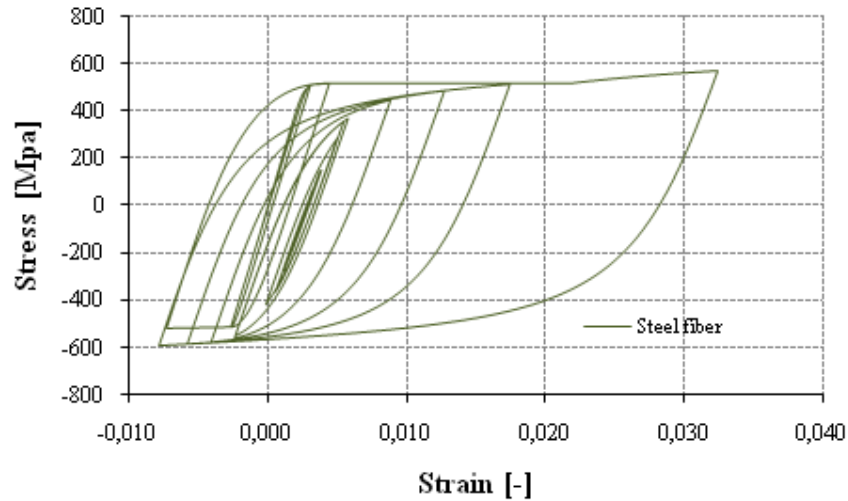


Figure 82 Steel fiber of the cross section of the as-build tall pier.-cyclic behavior of the model during the analysis (Displacements history applied at the top of the specimen during the pseudodynamic test (Kobe accelerogram))

3.2.2. Squat Piers

The squat specimen is representative of the central pier (7m height) of the irregular bridge (Figure 1). The applied dead axial load due to the deck is equal to 9288kN.

The OPENSEES model is a fiber model in which the cross-sectional area of a flexural member is divided into a number of longitudinal fibers. A description of the cross section (fibers subdivisions) can be found in the [3.2]. The OPENSEES model represents the scaled 1:6 squat specimen.

The material model for the concrete is Hosotani and Kawashima (1998) [84], [85]. The cover SCC is confined by CFRP whereas the inner SCC and the repaired concrete core are confined by CFRP and steel stirrups.

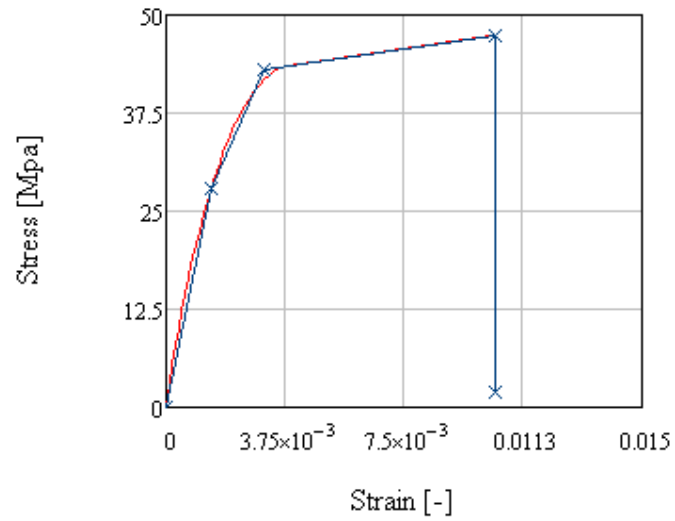


Figure 83 Hosotani and Kawashima (1998) - SCC confined by CFRP discontinuous wrapping - (cover).

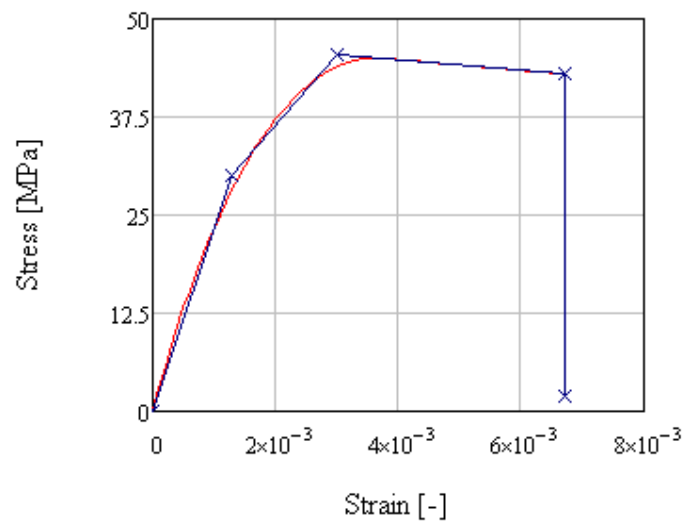


Figure 84 Hosotani and Kawashima (1998) - SCC confined by CFRP discontinuous wrapping and steel stirrups- (external part of the concrete core).

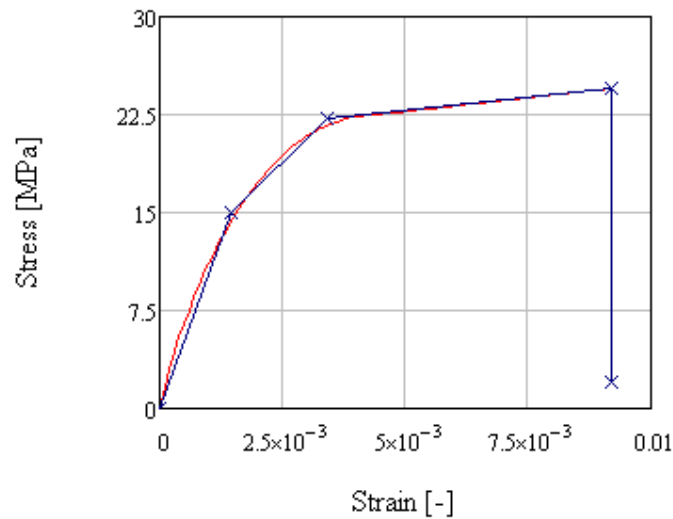


Figure 85 Hosotani and Kawashima (1998) - concrete confined by CFRP discontinuous wrapping and steel stirrups- (repaired concrete core).

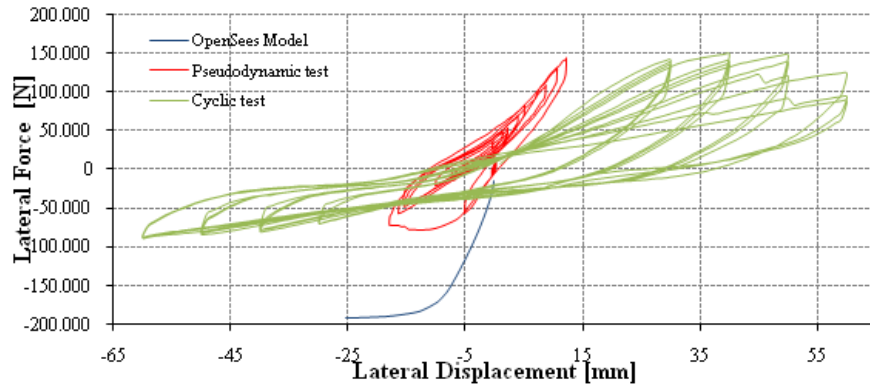


Figure 86 Comparison between the monotonic displacement responses of the OpenSees fiber model of the retrofitted squat pier and the pseudodynamic and cyclic response of the specimen.(scale of the specimen).

It is clear by **Figure 86** that the stiffness of the retrofitted specimen is smaller than that of the fiber model. The maximum force that the fiber model predicts is greater than the measured restoring force. The stiffness

can be modeled better by introducing the reduction of the concrete stiffness due to cracking of the concrete.

Note that the results of the preliminary test which are in progress shows that the contribution of the concrete core and of the two bars that have the broken anchorage does not seem justify the experimental behavior of the specimen. Finally it is necessary to refine the model to include the base rotation due to the wide cracks.

4. Conclusion

In this thesis the first results of the experimental research at the Laboratory of experiments on materials and structures of the University of Roma Tre on column specimens representative of repaired and retrofitted squat circular r.c. bridge piers, which were designed according to Italian code before 1986 for the design of concrete structures and previously tested until collapse by pseudo-dynamic and cyclic tests are presented. The tests carried out are of pseudo-dynamic type as well as cyclic.

Innovative techniques to fast repair of bridge piers, which are seriously damaged by severe earthquakes, are proposed and the practical problems in repairing and retrofitting of the piers are examined.

The proposed repairing techniques use adhesive resin, stainless steel bars and self compacting concrete and C-FRP discontinuous wrapping to increase the shear strength of the piers which are significantly damaged due to shear failure in order to match EC8 design requirements.

The experimental study includes the testing of five specimens at 1/6 scale: two undamaged tall piers and three damage squat piers.

All above specimens represent bridge piers which were designed according to previous Italian code of 1986 for the design of concrete structures.

Tall piers have insufficient transverse reinforcement and then the curvature ductility is smaller than that of the piers of the same bridge designed by Eurocode8. Therefore, the undamaged tall piers are retrofitted using C-FRP discontinuous wrapping to increase the ductility to match EC8 design requirements. The tests on tall piers are in progress.

Two squat specimens were considerably damaged during the previous pseudo-dynamic and cyclic test, and shear failure was detected. These specimens are repaired and retrofitted using the proposed techniques to improve the shear strength in order to evaluate the effectiveness of the applied repairing and retrofitting methods

In particular, it is important to note that, the material which are used to repair and strengthening the piers allow overcoming many of the difficulties that have previously limited similar solutions. However, it can be observed that:

- It is possible to use adhesive resin material with very low viscosity in order to restore by injection concrete element damaged by earthquakes. The resin passes also through the hairline cracks and penetrates deep down into the concrete core. The injection is easy to do and very fast. The effectiveness of the adhesive resin has to be investigated by means of numerical simulation. In fact, it is possible to evaluate analytically the contribution of the repaired concrete core using two fiber model in OPENSEES which include or not the concrete core.
- the SCC can restore the cover and the external part of the concrete core and guarantees the continuity of the structural member in spite of the narrow spaces of concrete casting (the destructive inspection after the cyclic test, proves this consideration). During the casting operation the SCC has not to be vibrated by means of external tools. A concrete pouring is carried out in stages in fast and easy way: the SCC is cast from above (upper part of the part of the specimen where it is necessary to restore the removed concrete) by means of buckets. The SCC concrete develops high mechanical resistance very quickly after it is poured and the framework can be removed just 24 hours after pouring. The SCC surface is uninterrupted without ridges and compact: occlusions or vacuums are not detected. The concrete jacket is practically not damaged after the pseudodynamic and the cyclic tests: only some cracks may be noted at the base of the column.
- It can be a difficult to connect the new portion of longitudinal bars to the original ones. The foundations can be congested with reinforcement and then it is difficult to anchor the new portion of

longitudinal bars. A possible solution is to weld the new portion of longitudinal bars to the preexistent anchorages if they are undamaged. However it is necessary to pay careful attention to welding design and procedures. In fact the welding can be the weak element.

- The different resistance of the inox bars (allowable by Italian code in the past) can causes the asymmetric behavior of the structural element if only yielding or break longitudinal bars are substituted. However this solution can provide cost saving benefits and limits the problem of making the connection between new longitudinal bars and the original ones. More focused studies will be needed to understand the behavior of this connection between the bars and to improve it. The disposition of the new bars can correct original irregularity (for instance the wrong disposition of the longitudinal bars during the pouring of concrete)
- The new inox stirrups are designed to take the maximum shear load that is equivalent to that of the original one and are placed externally the longitudinal bars applying a tension to the inox bars. The stirrups were connected by strong tying to the longitudinal bars and were closed by welding connection and enclosed the longitudinal bars (the new inox bars and the original ones).

The CFRP wrapping improves the shear resistance of the specimen and confines the repaired portion of the specimen. A CFRP discontinuous wrapping is placed on the surface of the repaired portion of the columns to improve the shear resistance of the specimen.

A discontinuous wrapping is placed because of the pre-existing transversal bars which are used as rigid support for the sensors in plastic hinge zone and to allow the survey of the crack patterns during the test.

The specimen is strengthened with one layer of CFRP. The monotonic moment-curvature relationship of the repaired and retrofitted section can be rather accurately traced using a fiber model. In particular, OpenSees was used to model accurately the repaired specimen and the nonlinear behavior of the material

(standard steel, inox, concrete and SCC confined by CFRP wrapping and/or steel stirrups) was included in this analysis.

The shear strength of the repaired and retrofitted piers was calculated and It is evident that the shear corresponding to the maximum moment obtained by the analysis can be sustained by the retrofitted pier. Thus, brittle shear failure before yielding is avoided.

In conclusion, the proposed repairing techniques are doable and are quite simple and fast.

Subsequently a pseudodynamic apparatus as well as the relative computer software has been developed and set up to test the repaired specimens.

In-house pseudo-dynamic test software is implemented in MATLAB and LabIEW 8.2.and pseudo-dynamic tests are performed on the one squat specimen to test the pseudo-dynamic test equipment and software.

The pseudodynamic software has been written using MATLAB in order to simplify the implementation starting from a previous FORTRAN version of the software.

However the National instruments hardware used to acquire the measures of the transducer and to control the actuator have to be controlled by LABVIEW. So dedicated LABVIEW structures are used to sends the m-code to MATLAB for execution and then reads the results back in to LabVIEW.

Finally, LabVIEW is used to develop easy human machine interface (HMI), sequential control, safety interlock and control the hardware (INVERTER, DAQ-board, acquisition modules), whereas MATLAB is employed to implement numerical analysis and simulation procedure. Several problems arise during the equipment setup. Some kinds of noise sources will appear similarly in all measurements; they have different origins and are of different types:

- motor control hardware gives so much electrical noise that they disturb the potentiometer. This spike noises are due to the electrical signals which are used to control the inverter and then the motors.
- Chassis power pack introduces periodic variation of all the measures. This noise appears as “a wave noise” that simultaneity

modify in the same way the amplitude of the measures of all the transducer (strain gauges, load cells and potentiometers)

In order to reduce this noise, a hardware filter is successfully used to reduce the effect of noise due to chassis whereas an in house software filter is successfully implemented in LABVIEW to filter the noise in real time during the test.

The new pseudodynamic software was tested and tuned performing two pseudodynamic test on a squat specimen that was already damaged but only a single large crack at the column base is observed. The structure tested by means of the pseudodynamic apparatus is an irregular concrete bridge.

The bridge has a continuous box girder hinged on the circular section piers and on the abutments. It consists of four bridge spans with an equal span length of 50m

The piers are of unequal height with the shortest pier 7m in the middle and two piers with different height (14m and 21m) on sides (irregular configuration).

Two pseudodynamic test were performed using Tolmezzo earthquake acceleration records (PGA=0.35) for the first test and Tolmezzo earthquake acceleration records scaled up to two (PGA=0.7) for the second test.

Then nonlinear dynamic analyses of the bridge are carried out by means of the previous FORTRAN pseudo-dynamic software that has been used with success in previous pseudo-dynamic test [52]. In this simulation the response (force-displacement) of each pier (including the experimental behavior of the specimen 7) is modeled using the Takeda model and the input files are the same, which are used for the actual pseudo-dynamic test on the specimen 7.

The comparison between the results of the actual test and result obtained by the numerical simulation using FORTRAN version of the software shows a general good agreement with the experimental results of the actual pseudo-dynamic test on the squat specimen. Therefore the new software and the pseudo-dynamic test equipment work correctly.

In-house test apparatus is designed and work correctly. The vertical frame can potentially apply load up to 1600kN and the design solution allows testing also the tall piers despite the free space in height available.

The 500kN actuator is controlled through a closed-ring control system. In this way the accuracy of velocity control is guaranteed. In house control and acquisition software are developed using LABVIEW.

Therefore two pseudo-dynamic tests using the same above accelerograms and one cycles test are performed on one repaired squat piers. The results of the survey show that after the test:

- The CFRP wrapping is not damaged after the cyclic test. The external concrete confined by CFRP is damaged only near the base and the damage is limited.
- Only one large crack was observed near the base of the specimen after the tests.
- Some welding connection of the longitudinal bars are broken

The performance of the repaired pier is compared with that of the as-built squat pier during pseudo-dynamic test. The bridge structure and the input excitation are the same used during the previous test on the as-built piers. The comparison between the experimental results of the as-build pier and the repaired one shows that:

- the rupture of the welding between inox longitudinal bars and the original one can affect the response of the structure to loading. In fact, the stiffness of the specimens abruptly drops maybe because of the rupture of one welding connection.
- the proposed repair techniques provide satisfactory seismic performance of the repaired specimen and have improved the strength and the stiffness of the damaged piers. In addition it is possible to recover the seismic performance of the as-build piers which show a severe damage state.
- The initial stiffness of the repaired pier is better than that of the "as build pier" in each loading directions.
- The different stiffness in the negative direction could be due to the anchorage failure during the first pseudo-dynamic test. It is

evident that this great reduction of the stiffness is a problem about which it is necessary to reflect.

The comparison between the seismic response of the irregular bridge with as-build piers and the same bridge with the repaired pier shows that:

- the maximum displacements of the as- build central pier are greater than those of the repaired one in the positive direction, whereas the maximum displacements are about the same in the opposite direction during the time interval in which the displacements are greater. The difference is of about 25mm (real scale) in the positive direction. The displacement trend is the same in both analyses
- The displacements are different in both direction (positive/negative) during the final displacement cycles and the as-build has greater displacements than the repaired one of about 15-20mm.

Flexural displacements of the top of the repaired specimen were computed by integrating curvatures along the height of the specimen and the contribution due to shear was then found as the difference between the pier top total displacement measured during the cyclic test and the computed flexural one. The curvatures were obtained using the displacement measured by vertical transducer in the “critical zone” at the base of the specimen (that includes the “plastic hinge zone” where the plastic deformations are dominantly concentrated). The displacements due to the shear are small. In fact the CFRP wrapping works correctly and the damaged is concentrated at the base section of the specimen where large rotations occur.

The CFRP deformations (in the fiber direction) are limited to 2 mEpsilon during the cyclic tests. These deformations are measured on the FRP strips at the base of the specimen and one strain gauge has measured a deformation of about 4 mEpsilon but maybe it was broken or placed where the failure occurred.

The OPENSEES model for the tall piers can correctly reproduce the experimental behavior of this element if the strain penetration effect is taken in account. The model represents the scaled 1:6 tall specimen. The

displacements history of the top of the lateral piers that was imposed on the specimen during the pseudodynamic test (Kobe accelerogram) and the constant axial load (300kN) are applied to the node that corresponds to the top of the model during the analysis.

The squat piers can be model using a refined fiber model in OpenSees which includes the nonlinear behavior of the repaired concrete and the new external portion of the core (SCC) confined by discontinuous CFRP wrapping and steel stirrups, the SCC cover confined by CFRP wrapping, the undamaged original longitudinal bar and the new inox longitudinal bars. The analytical model for the concrete is proposed by Hosotani and Kawashima (1998).

The monotonic displacements are imposed on the top of the fiber model where is applied a vertical load of about 258Kn.

Finally the research is in progress and:

- we will test the second squat piers as soon as possible. This pier is similar to tested squat piers and the repair procedure is the same. The experimental results will be compared with those of the first repaired squat specimen. The pseudodynamic tests will carry out using the same input (structure, integration parameters and input excitation). Finally cyclic test will perform.
- The welding connection between inox longitudinal bars and the original ones has to be investigated in order to understand if the welding techniques can be improved or if a new connection technique has to be used.
- The damaged specimen 7 will repair using inox longitudinal bars which are allowed by the new Italian code. The resistance of this bar is comparable with that of the standard bars. It is necessary to reflect on the type of anchorage between the new longitudinal bars and the original ones that can be used.
- Retrofitted tall piers will test and the experimental results will help determine and understand the CFRP effects to improve also the accuracy of the OPENSEES fiber model of the repaired squat piers

- OPENSEES model for squat piers has to be improved to take account of the correct cyclic behavior of the SCC confined by CFRP and/or stirrups and to model the experimental behavior of the specimen in order to understand the effect of:
- the rupture of the welding connection
- The contribution of the repaired concrete core

Acknowledgments

Research carried out under the partial financial support of “convenzione Dipartimento di Protezione Civile- Consorzio RELUIS, signed 11/07/2005 (repertorio n. 540), research line 2.

REFERENCE

[1] Bayer, V., Dorka, U.E., and Fullekrug, U. (2000), “A New Algorithm for Real-Time Sub-Structure Pseudodynamic Tests,” Proc. of 12th World Conference on Earthquake Engineering, Auckland, New Zealand.

[2] Darby, A.P., Blakeborough, A, and Williams, M.S. (1999), “Real-Time Substructure Tests using Hydraulic Actuators,”

Journal of Engineering Mechanics, American Society of Civil Engineers, 125, 1133-1139.

[3] Dermitzakis, S.N. and Mahin, S.A. (1985), “Development of Substructuring Techniques for On-Line Computer Controlled Testing,”

UBC/EERC-85/04, Earthquake Engineering Research Center, University of California, Berkeley, CA.

[4] Hakuno, M., Shidawara, M., and Hara, T. (1969), "Dynamic Destructive Test of a Cantilever Beam Controlled by an Analog Computer," Trans. Japanese Society of Civil Engineers, 171, 1-9.

[5] Horiuchi, T., Nakagawa, M., Sugano, M., and Konno, T. (1996), "Development of a Real-Time Hybrid Experimental System with Actuator Delay Compensation," Proc. of 11th World Conference on Earthquake Engineering, Paper No.660, Acapulco, Mexico.

[6] Hughes, T.J.R. (1983), "Analysis for Transient Algorithms with Particular Reference to Stability Behavior," Belyschko T, [02] Hughes T.J.R., Editors. Computational Methods for Transient Analysis. Amsterdam, North-Holland.

[7] Jung, R. and Shing, P.B. (2006), "Performance Evaluation of a Real-time Pseudodynamic Test System," Earthquake Engineering and Structural Dynamics (in press).

[8] Magonette, G., Pegon, P., Molina, F.J., and Buchet, P. (1998). "Development of Fast Continuous Pseudodynamic Substructuring Tests," Proc. of 2nd World Conference on Structural Control, Kyoto, Japan.

[9] McKenna, F. and Fenves, G.L. (2000), "An Object-Oriented Software Design for Parallel Structural Analysis," Proc. of the SEI/ASCE Structures Congress, Philadelphia, PA.

[10] Mahin S.A. and Shing P.B., "Pseudodynamic method for seismic testing." Journal of Structural Engineering (ASCE), 1985; 111: 1482-1503.

[11] Nakashima, M. and Kato, H. (1987), "Experimental Error Growth Behavior and Error Growth Control in On-Line Computer Control Test Method," BRI Research Paper No. 123, Building Research Institute, Ministry of Construction, Japan.

-
- [12] Nakashima, M., et al. (1990), "Integration Techniques for Substructure Pseudodynamic Test," Proc. of 4th U.S. National Conference on Earthquake Engineering, II, Palm Springs, CA, 515-524.
- [13] Nakashima, M., Kato, H., and Takaoka, E. (1992), "Development of Real-Time Pseudo Dynamic Testing," Earthquake Engineering and Structural Dynamics, 21, 79-92.
- [14] Nakashima, M. and Masaoka, N. (1999), "Real-Time On-Line Test for MDOF Systems," Earthquake Engineering and Structural Dynamics, 28, 393-420.
- [15] Pinto, A.V., Pegon, P., Magonette, G., and Tsionis, G.. (2004), "Pseudo-Dynamic Testing of Bridges using Non-Linear Substructuring," Earthquake Engineering and Structural Dynamics, 33, 1125-1146.
- [16] Reinhorn, A.M., Sivaselvan, M.V., Weinreber, S., and Shao, X. (2004), "Real-Time Dynamic Hybrid Testing of Structural Systems," Proc. of 3rd European Conference on Structural Control, Vienna, Austria.
- [17] Shing P.B. and Mahin, S.A. (1983), "Experimental Error Propagation in Pseudodynamic Testing," UCB/EERC-83/12, Earthquake Engineering Research Center, University of California, Berkeley, CA.
- [18] Shing, P.B., Vannan, M.T., and Carter, E. (1991), "Implicit Time Integration for Pseudodynamic Tests," Earthquake Engineering and Structural Dynamics, 20, 551-576.
- [02] Shing, P.B., Bursi, O.S., and Vannan, M.T. (1994), "Pseudodynamic Tests of a Concentrically Braced Frame using Substructuring Techniques," Journal of Constructional Steel Research, 29, 121-148.
- [19] Shing, P.B., Wei, Z., Jung, R., and Stauffer, E. (2004), "NEES Fast Hybrid Test System at the University of Colorado," Proc. of 13th World Conference in Earthquake Engineering, Vancouver, Canada.
- [20] Shing, P.B., Bursi, O.S., and Vannan, M.T. (1994), "Pseudodynamic Tests of a Concentrically Braced Frame using Substructuring Techniques," Journal of Constructional Steel Research, 29, 121-148.

[21] Takanashi, K., et al. (1974), "Seismic Failure Analysis of Structures by Computer-Pulsator On-Line System," Journal of Institute of Industrial Science, 26(11), University of Tokyo, Tokyo, 13-25.

[22] Takanashi K. et al., "Non-linear earthquake response analysis of structures by a computer actuator on-line system, part 1 – details of the system." Trans. of Architectural Inst. of Japan, Tokyo, Japan, 1975; 229: 77-83.

[23] Yang, C.-S., Leon, R.T., and DesRoches. R. (2006), "On the Development of Zipper Frames by Pushover Testing," Proc. of 5th Conference on the Behavior of Steel Structures in Seismic Areas, Yokohama, Japan.

[24] Nakashima M., Kaminosono T., and Ishida M., "Integration techniques for substructure pseudodynamic test." Proceedings of 4th US National Conference on Earthquake Engineering, 1990; II: 515-524.

[25] Shing P.B., Nakashima M., and Bursi O., "Application of pseudodynamic test method to structural research." Earthquake Spectra, 1996; 12(1): 29-56.

[26] . Pinto A.V., Pegon P., Magonette G., and Tsionis G., "Pseudo-dynamic testing of bridges using non-linear substructuring." *Earthquake Engineering and Structural Dynamics*, 2004; 33: 1125-1146.

[27] . Nakashima M. and Masaoka N., "Real-time on-line test for MDOF systems." *Earthquake Engineering and Structural Dynamics* 1999; 28: 393-420.

[28] . Horiuchi T., Nakagawa M., Sugano M., and Konno T. (1996), "Development of a real-time hybrid experimental system with actuator delay compensation," Proc. of 11th World Conference on Earthquake Engineering, Paper No. 660, Acapulco, Mexico.

-
- [29] Williams D.M., Williams M.S., and Blakeborough A., "Numerical modeling of a servo-hydraulic testing system for structures." *Journal of Engineering Mechanics*, 2001; 127(8):816-827.
- [30] . Zhao J. et al., "Considerations for the development of real-time dynamic testing using servo-hydraulic actuation." *Earthquake Engineering and Structural Dynamics*, 2003; 32:1773-1794.
- [31] . Chang S.Y., "Explicit pseudodynamic algorithm with unconditional stability." *Journal of Engineering Mechanics*, 2002; 128(9):935-947.
- [32] . Bonelli A. and Bursi O.S., "Generalized- α methods for seismic structural testing." *Earthquake Engineering and Structural Dynamics*, 2004; 33: 1067-1102.
- [33] . Wu B., Xu G., Wang Q., and Williams M.S., "Operator-splitting method for real-time substructure testing." *Earthquake Engineering and Structural Dynamics*, 2006; 35(3): 293-314.
- [34] . Bursi O. and Shing P.B., "Evaluation of some implicit time-stepping algorithms for pseudodynamic tests." *Earthquake Engineering and Structural Dynamics* 1996; 25: 333-355.
- [35] . Jung R.-Y., "Development of real-time hybrid test system." Doctoral Thesis, University of Colorado at Boulder, 2005.
- [36] Bayer V., Dorka U.E., Füllekrug U., and Gschwilm, J., "On real-time pseudodynamic sub-structure testing: algorithm, numerical and experimental results." *Aerospace Science and Technology*, 2005; 9: 223-232.
- [37] . Jung R.-Y. and Shing P.B., "Performance evaluation of a real-time pseudodynamic test system." *Earthquake Engineering and Structural Dynamics*, 2006; 35(7): 789-810.
- [38] . Hughes T.J.R., "Analysis for transient algorithms with particular reference to stability behavior." Belyschko T., Hughes T.J.R (Ed.). *Computational Methods for Transient Analysis*. Amsterdam: North-Holland, 1983.

[39] . Shing P.B., Vannan M.T., and Carter E., "Implicit time integration for pseudodynamic tests." *Earthquake Engineering and Structural Dynamics*, 1991; 20(6):551-576.

[40] . Shing P.B. and Vannan M.T., "Implicit time integration for pseudodynamic tests: convergence and energy dissipation." *Earthquake Engineering and Structural Dynamics*, 1991; 20(6):809-819.

[41] Wu B., Wang Q., Shing P.B., and Ou J., "Equivalent force control method for generalized real-time substructure testing with implicit integration." *Earthquake Engineering and Structural Dynamics*, 2007. (in press)

[42] . Wei Z., "Fast hybrid test system for substructure evaluation." Doctoral Thesis, University of Colorado at Boulder, 2005.

[43] . Shing P.B., Stavridis A., Wei Z., Stauffer E., Wallen R., and Jung R., "Validation of a fast hybrid test system with substructure tests." *Proc. of 17th Analysis and Computation Conference, SEI/ASCE, St. Louis, May, 2006.*

[44] . Dorf R.C. and Bishop R.H., *Modern Control Systems*, 9th ed., Prentice Hall, NJ, 2000.

[45] Goodwin G.C., Graebe S.F., and Salgado M.E., *Control System Design*, Prentice Hall, NJ, 2001.

[46] T. Albanesi, D. Lavorato, & C. Nuti, "Prove sperimentali monotone e cicliche su barre di acciaio inox". *Sperimentazione su materiali e strutture, Convegno nazionale, Venezia: 357-366 (2006).*,

[47] T. Albanesi, C. Nuti, F. Paolacci, & S. Santini, "Cyclic tests of existing r.c. columns repaired or retrofitted by mean of jacketing technique", *Fib Congress, Naples, paper 0521(2006).*

[48] T. Albanesi, C. Nuti, F. Paolacci, & S. Santini, "Comportamento ciclico di colonne in c.a. riparate ed adeguate con fasciature in FRP" ,

ANIDIS: XII Convegno L'Ingegneria Sismica in Italia, Pisa, 10-14 giugno (2007).

[49] T. Albanesi, C. Nuti, & I. Vanzi, "Closed form constitutive relationship for concrete filled FRP tubes under compression", *Construction and Building Materials*, 21, 409-427 (2007).

[50] CNR-DT 200 2004. "Istruzioni per la Progettazione, l'Esecuzione ed il Controllo di Interventi di Consolidamento Statico mediante l'utilizzo di Compositi Fibrorinforzati".

[51] L. Coppola, "Concrete durability and repair technology", *Proceedings of 5th CANMET/ACI International Conference on Durability of Concrete*, Barcellona, Spain: 1209-1220 (2000).

[52] A. De Sortis, C. Nuti, "Seismic response by pseudodynamic tests of RC bridges designed to EC8", *Proceedings of 11th World Conference on Earthquake Engineering*, Acapulco, Mexico (1996).

[53] A. De Sortis, G. Monti, & C. Nuti, "Problemi di scala nella sperimentazione pseudodinamica di pile da ponte in c.a", *Atti del Workshop su Danneggiamento, Prove Cicliche e Pseudodinamica*, Dip. Analisi e Prog. Str., Università "Federico II", Napoli, Italia (1994).

[54] D.M. LL.PP. 24.01.86. "Norme tecniche per le costruzioni in zone sismiche".

[55] DM 14.1.2008 "Norme Tecniche per le Costruzioni". GU del 4 febbraio 2008, supplemento ordinario n. 30.

[56] Eurocode 8. 1998. "Design of structures for earthquake resistance, Part 2: Bridges. (Draft March 2005)".

[57] Eurocode 8. 1998. "Design of structures of earthquake resistance, Part 3: Assessment and retrofitting of buildings" (Draft November 2004)

[58] Fib Bulletin no.14, "Design and use of externally bonded FRP reinforcement (FRP EBR) for reinforced concrete structures", prepared by

sub-group EBR (Externally Bonded Reinforcement) of fib Task Group 9.3 'FRP Reinforcement for Concrete Structures', (2001).

[59] Fib Bulletin no.39, "Seismic bridge design and retrofit - structural solutions", (May 2007).

[60] D. Lavorato, "Prove pseudodinamiche su pile da ponte in cemento armato riparate e/o rinforzate con materiali innovativi" tesi di dottorato (2008). [in preparazione].

[61] L. Moléz, "Comportement des reparations structurales en béton: couplage des effets hydriques et mécaniques". PhD thesis, École Normale Supérieure de Cachan, France (2003).

[62] G. Monti, N. Nisticò & S. Santini, "Design of FRP jackets for upgrade of circular bridge piers", *Journal of Composite for Construction*, ASCE, 5(2): 94-101 (2001).

[63] M. Nakashima, et al., "Integration Techniques for Substructure PseudoDynamic Test," *Proceedings of the Fourth U.S. National Conference on Earthquake Engineering*, Palm Springs, USA, , Vol.2, pp.515-524. (14),(May 20-24, 1990).

[64] P. B. Shing, M. T. Vannan & E. Cater, "Implicit time integration for pseudodynamic tests", *Earthquake Engineering & Structural Dynamics* Volume 20, Issue 6, , Pages: 551-576 (1991).

[65] P. B. Shing, M. T. Vannan. "Implicit time integration for pseudodynamic tests: Convergence and energy dissipation", *Earthquake Engineering & Structural Dynamics* Volume 20, Issue 9, Pages: 809-819 (1991).

[66] C. Talbot, M. Pigeon, D. Beaupré & D.R. Morgan, "Influence of surface preparation on long-term bonding of shotcrete" *ACI Material Journal* 91(6): 560-566 (1994).

[67] UNI EN 10002-1:2004. "Materiali metallici Prova di trazione - Parte 1: Metodo di prova a temperatura ambiente".

[68] UNI 11040:2003. "Calcestruzzo autocompattante Specifiche caratteristiche e controlli".

[69] McKenna, F. and Fenves, G. L. (2000). The OpenSees Command Language Primer [Z], PEER, Univ. of California, <http://OpenSees.Berkeley.edu>.

[70] Chang, G. and Mander, J. (1994). Seismic Energy Based Fatigue Damage Analysis of Bridge Columns: Part I – Evaluation of Seismic Capacity. NCEER Technical Report 94-0006.

[71] Gomes, A., and Appleton, J. (1997). "Nonlinear cyclic stress-strain relationship of reinforcing bars including buckling." *Eng. Struct.*, 19(10), 822–826.

[72] Brown, J. and Kunnath, S.K. (2000). Low Cycle Fatigue Behavior of Longitudinal Reinforcement in Reinforced Concrete Bridge Columns. NCEER Technical Report 00-0007.

[73] Mander, J. B., Priestley, M. J. N., and Park, R. (1988). "Theoretical stress-strain model for confined concrete." *Journal of Structural Engineering ASCE*, 114(8), 1804-1825.

[74] Popovics, S. (1973). "A numerical approach to the complete stress strain curve for concrete." *Cement and concrete research*, 3(5), 583-599.

[75] Karsan, I. D., and Jirsa, J. O. (1969). "Behavior of concrete under compressive loading." *Journal of Structural Division ASCE*, 95(ST12).

[76] Zhao, J., and S. Sritharan. (2007) Modeling of strain penetration effects in fiber-based analysis of reinforced concrete structures. *ACI Structural Journal*, 104(2), pp. 133-141

[77] Chang, G. and Mander, J. (1994). "Seismic Energy Based Fatigue Damage Analysis of Bridge Columns: Part I – Evaluation of Seismic Capacity." NCEER Technical Report 94-0006.

[78] Dodd, L. and Restrepo-Posada, J. (1995). "Model for Predicting Cyclic Behavior of Reinforcing Steel" *J. Struct. Eng.*, 121(3), 433-445.

- [79] Gomes, A., and Appleton, J. (1997). "Nonlinear Cyclic Stress-Strain Relationship of Reinforcing Bars Including Buckling." *Eng. Struct.*, 19(10), 822–826.
- [80] Brown, J. and Kunnath, S.K. (2000). "Low Cycle Fatigue Behavior of Longitudinal Reinforcement in Reinforced Concrete Bridge Columns." NCEER Technical Report 00-0007.
- [81] Dhakal, R. and Maekawa, K. (2002). "Modeling for Postyield Buckled of Reinforcement" *J. Struct. Eng.*, 128(9), 1139-1147.
- [82] Menegotto, M. and Pinto, P.E.: (1973). Method of analysis of cyclically loaded RC plane frames including changes in geometry and non-elastic behavior of elements under normal force and bending, Preliminary Report, IABSE, Vol. 13, pp. 15–22.
- [83] Mazzoni S, McKenna F, Scott M H, Fenves G L. (2006) *OpenSEES Command Language Manual*, http://OpenSEES.Berkeley.edu/OPENSEES/manuals/usermanual/OpenSEES_Command_Language_Manual_June_2006.pdf.
- [84] Hosotani M, Kawashima K. (1998) "A Stress-Strain Model for Concrete Cylinders Confined by Both Carbon Fiber Sheets and Hoop Reinforcement". Department of Civil Engineering, Tokyo Institute of Technology, *Report No. TIT/EERG 98-3*
- [85] Hosotani M and Kawashima K. (1999) "A Stress-Strain Model for Concrete Cylinders Confined by both Carbon Fiber Sheets and Tie Reinforcement", *Journal of Concrete Engineering*, JSCE, 620/V43, pp 25-42
- [86] Lowes, L.N., Mitra, N., and Altoontash, A. (2004). "A beam-column joint model for simulating the earthquake response of reinforced concrete frames." *PEER Report 2003/10*, Pacific Earthquake Engineering Research Center, College of Engineering, University of California, Berkeley
- [87] NUOVE NORME TECNICHE PER LE COSTRUZIONI - DM 14 gennaio 2008 Pubblicato su S.O. n. 30 (NNT)

APPENDIX I

This appendix shows the different possible comparisons between the Force-Displacement cycles of the as-build Italian central pier and the repaired one (same irregular bridge).

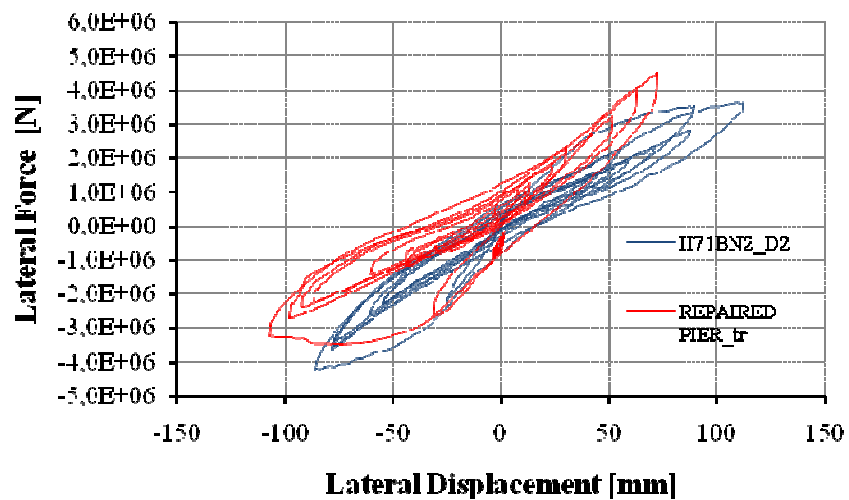


Figure 87 Repaired Italian irregular bridge and irregular Italian bridge – first pseudo-dynamic test with Tolmezzo PGA=0.35g. Comparison between the response of the repaired specimen 8 including the initial horizontal load(REPAIRED PIER_tr) and the as-build Italian pier II71BN2 if the initial displacements are imposed in the direction D2(II71BN2_D2).

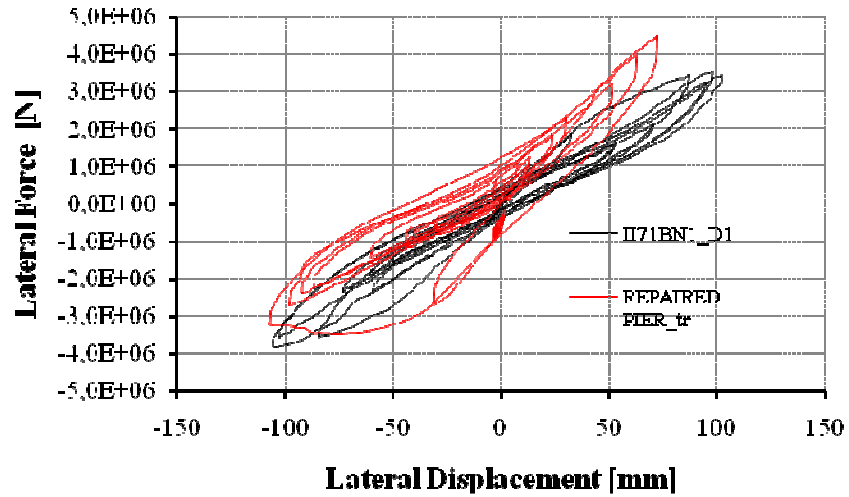


Figure 88 Repaired Italian irregular bridge and irregular Italian bridge – first pseudo-dynamic test with Tolmezzo PGA=0.35g. Comparison between the response of the repaired specimen 8 including the initial horizontal load (REPAIRED PIER_tr) and the as-built Italian pier II71BN1 if the initial displacements are imposed in the direction D1 (II71BN1_D1).

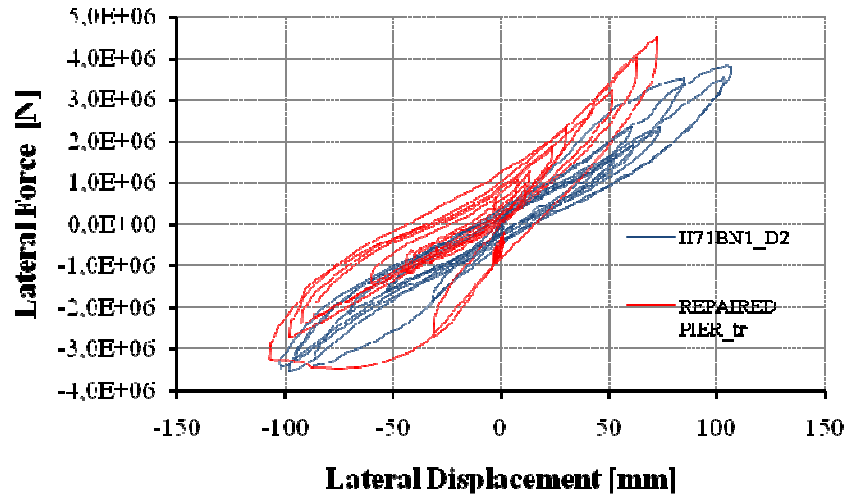


Figure 89 Repaired Italian irregular bridge and irregular Italian bridge – first pseudo-dynamic test with Tolmezzo PGA=0.35g. Comparison between the response of the repaired specimen 8 including the initial horizontal load(REPAIRED PIER_tr) and the as-build Italian pier II71BN1 if the initial displacements are imposed in the direction D2(II71BN1_D2).

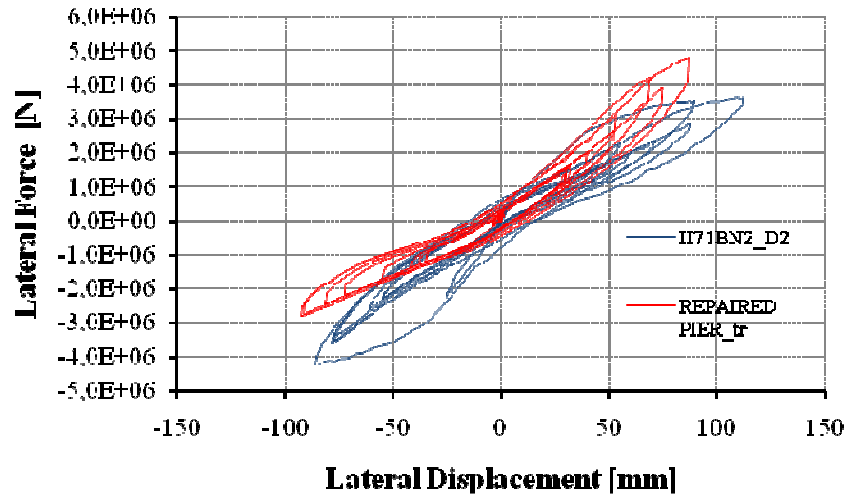


Figure 90 Repaired Italian irregular bridge and irregular Italian bridge – second pseudo-dynamic test with Tolmezzo PGA=0.35g. Comparison between the response of the repaired specimen 8 without the initial horizontal load (REPAIRED PIER_tr) and the as-built Italian pier II71BN2 if the initial displacements are imposed in the direction D2 (II71BN2_D2).

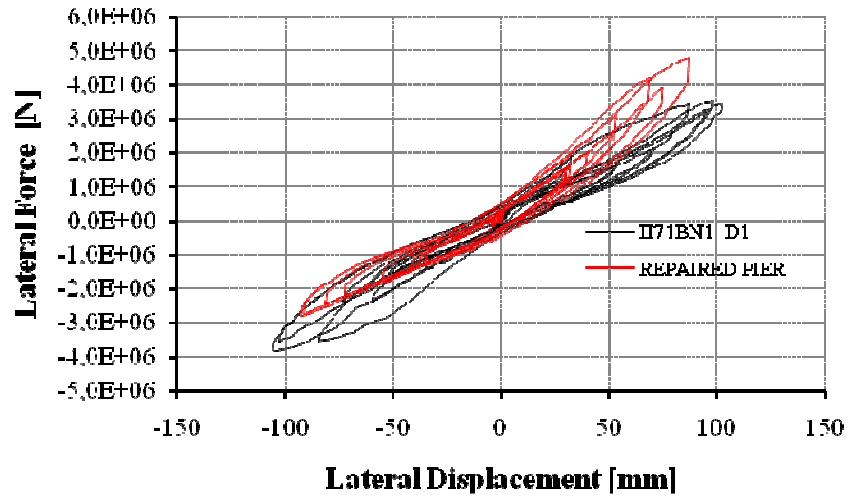


Figure 91 Repaired Italian irregular bridge and irregular Italian bridge – second pseudo-dynamic test with Tolmezzo PGA=0.35g. Comparison between the response of the repaired specimen 8 without the initial horizontal load (REPAIRED PIER_tr) and the as-built Italian pier II71BN1 if the initial displacements are imposed in the direction D1 (II71BN1_D1).

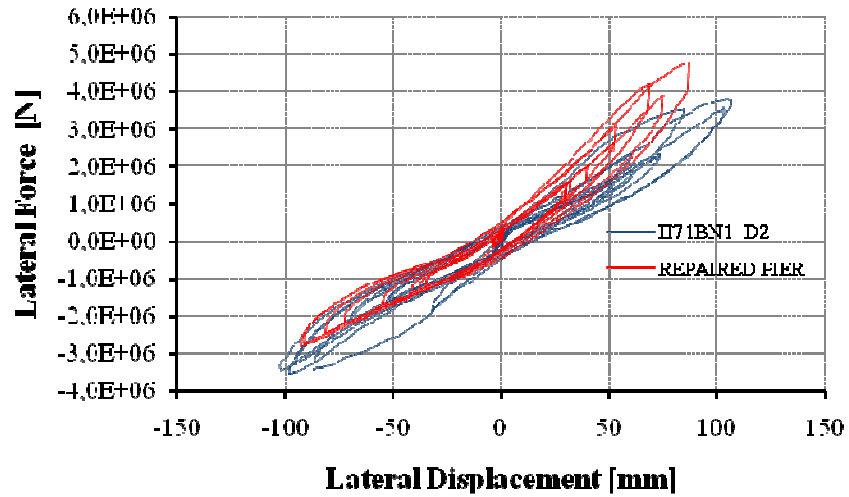


Figure 92 Repaired Italian irregular bridge and irregular Italian bridge – second pseudo-dynamic test with Tolmezzo PGA=0.35g. Comparison between the response of the repaired specimen 8 without the initial horizontal load (REPAIRED PIER_tr) and the as-built Italian pier II71BN1 if the initial displacements are imposed in the direction D2 (II71BN1_D2).

APPENDIX II

Pseudodynamic test program. User interface and block diagram



Figure 93 Pseudodynamic test software –USER INTERFACE

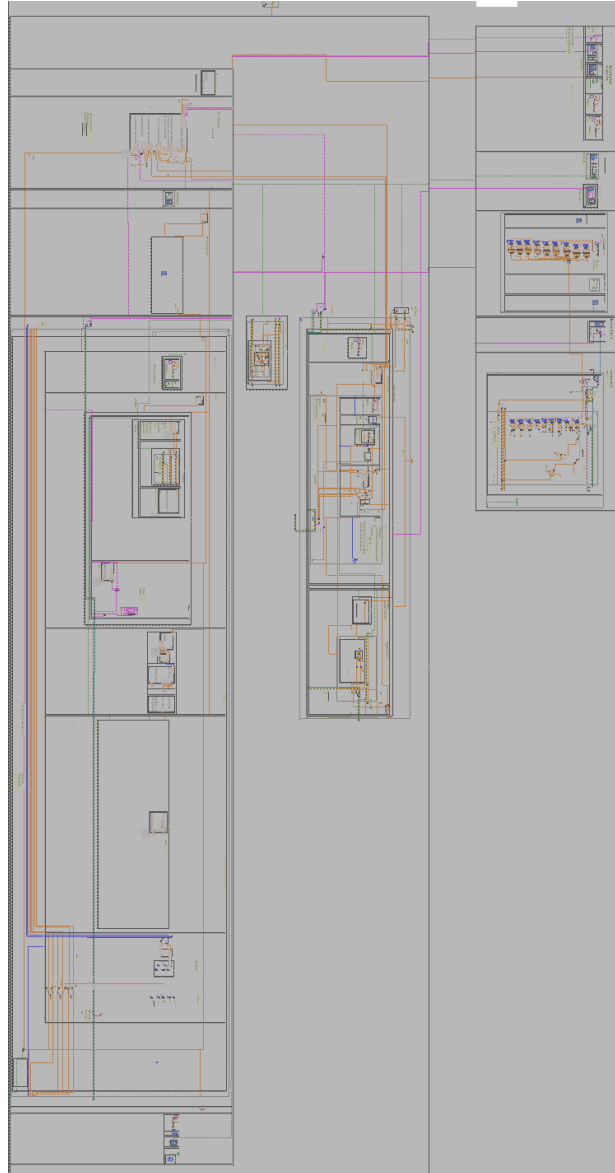


Figure 94 Pseudodynamic test software –Block diagram-